Thermo-Economic Evaluation of the Production of Liquid Fuels from Biomass

TOCK Laurence

Section of Chemistry and Chemical Engineering
Master in Chemical and Biochemical Engineering

January 16, 2009

Professor: Dr. MER François Maréchal
Responsible Engineer: Martin Gassner

Master project accomplished at the Industrial Energy Systems Laboratory of the Swiss Federal Institute of Technology

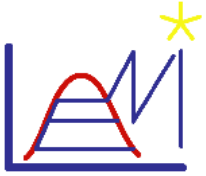

EIDGENÖSSISCHE TECHNISCHE HOCHSCHULE LAUSANNE

POLITECNICO FEDERALE DI LOSANNA

PSWISS FEDERAL INSTITUTE OF TECHNOLOGY LAUSANNE

ÉCOLE POLYTECHNIQUE FÉDÉRALE DE LAUSANNE

Laboratoire d'énergétique industrielle (LENI)

Industrial energy systems laboratory (LENI)

Projet de master de TOCK Laurence

Evaluation thermo-économique des productions de carburants liquides à base de biomasse

Contexte

Dans le contexte global de réduction des émissions de CO2, la dépendance de l'approvisionnement énergétique etc, l'intérêt dans la production des carburants à partir des ressources renouvelables croît. Dans le débat actuel, les carburants liquides sont cependant considérés comme particulièrement intéressants, à cause de leur densité énergétique et de leur compatibilité avec la technologie actuelle des moteurs à combustion interne. Les carburants les plus favorisés sont l'éthanol produit par fermentation et distillation, ainsi que différents carburants produits par voie thermochimique (carburants Fischer-Tropsch (FT), diméthyl éther (DME), méthanol).

Objectifs

Dans des projets antérieurs, des modèles thermo-économiques de différentes technologies et procédés entiers pour la production de carburants à base de biomasse ont été élaborés (SNG, DME, FT, Ethanol). Notamment dans les voies liquides, la séparation du produit brut n'a cependant pas été simulée de manière rigoureuse, l'intégration énergétique n'a pas été menée jusqu'au bout et les études n'incluent pas la dimension économique. L'objectif de ce travail de master est de compléter ces études, afin de comparer les voies de production de carburants liquides et gazeux par rapport à l'efficacité énergétique, les coûts de production et leurs échelles de production économiques.

Réalisation

- étude des modèles existants
- réconciliation des modèles non-vérifiés (synthèse FT, distillation éthanol-eau)
- développement des modèles thermodynamiques des unités manquantes (séparation d'air, synthèse méthanol, distillation DME-méthanol-eau, év. distillation FT brut)
- dimensionnement des unités et estimation des coûts d'investissements
- intégration énergétique
- comparaison environomique (énergétique, économique et environnementale) des différents carburants et leur voies de production

Lausanne, le 16/09/2008

Validation du projet:

Ingénieur responsable: **Martin Gassner**
martin.gassner@epfl.ch

Enseignant responsable: **Dr. MER F. Maréchal**
(tél: 021/693 3516) / Francois.Marechal@epfl.ch

#Project ID: 351

Imprimer cette page Fermer cette page

Abstract

A detailed thermo-economic model considering different technological alternatives for the thermochemical production of fuels from biomass (i.e.wood) is presented. Energetic and economic models for the production of Fischer-Tropsch fuel (FT), methanol (MeOH) and dimethyl ether (DME) by the means of different options of wood drying (flue gas and steam), gasification (directly and indirectly heated, fluidized bed and entrained flow), gas cleaning (hot and cold), synthesis and upgrading are reviewed and developed. Based on these models, the process is integrated and the optimal utility system is computed. Furthermore, economic models are elaborated and the competitiveness of the different process options is compared on the basis of the energetic, economic and environmental performance. The recommended technical alternatives for the production and treatment of producer gas are: air drying, indirectly heated fluidized bed gasification followed by steam methane reforming and cold gas cleaning. For the three different synthesis processes, the total energetic efficiencies are 59.8% (FT), 52.5% (MeOH) and 53.4% (DME), and the production costs are 126.6, 184.8 and 163 US$/MWh with investment costs of 24.6, 35.9 and 31.1 MUS$ for a plant capacity of $20 MW_{th}$ nominal power based on LHV. Compared to fuels from fossil sources, these biomass-derived fuels are more sustainable and emit less greenhouse gases. On the long term the economic performance can be increased by cheaper biomass, technological learning and development, and large scale applications. In the prospect of resolving the environmental problems related to the fossil fuel consumption, investigations in the R&D of these alternative thermochemical processes should be pursued in the future.

Key words: biofuels (dimethyl ether, Fischer-Tropsch fuel, methanol), biomass, process design, process integration, thermo-economic modeling

Résumé

Des modèles thermo-économiques de différentes technologies pour la production thermochimique de carburants à base de biomasse sont élaborés. Pour les différentes étapes de la production de carburant Fischer-Tropsch (FT), de méthanol (MeOH) et d'éther méthylique (DME) passant par le séchage, la gazéification, le lavage, la synthèse et la purification, des modèles existants sont complétés et de nouvelles alternatives sont dévelopées. Des modèles économiques sont créés et l'intégration énergétique est effectuée. Sur la base de ces modèles, les différentes alternatives sont comparées par rapport aux performances énergétiques, économiques et environnementales. Il s'avère que les meilleures options de prétraitement et de production du gaz de synthèse sont le séchage à l'air, la gazéification indirecte à lit fluidisé suivie du reformage du méthane et le lavage à froid. L'efficacité énergétique globale des trois voies de synthèse est relativement élevée (59.8% (FT), 52.5% (MeOH), 53.4% (DME)) et les coûts de production sont de l'ordre de 126.6, 184.8 et 163 US$/MWh pour un investissement de 24.6, 35.9 et 31.1 MUS$ pour une installation ayant une capacité thermique de $20 MW_{th}$ basée sur le pouvoir calorifique inférieur. Ces carburants produits à partir de ressources renouvelables et émettant moins de gaz à effet de serre, constituent une alternative prometteuse aux carburants fossiles pour le futur. Le plus grand potentiel réside dans le secteur du transport où ces carburants peuvent substituer les carburants actuels dans les moteurs à combustion interne sans modifications importantes. La substitution des carburants fossiles pourra aider à résoudre le problème du réchauffement climatique lié en grande partie aux émissions du transport. À l'heure actuelle, seule la compétitivité économique défavorise encore ces biocarburants sur le marché. Cependant, le développement d'installations à grande échelle, des progrès dans le développement et la commercialisation de nouvelles technologies, ainsi que la disponibilité de la biomasse à prix réduit, pourraient augmenter considérablement la compétitivité économique de ces carburants. Dans la lutte contre les problèmes environementaux liés à la consommation de l'énergie, la recherche et le développement dans ce domaine doivent être poursuivis et encouragés dans le futur.

Abbreviations and Acronyms

	Abbreviations
ATR	Autothermal Reformer
BTL	Biomass To Liquid process
BTX	Benzene, Toluene and Xylenes
C_{BM}	Bare Module Cost
C_{GR}	Grass Roots Cost
C_{TM}	Total Module Cost
C_{OL}	Operating Labor Cost
C_{RM}	Raw Material Cost
C_{UT}	Utilities Cost
C_p	Purchased Cost
COM	Cost Of Manufacturing
CFB	Circulized Fluid Bed reactor
CGCL	Cold Gas Cleaning
CHP	Combined Heat and Power (Cogeneration)
DEA	Diethanolamine
DM	Dry Matter
DME	Dimethyl Ether
DMFC	Direct Methanol Fuel Cells
ECN	Energy research Centre of the Netherlands
EF	Entrained Flow reactor
EJ	Exajoule ($10^{18}J$)
EtOH	Ethanol
FB	Fixed Bed reactor
FICFB	Fast Internally Circulating Fluidized Bed gasifier
FT	Fischer-Tropsch
GCC	Grand Composite Curve
GCL	Gas Cleaning
GHG	Greenhouse Gas
HETP	Height Equivalent of Theoretical Plate
HGCL	Hot Gas Cleaning
HHV	Higher Heating Value [kJ/kg , kJ/kmol]
HTFT	High Temperature Fischer-Tropsch Process
IR	Interest Rate
ITM	Ion Transfer Membranes
LHV	Lower Heating Value [kJ/kg , kJ/kmol]
LPG	Liquefied Petroleum Gas
LTFT	Low Temperature Fischer-Tropsch process

MEA	Monoethanolamine
MER	Minimum Energy Requirement
MeOH	Methanol
MTBE	Methyl Tertiary Butyl Ether
MTG	Methanol To Gasoline process
PFD	Process Flow Diagram
PG	Producer Gas: mixture of H_2, CO, CH_4, higher hydrocarbons (CO_2, H_2O, possibly N_2)
ppb	Parts per Billion
ppbv	Parts per Billion (volume per volume ratio)
ppm	Parts per Million
ppmv	Parts per Million (volume per volume ratio)
PSA	Pressure Swing Absorption
RCRA	Resource Conservation and Recovery Act
SAS	SASOL Advanced Synthol reactor
SB	Slurry Bed reactor
SG	Syngas: mixture of H_2 and CO (CO_2, H_2O, possibly N_2)
SNG	Synthetic Natural Gas
SMR	Steam Methane Reforming
TEA	Triethanolamine
TGRC	Total Grass Roots Cost
tpd	tons per day
TOP	Torrefaction and Pelletization Process

Roman and Greek Letters

c	Specific heat capacity [J/Kkg]
d	Diameter [m]
$\Delta\tilde{h}_r^o$	Standard molar enthalpy change of reaction [kJ/mol]
ϵ_{cc}	Carbon Conversion Efficiency
ϵ_{chem}	Chemical Efficiency or Fuel Efficiency
ϵ_{tot}	Total Energetic Efficiency
$\epsilon_{Murphey}$	Murphey Efficiency
$\dot{E}$	Mechanical Power [kW]
G	Superficial gas mass flow [kg/sm^2]
h	Height [m]
K_p	Equilibrium Constant
$\dot{m}$	Mass flow rate [kg/s]
$\%mol$	Mole Percent
N	Number of plates of distillation columns
P	Pressure [bar]
$\dot{Q}$	Thermal Power [kW]
T	Temperature [^oC or K]
u_{mean}	Mean Gas Velocity [m/s]
$\dot{V}$	Volumetric flow rate [m^3/s]
$\%vol$	Volume Percent
$\%wt$	Weight Percent

Contents

Chapter 1

Introduction

1.1 Context

In modern life, energy plays a crucial role because it is needed all-over for heating, lighting, cooking and for industrial, commercial and transport activities. Over the last 50 years, the world's energy consumption has increased drastically due to the economic and demographic growth. The major energy resources covering the demand are fossil fuels (e.g. oil, natural gas and coal), nuclear power and renewables in a lesser extent (figure 1.1a)). With the depletion of the fossil resources, the increased global warming caused by the greenhouse gas emissions, and the geographical imbalance between major producers and large consumers, alternative energy resources have to be privileged in the future to assure the security of energy supply and sustainability.

In the prospect of reducing the CO_2 emissions according to the Kyoto Protocol, renewable energy resources, like solar energy, hydropower, geothermal heat, waste and biomass become more and more popular. Biomass is however the only renewable resource that offers the possibility to produce a wide variety of products: heat, electricity, chemicals, solid fuels, gaseous fuels and liquid transportation fuels being compatible with the present technology of internal combustion engines. Since the transportation sector represents nearly one third of the global energy consumption (figure 1.1b)) and is responsible for a large part of the global CO_2 emissions, these carbon neutral biofuels, could offer potential alternatives for fossil transportation fuels. The most important fuels produced from biomass are: hydrogen, ethanol, methanol, dimethyl ether (DME) and other hydrocarbons synthesized by thermochemical processes like the Fischer-Tropsch synthesis (FT).

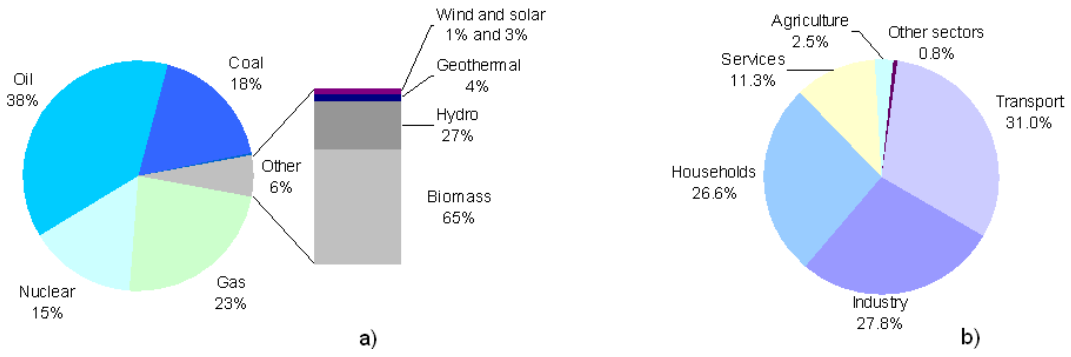

Figure 1.1: a) Breakdown of energy consumption in the EU-25 (adapted from [1, 2]) b) Final energy consumption by sectors, EU-27, 2005 (adapted from [2])

The research and development of these alternative fuels produced from biomass is justified by the three main problems: emissions on short-term, climate change on medium-term and security of supply on long-term. However, a non-sustainable exploitation of the biomass resource could create additional environmental pressures, such as on biodiversity, soil and water resources. Moreover, not all the existing biomass resources can be used for energy purposes, because the requirements of the food and wood products, and the paper sector have to be met at the same time. Research is therefore focusing on so-called second generation biofuels based on non-food biomass.

The energy targets in the European Union (EU-25) for 2010 are to increase the share of renewable energies to 12% of the gross energy consumption, of green electricity to 21% of gross electricity production and of liquid biofuels to 5.75% of total fuel consumption. However, the current trend in Europe leads to only approximately 3.5% biofuels in 2010 (vs. target 5.75%). The vision goal of the European Technology Platform Biofuels is 25% biofuels in 2030, compared to the world's average accounting for 0.5% biofuels in 2003. Preliminary results indicate that enough biomass is available to reach these targets, even after taking the environmental constraints into account [1, 3, 4]. However, to reach these targets additional technological progress has to be made to convert biomass efficiently into fuels through gasification, gas processing and chemical synthesis.

1.2 Purpose of Study

The purpose of the present work is to analyze different technologies for the thermochemical production of fuels (Fischer-Tropsch fuel, dimethyl ether and methanol) from biomass. Thermo-economic models of different technologies have already been developed in previous works [5, 6], however several steps haven't been elaborated in detail, such as the purification of the crude products, the energy integration and the economic analysis. The aim is hence to verify and complete these existing models for the different process alternatives, in order to compare the competitiveness of the different options for the production of biofuels with regard to energetic, economic and environmental considerations.

1.3 Methodology

The general methodology applied to study the different processes is based on the development of separate energy-flow, energy-integration and economic models. After the assessment of the different technologies for gasification, gas-cleaning, syngas processing and conversion (FT, MeOH and DME synthesis), the process flow superstructure, including the different options, is defined. For each unit, thermodynamic and economic models are developed and the technical and economic performance is analyzed. The models are improved step by step from intermediate results by including different options and optimizing key parameters. The purpose of the thermo-economic model is to compute the systems' efficiency as a function of the decision variables and to identify critical parameters and opportunities for process improvements.

The thermodynamic model contains two parts: the energy-flow model representing the transformations from feedstock to product and the energy-integration model representing the heat recovery in the system. The commercial software, Belsim-Vali [7], which is suitable for design, as well as for data reconciliation purposes, is used for the flowsheet calculations. This tool using an equation solver approach, generates relevant information about the process streams, especially

mass balances, flow compositions and physical properties, as well as mechanical and thermal energy balances.

From these data, thermodynamic calculations such as the minimum energy requirement and the optimal utility network with regard to minimal operating costs, are figured out with the aid of the energy integration software Easy2 [8]. The heat and power integration model maximizes the combined production of heat and power, while solving the energy balance of the plant and the heat cascade constraints of the pinch analysis.

The interface for the information transfer between the different models is managed by the OSMOSE framework developed at the Laboratory of Industrial Energy Systems (LENI). OSMOSE also affords with the help of the integrated optimization software Moo, the possibility for optimizations by performing sensitivity analysis on key parameters of the model. The MATLAB programming language was used to develop the software and to implement the economic models. With all these data the investment costs are evaluated for different process conditions.

This methodology based on separate flowsheet models and process integration, has the advantage, contrary to the conventional simulations based on a scenario approach, to offer the possibility to consider many potential solutions without excluding one right from the design definition. By considering various combinations between the different process options, optimal process conditions and an optimal process layout can be determined from the integration step and the different options can be compared from an energetic and economic point of view. However, one drawback is that the energy integration is performed on a theoretical level by targeting the minimal energy requirement and consequently the resulting heat exchanger network generally isn't an industrial solution. Nevertheless, this method is appropriate for preliminary process design and comparison. By identifying promising system configurations, it is a good starting point for the detailed design of an optimal plant.

1.4 Outline of Report

After the introduction of the subject in chapters 1 and 2, a general description of the different processes including their main steps and technological options is given in chapter 3. The flowsheets of the different options and the modeling assumptions are then presented in chapter 4. The energy integration principle is discussed in chapter 5 and the economic evaluation is presented in chapter 6. The influence of key parameters on the productivity and the energetic performance is analyzed in chapter 7, leading to the improvement of the models. Finally, the performance of the overall processes for different gasification and synthesis options are compared and discussed in chapter 8 and a conclusion is drawn in chapter 9. Additional details are reported in the appendices.

Chapter 2

Biomass and Sustainable Development

Today, industrialized countries become more and more aware that with the increased energy consumption and without any changes in the energy supply and the living customs, the world is already and will be confronted in the future, to some major environmental problems: increased greenhouse gas emissions (GHG) leading to global warming and climate change, and depletion of the fossil resources. With this awareness, many initiatives were taken and novel concepts were born in the last decades having as goal a more sustainable development with the objective to limit the environmental damages; reduce the CO_2 and NO_x emissions, reduce and optimize the energy consumption, increase the energy efficiency, avoid the spoilage of resources and energy, reduce wastes, use water in a rational way and promote renewable energy resources. The main objectives can be summarized by the 3 Rs: Reduce, Reuse and Recycle. In this context some relevant key concepts are: sustainability, GHG emission reduction, cleaner production, waste management, green chemistry, industrial ecology, life cycle assessment, eco-efficiency, 2000Watt Society (in Switzerland) and many others.

To achieve these objectives one essential step is to promote the exploitation of renewable energy sources. In this context, the potential of the biomass for the production of biofuels is studied in this work.

2.1 Biomass

Biomass can be considered as renewable resource because biomass, including wood, energy crops, agricultural and forest residues, by-products, sludges and wastes from industrial and municipal processes, is replenished by natural processes and is abundant in most parts of the world. Moreover, the use of biomass doesn't increase the net CO_2 content in the atmosphere. In fact, trees and plants remove carbon from the atmosphere through photosynthesis, forming new biomass as they grow. The carbon is stored in the biomass and when biomass is burned, carbon returns to the atmosphere in the form of CO_2 and the cycle is closed. However, if the processing of biomass consumes any fossil fuel, additional biomass would need to be grown to offset the carbon released from the fossil fuel.

Therefore, biomass has many advantages as energy source producing a wide variety of product types: heat, electricity, biofuels and others. But not all the available biomass resources can be used for energy purposes. Food, timber, paper and certain high-value chemicals are also derived from biomass. Therefore, the bio-energy production must be integrated with the other priority applications. Biomass has to be used in a wise and sustainable way.

The energetic potential of a particular biomass resource depends on its composition and moisture content. Woody biomass consists essentially of hemicellulose, cellulose, lignin and glycoproteins (figure 2.1).

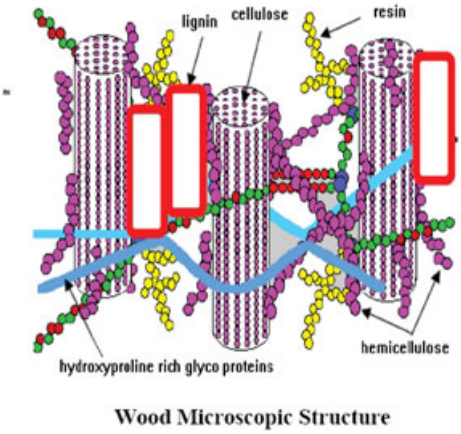

Figure 2.1: Microscopic structure of woody biomass [9]

2.2 Syngas

Syngas or synthesis gas, a mixture of hydrogen and carbon monoxide is an important intermediate in chemicals production and an important fuel source. The name is derived from the use as an intermediate in generating synthetic natural gas and to create ammonia and methanol. Syngas is also an intermediate in creating synthetic petroleum to be used as a lubricant or fuel. It is essentially produced from fossil energy sources by coal gasification and steam reforming of natural gas to generate hydrogen. However syngas, or more exactly producer gas [1], can also be generated from biomass via gasification. Consequently, syngas produced from renewable biomass sources could play an important role in a more sustainable development due to its multiple applications: source for pure hydrogen, produce electricity and heat in a gas turbine, produce chemicals (ammonia, methanol, etc.) and fertilizers and finally produce biofuels for transportation (methanol, DME, FT-fuels, Diesel).

Today, around 6EJ of syngas are produced annually worldwide (figure 2.2). The market is dominated by the ammonia industry, the production of hydrogen for use in refineries and the production of methanol. The use for the production of transportation fuels (gas-to-liquid (GTL) process) only represents 8%.

Even if today the syngas is produced essentially from fossil resources, progress notably in the gasification technology would allow to increase the efficiency of the production of syngas from biomass. Since syngas and second generation biofuels from biomass are expected to become increasingly important in the future due to environmental concerns, many institutes and companies are involved in gasification research, development, demonstration and commercialization [10, 11].

[1] Producer gas contains in addition to syngas, methane and higher hydrocarbons

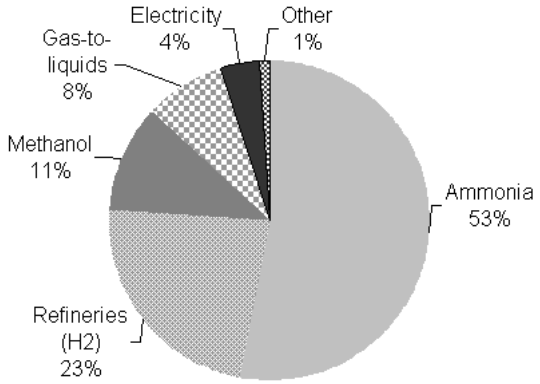

Figure 2.2: Present world's syngas market, total ≈6EJ/year [4, 10]

2.3 Biofuels

Biofuels are an emerging business worldwide, driven by threatened fuel supply, climate change concerns and attractive policies. A few main routes can be distinguished to produce biofuels: extraction of vegetable oils, fermentation of sugars to alcohol, gasification and chemical synthesis. Biofuels are often classified in terms of "first" versus "second" generation. First generation biofuels are produced from traditional agricultural crops (e.g. biogas and ethanol from starch an sugar) while second generation biofuels are generated from lignocellulosic feedstock. These second generation biofuels have the advantage that no food crops are used as feedstock, that the yield of biofuel per hectare of land is higher and that the greenhouse gas emissions are lower. In addition, biofuel from algae is sometimes designated by third generation biofuel. Second and third generation biofuels are also called advanced biofuels.

Today biomass is already used for the production of transportation fuels, such as biodiesel from vegetable oils or bioethanol from sugars and starches (first generation biofuels). However, biomass in the form of woody and grassy energy crops and residual streams of the wood industry has the potential to produce more sustainable second generation biofuels. Biomass derived transportation fuels can have low lifecycle CO_2 emissions if the biomass feedstock is sustainably grown, transported, converted and consumed. This could also partly reduce local air pollution. Two types of processes can be used to produce transportation fuels from woody and grassy biomass: biochemical processes with bacteria, yeasts or fungi, or thermal processes [10]. In this work, thermal processes producing biofuels via syngas are studied exclusively. Potential fuels are: methanol, DME and Fischer-Tropsch fuels, as well as hydrogen, ethanol and propane (the last ones aren't investigated in this work).

Alternative transportation fuels for gasoline or diesel need to have some characteristic physical and combustion properties, such as volumetric heating values, cetane number (for diesel fuels), octane value (for gasoline fuels) and vapor pressure. Fuel regulations suggest that motor vehicle fuels should have sufficient vapor pressure to cold start, even at temperatures of -30^oC. A comparison of the properties of alternative fuels and conventional transportation fuels is given in table 2.1.

For conventional diesel fuel the cetane number is around 40-55. Fuels with a higher cetane number such as DME, result in reduced emissions of NO_x, particulate matter, hydrocarbons and CO.

Methanol, having a higher octane rating than gasoline, can be used as alternative fuel in different ways in transportation: direct use, use as a blend with gasoline, methanol to gasoline

and methanol to hydrogen process. Despite the various benefits as a transportation fuel, it has some safety drawbacks due to the wider flammability limits, the invisible burning and the formation of toxic and possibly carcinogenic formaldehyde.

Alcohols have moreover the advantage that they can be used in fuel cells converting chemical energy into electrical energy. Compared to hydrogen gas requiring large storage tanks due to the low volumetric heating value, the advantage of alcohols consists in the easy storage and transport. In addition, alcohols have high hydrogen storage capacities and could offer an alternative to produce hydrogen for fuel cell-powered motor vehicles by onboard autothermal reforming [12].

Properties	Gasoline	Diesel	Methanol	DME	Ethanol	Methane	Propane
Chemical formula	$C_5 - C_{12}$	$C_{12} - C_{25}$	CH_3OH	CH_3OCH_3	C_2H_5OH	CH_4	C_3H_8
H/C ratio	1.9	1.88	4	3	3	4	2.7
Liquid density [kg/l]	0.72-0.78	0.84-0.88	0.792	0.67	0.785	0.422	0.51
Boiling Point [^oC]	37-205	140-360	65	-25.1	79	-161.6	-42.15
Auto-ignition T [^oC]	257	320	460	350	423	532	470
Flammability limits [vol%]	1.4-7.6	0.6-6.5	5.5-36	3.4-17	4.3-19	5-15	2.1-19
Energy content (LHV) [MJ/kg]	44.0	42.5	20.0	28.8	26.9	50.0	46.4
Cetane Number	0-5	45-55	5	55-60	5	0	-2
Research Octane Number	92-98	-	106	-	107	120	112
Motor Octane Number	80-90	-	92	-	89	120	97
Reid Vapor Pressure [psi]	8-15	0.2	4.6	-	2.3	2400	208

Table 2.1: Properties of different types of fuels (adapted from [12, 13])

2.4 Outlook

The exploitation of the energetic potential of the renewable resource biomass can contribute in the future to security in the energy supply, to the reduction of the CO_2 emissions and to a more sustainable development. Notably, by the production of biofuels for the transportation sector by the thermo-chemical production routes studied in this work. Besides the production of transportation fuels, heat and electricity, the potential of biomass could be used essentially for the sustainable production of syngas. With syngas as starting reactant, many chemicals and even hydrogen can be produced. Therefore, the potential of biomass in the production of hydrogen, the energy carrier of the hydrogen economy, could also be investigated. In this context, the methanol economy in which methanol replaces fossil fuels as a mean of energy storage, fuel and raw material for synthetic hydrocarbons, could be proposed as alternative to the hydrogen economy. The advantage of a methanol economy compared to a hydrogen economy is the compatibility with the existing infrastructures and the efficient energy storage, and compared to an ethanol economy the non-dependence on food feedstocks.

Biomass can be used for many applications and has many advantages as an energy resource. In future, biomass is a promising alternative to the fossil resources.

Chapter 3

Principles and Technologies

3.1 General Process Layout

The general layout of the processes converting biomass to fuels consists in different steps: the upstream units for the pre-treatment, the chemical conversion process itself and finally the downstream units for the product separation, purification and upgrading. The conversion of biomass to fuel is achieved through mechanical, thermal, chemical or biological processes. The main steps, illustrated by the general block flow diagram in figure 3.1, are:

1. Conditioning of the feed: sizing and drying.
2. Pyrolysis to break the dried feedstock down into a gaseous, liquid (tar) and solid (char) part.
3. Gasification to produce raw synthesis/producer gas.
4. Gas clean-up and treatment: Purification by removing catalyst poison and other impurities (e.g. SMR and gas cleaning) and adjustment of the H_2/CO ratio by the water-gas shift reaction and by CO_2 removal (optional).
5. Fuel synthesis: conversion of carbon monoxide and hydrogen to FT-fuel, methanol or DME.
6. Refining and upgrading of the crude fuel products.

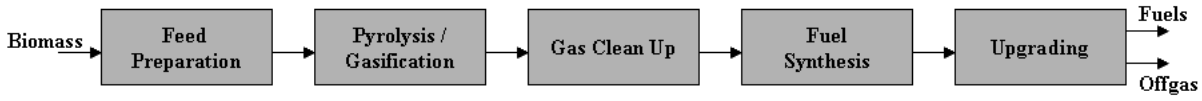

Figure 3.1: Block flow diagram of the overall biomass conversion process

3.2 Producer Gas Production

Depending on the biomass feedstock, different pre-treatment steps prior to gasification are required and syngas of different qualities is produced. The gasification converting carbonaceous feedstock to combustible gas, is characterized by the same thermochemical reactions as combustion, however the difference is, that oxidation is not complete. Drying, pyrolysis and gasification is an overall endothermic process requiring heat supply, either by external heating or by supplying sufficient oxygen to oxidize part of the product. The different steps are characterized by the process temperature and the amount of oxygen that is present.

A general overview is given in [14, 15] and figure 3.2 summarizes the physical and chemical changes of coal being similar for biomass.

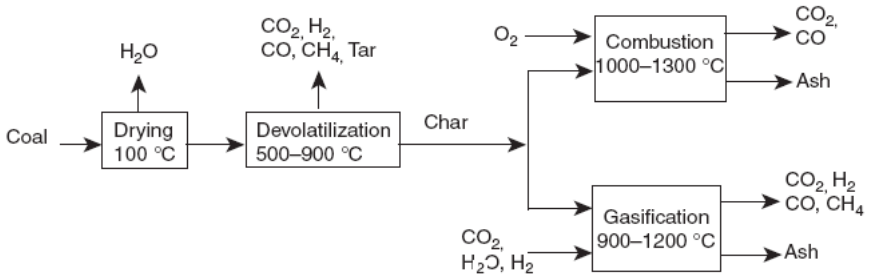

Figure 3.2: Chemical and physical changes of coal [15]

3.2.1 Drying

Drying is generally the most important pre-treatment step prior to gasification and requires a high amount of energy, which can be the synthesis process heat itself or can be extracted from the plant's offgas or from a steam cycle. This step is necessary to reduce the moisture content of wood to 10-15%, because otherwise the high moisture content would decrease the gasifier's performance owing to exergetic losses. The moisture is made up of free water within the pores and of bound water adsorbed in the interior surface structure. By heating up to around 100^oC water vaporizes, free water is forced out and thereby the humidity decreases. An efficient drying stage needs therefore thermal energy at a temperature above the boiling point of water. The most common biomass drying techniques are steam drying and flue gas drying [16, 17] using steam respectively air as drying agent. The choice of the technique depends among others on the steam demands within the process and the extent of electricity co-production.

3.2.2 Pyrolysis and Gasification

Process Principles

Pyrolysis is an anaerobic process transforming biomass into reactive intermediate products by heating up. It is therefore a slightly endothermic process. At around 150^oC, thermal decomposition starts. The main products that are released are char, light molecular weight gases and heavy molecular compounds (tar) that condense when cooled down. At the end of the pyrolysis the mass is reduced up to 15% of the initial mass and the solid part is mainly composed of char.

In the gasification, starting around 450^oC, the heavy compounds further break down into gases by cracking and the char is converted into gases by reaction with the gasifying agents.

The exact composition of the product depends on the operating pressure and temperature and the technology used.

Pyrolysis Process

Different types of pyrolysis (e.g. slow, fast, flash and torrefaction) are distinguished according to the process temperature, the residence time of the biomass in the reactor, the heating method (direct or indirect) and the reactor type (fixed bed, screw reactor (Augers), fluidized bed, ablative processes, etc.). Detailed information on the pyrolysis technology are found in [18, 19, 20].

One type of pyrolysis is torrefaction, consisting of a decomposition reaction. Water is released by the decomposition and the biomass becomes dried. The tenacious and fibrous structure of wood is altered; the lignins are loosened and the hemicellulose bound to cellulose is burned away and so the wood is unbound and more brittle (figure 2.1). Besides water, other decomposition products are: carbon monoxide, carbon dioxide, methane (CH_4) and acetic acid (CH_3COOH). The yield of mass and energy from original biomass to torrified biomass is dependent on the temperature, the reaction time and the biomass type. For wood feedstock a possible stoichiometry of the reaction is:

$$\begin{aligned} C_6H_{8.6}O_{3.65} \quad \rightarrow \quad & 0.92C_6H_{7.5}O_{3.3} + 0.28H_2O + \\ & 0.037CH_3COOH + 0.21CH_4 + 0.076CO_2 + 0.12CO \end{aligned} \tag{3.1}$$

Torrified biomass having a high grindability, has consequently properties similar to coal and is therefore attractive for combustion and gasification. During the torrefaction process most of the energy value of the wood is preserved (90% of its energy), while the product can loose up to 30% of its mass.

Torrefaction, being a relatively new development for biomass upgrading, isn't commercially prevalent yet. On a demonstration plant of the Pechniney process an indirectly heated jacketed screw reactor was used for biomass torrefaction, however this kind of reactor has low scale-up characteristics. In the TOP process (torrefaction and pelletization process) from ECN a directly heated moving bed reactor was developed for torrefaction [21]. Other potential torrefaction reactors could have designs similar to dryers. Steam tube dryers, possibly with rotation to promote contact between the solid particles and hot steam tubes may be used. Transnational Technology LLC, a market place for technology transfer and innovation [22], suggests in an industrial torrefaction process the use of Wyssmont's Turbo-Dryer®(figure 3.3) consisting of a stack of slowly rotating circular trays.

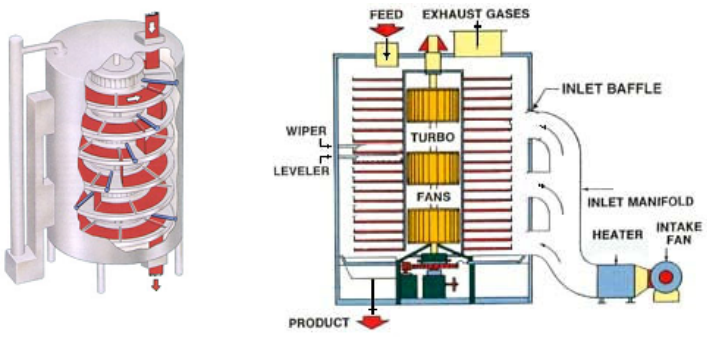

Figure 3.3: Wyssmont's Turbo-Dryer®[23]

Gasification Process

The gasification process, where carbonaceous materials are broken at high temperature into mainly hydrogen, carbon monoxide, carbon dioxide, hydrocarbons, tars and ash, is very efficient for extracting energy from many different types of organic materials. Gasification is essentially an incomplete combustion and the chemical and physical processes are quite similar; however the difference from a processing point of view is that gasification consumes heat evolved during combustion. In fact, gasification is generally operated at the point where just enough oxygen is added to the process that, the heat generated equals the energy that is required to volatilize the feedstock. Contrary to combustion, gasification produces a gas that is combustible. Commercial applications, ranging from small scale applications up to industrial scale installations, such as advanced integrated gasification combined cycle plants, exist.

In a simplified form, the reaction can be regarded as the reaction of carbon with the gasifying agent [15].

$$\text{Steam/carbon reaction}: \quad C_{(s)} + H_2O \rightleftharpoons CO + H_2 \qquad \Delta\tilde{h}_r^o = 131kJ/mol \tag{3.2}$$

$$\text{Partial oxidation}: \quad C_{(s)} + \tfrac{1}{2}O_2 \rightleftharpoons CO \qquad \Delta\tilde{h}_r^o = -111kJ/mol \tag{3.3}$$

$$\text{Bouduard reaction}: \quad C_{(s)} + CO_2 \rightleftharpoons 2CO \qquad \Delta\tilde{h}_r^o = 172kJ/mol \tag{3.4}$$

In addition, water-gas shift and reverse methanation (steam methane reforming) reactions proceed to near chemical equilibrium in most gasifiers.

$$\text{WGS}: \quad CO + H_2O \rightleftharpoons CO_2 + H_2 \qquad \Delta\tilde{h}_r^o = -41kJ/mol \tag{3.5}$$

$$\text{SMR}: \quad CH_4 + H_2O \rightleftharpoons CO + 3H_2 \qquad \Delta\tilde{h}_r^o = 206kJ/mol \tag{3.6}$$

The composition of the producer gas depends on the feedstock, the operating conditions and the reactor type. At high temperature the conversion of carbon to CO and H_2 increases while the production of H_2O, CH_4 and CO_2 decreases [24].

Different gasification methods, including atmospheric and pressurized, steam-blown, oxygen-steam-blown and air-blown, indirectly and directly heated gasification, produce a wide range of syngas compositions, with H_2/CO ratios varying from 0.45 to 2. Since the gasification is an endothermic process, heat supply has to be assured by the reactor design. Directly heated gasifiers use the exothermic reaction between oxygen and organics to provide the heat required to devolatilize biomass and to convert residual carbon-rich chars. The heat to drive the process is hence generated inside the gasifier by burning some char or biomass. Indirectly heated gasification on contrary takes place without combustion of the feedstock, instead the heat is transferred through a heat exchange mechanism, either from a hot solid (i.e. sand) or through a heat exchange surface. The advantage is that no oxygen production is required and that steam can be used as gasification agent leading to lower nitrogen impurities but higher methane content in the producer gas. In general, air-blown gasifiers produce low heating value fuel gas for use as industrial fuel and for power production, whereas oxygen-blown gasifiers produce medium heating value fuel gas for use in the production of chemicals and transportation fuels. Commonly, a cyclone is present after the gasifier to remove ash, unreacted char and particulates from the product.

Biomass gasification is inspired from fossil-fuel based gasifier concepts. Some concepts seem to work also for biomass, however some challenges are still to be overcome for large scale applications and to compete on the energy market. Commercial available reactors include fixed and fluidized bed (bubbling and circulating), as well as entrained flow reactors [5, 15, 17] (figure 3.4). A detailed description of each type of gasifier can be found in [10, 15, 25, 26].

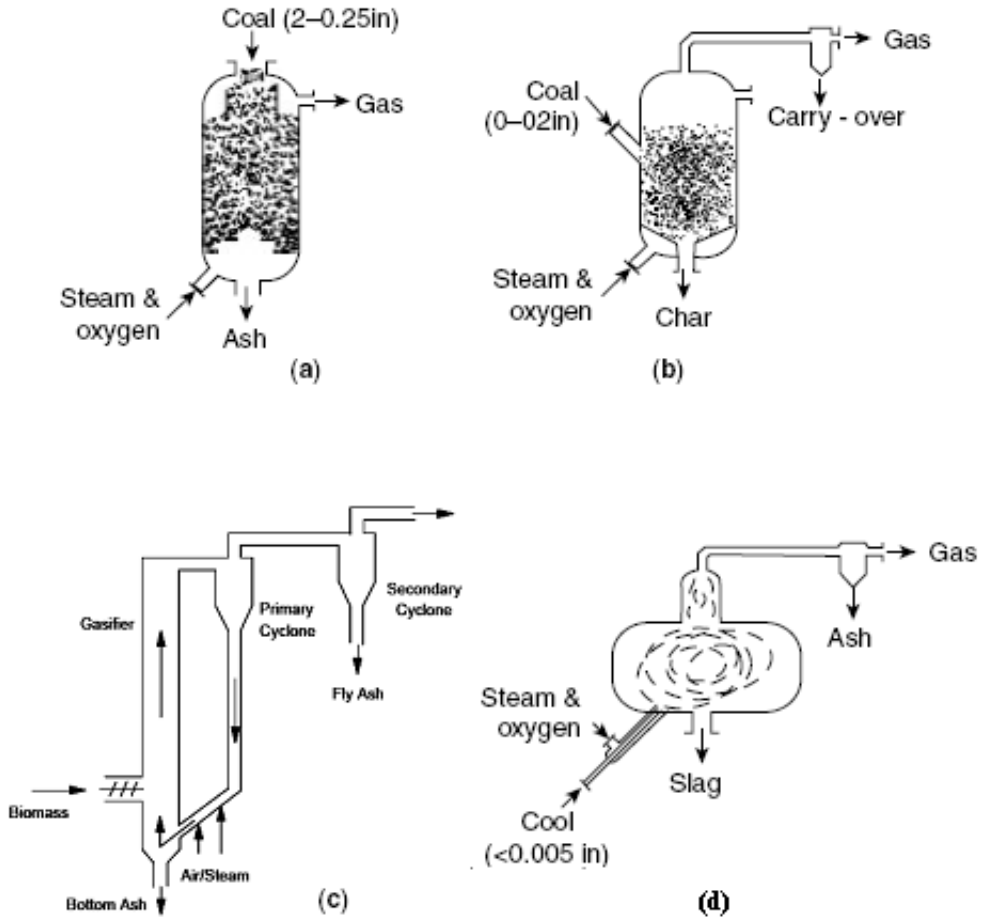

Figure 3.4: Types of gasifiers [15]: a) fixed bed, b) bubbling fluidized bed, c) circulating fluidized bed [26] and d) entrained-flow

The fixed bed gasifier is composed of a slowly moving packed bed of coal with a fixed height. This is a relatively simple technology, but is either limited in scale (downdraft fixed-bed) or produces a lot of tar (updraft fixed-bed). Moreover, the fuel flexibility is limited and the inhomogeneous process induces problems with process control and syngas quality. Regarding biomass applications, the updraft gasification has the advantage that size, shape and moisture content of the biomass are not critical and that syngas with a high heating value is produced.

The fluidized bed gasifier (bubbling or circulating (CFB)) is a highly fuel flexible and can be used at large scale. The fluidized beds normally use a quartz sand bed and this inert heat carrier (i.e. silica sand) moving within the reactor like a boiling fluid increases mixing and kinetics and creates high process temperature control. Consequently, the overall gasifier efficiency and the fuel throughput is high. For biomass applications, the major disadvantage is the risk for bed agglomeration, inducing ash related problems at relatively low temperatures. In fact, the sand grains in the bed agglomerate since the ashes begin to get pasty or melt; as the agglomerate grows the differential pressure over the bed drops and the bed defluidizes and in the worst case can collapse. To overcome this problem, the gasification temperature has to be decreased, the sand bed has to be exchanged frequently or mineral binding products have to be added. An

advantage of air or oxygen-blown fluidized bed gasifiers is that the methane content in the syngas is often relatively low, since the reactor functions as a high-temperature auto-thermal methane reformer.

The entrained-flow gasifier is described as a practically empty vessel in which the fuel is entrained with the gasifying agent to react in a cocurrent flow. The pulverized feed is fed continuously in form of gas, powder or in a slurry into a pneumatic-flow reactor along with a relatively large amount of oxygen or steam, and converted quickly in a turbulent powderized flame. For oxidative heating, the very high temperatures (typically 1300-1400^oC) caused by adding oxygen, destroy oils and tars and remove ash as liquid slag. One drawback is that a high percentage of energy is converted into sensible heat that has to be used for electric power generation and steam production to achieve reasonable process efficiencies. This type of gasifier has been essentially developed for coal gasification by Shell, Chevron Texaco and Koppers-Totzek and only limited testing for biomass has been performed. The lack of applications to biomass is related to the high costs of feed preparation to reduce moisture content to low levels and reduce particle size. When using biomass as fuel, it must either be grinded to powder or in some cases pyrolyzed to gas, pyrolysis oil and coke, the latter converted to slurry. Indirectly heated entrained-flow gasification for biomass is investigated and developed among others by Brightstar Environmental and Pearson Technology [26]. The heat for the endothermic gasification reaction is supplied by circulating hot synthetic olivine (calcined magnesium silicate).

A special type of gasifier called indirect (allothermal) gasifier was developed lately (figure 3.5). It consists of two separate fluidized bed reactors, the gasifier and the combustor coupled together by circulating bed material. In the combustor the residual char received from the gasifier is burned to produce heat before it passes with hot inert sand through the cyclone into the gasifier reactor. Here the hot sand provides the heat necessary to gasify the reactor's feedstock [25]. Examples of gasifiers developed based on this concept are: FICFB (Fast internally circulating fluidized bed gasifier, Guessing Plant) [27] and Milena gasifier [10, 28]. This process produces essentially N_2-free gas without the need of steady supply of oxygen and with a high rate of throughput. The produced gas has a high energy content. This is one of the most interesting gasification systems for large scale biomass power or fuel generation if coupled with the proper systems for gas cleanup and heat recovery. However, one drawback remains; the complicated construction inducing high investment costs.

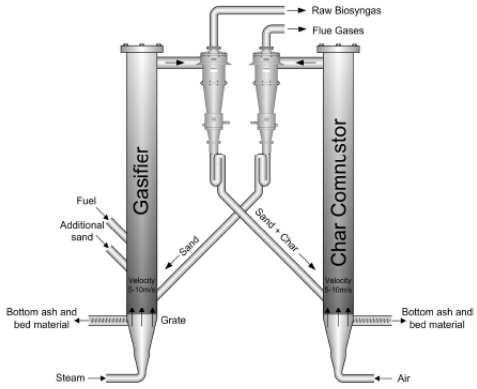

Figure 3.5: Char indirect, two-stage gasifier with steam reforming [25]

Oxygen supply

The oxygen used as gasification medium in the directly heated gasification can be provided as air, enriched air or pure oxygen. The use of pure oxygen reduces on the one hand the amount of nitrogen contaminants in the final product and on the other hand the volume flow and so the investment costs. The oxygen can be produced on site by adsorption or cryogenic distillation technology. For lower purity (<93.5% O_2) and quantity (120-150tpd) pressure swing adsorption is the preferred technology, while above this range cryogenic separation is in general more economical. Since air is freely available the costs are directly related to the costs for air compression and refrigeration [29].

Alternatives are the newer developments in ceramic ion transfer membranes (ITM) operating on the partial pressure differential to passively produce pure oxygen. This process might be economically advantageous with regard to capital, as well as utility costs. Although, research and development of ITM are still in demonstration phase and no commercial installations at industrial scale are built yet. Technical development of ITM is done by: Air Products, U.S. Department of Energy and ChevronTexaco [30, 31].

The ITM oxygen separation process is based on a nonporous pervoskite ceramic material which, under a pressure gradient at the appropriate temperature, electrochemically ionizes oxygen molecules from air and diffuses the ions and electrons through a wafer-type membrane, where they recombine as oxygen molecules on the other side without any external source of electrical power [32]. By integrating the energy-rich, vitiated, non-permeate stream with a gas turbine system, the overall process can co-produce high purity oxygen, power and steam [30, 31].

3.2.3 Syngas Cleaning

The syngas produced by the biomass gasification mainly consists of H_2, CO, CO_2 and CH_4. The fraction of each compound can be adjusted to the needs of the subsequent process by different treatments reducing for example, the amount of inert gases (CH_4 and CO_2) and thereby increasing the efficiencies of fuel catalysts.

Steam Methane reforming

After the gasification, the producer gas can be tailored to the needs of the process by steam methane reforming (SMR) converting the inert methane with steam into hydrogen and carbon monoxide at high temperature (700-1100^oC) in the presence of a catalyst (e.g. Ni).

$$CH_4 + H_2O \quad \rightleftharpoons \quad CO + 3H_2 \quad \Delta\tilde{h}_r^o = 206kJ/mol \tag{3.7}$$

In SMR, coking and carbon deposition may cause some problems if the biomass syngas has a high CO and C_+ content. To prevent it partly, additional steam has to be added.

Water-gas shift

The H_2/CO ratio can be adapted by a water-gas shift reaction (WGS), converting carbon monoxide and steam to hydrogen and carbon dioxide in the presence of a catalyst.

$$CO + H_2O \quad \rightleftharpoons \quad CO_2 + H_2 \quad \Delta\tilde{h}_r^o = -41kJ/mol \tag{3.8}$$

The main objective of the water-gas shift process is to remove H_2 by a CO_2-selective membrane and shift the unfavorable equilibrium to produce more H_2 at high temperatures and pressures (figure 3.6). The WGS-process is normally performed at 20 bar and 400-600^oC or even up to 900^oC depending on the membrane and reactor walls.

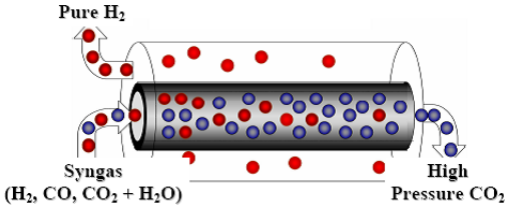

Figure 3.6: Sketch of the WGS-reactor [25]

CO_2 removal

Since the fuel catalysts effectiveness is influenced by the presence of inert CO_2, and since the concentration of CO_2 influences the reaction equilibrium and hence the product synthesis and purity, CO_2 is often removed before the synthesis to increase the efficiency by optimizing the reactants' composition. Common techniques are chemical and physical absorption, solid physical adsorption (PSA), cryogenic separation and the use of membrane systems. These processes are already widely used in fossil natural gas treatment and in carbon dioxide removal for enhanced oil recovery.

In chemical absorption aqueous solutions of ethanolamines like mono- (MEA), di- (DEA) and triethanolamines (TEA) are often used for scrubbing acidic gases like CO_2 from flue gas. The MEA acts as a weak base, neutralizing the acidic compounds to turn the molecules into ions (i.e. CO_2 into HCO_3^-) and dissolving them in the gas-scrubbing solution. This chemical absorption process is illustrated in figure 3.7 [33].

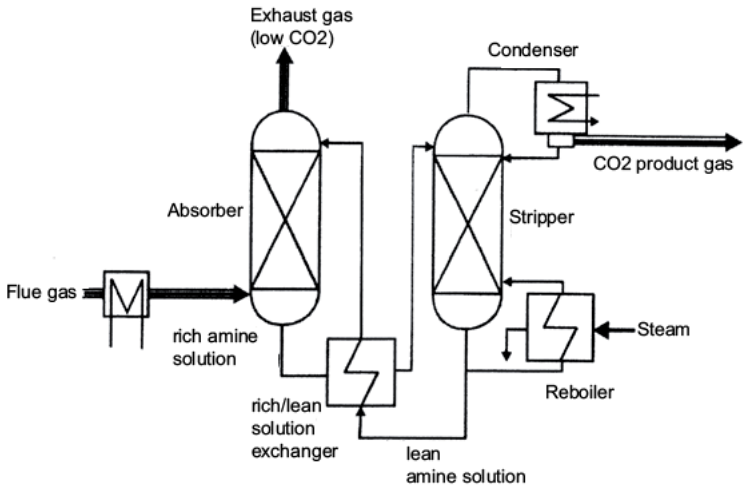

Figure 3.7: Illustration of the MEA chemical absorption process (adapted from [33])

The flue gas raises in the absorber column, while the MEA solvent trickles down in counter-current and reacts with the carbon dioxide according to the reaction eq.: 3.9:

$$CO_2 + R - NH_2 + H_2O \quad \rightleftharpoons \quad R - NH_3HCO_3 \tag{3.9}$$

After the extraction of the CO_2 from the gas stream, the saturated solution is heated and passes a stripper where the chemical bounds are broken and the acid gas is released from the solvent (120^oC). The MEA solution is recovered and reused in the absorber. A considerable amount of energy is consumed for the regeneration of the solvent, the compression of the flue gas and the pumping of the amine through the removal plant. [18, 33]

When the CO_2 content is high, the costs of removing it by the mean of these heat regenerable solvents are too high and physical absorption processes become more advantageous. Physical absorption is based on the use of anhydrous organic solvents which dissolve the acids and can be stripped by reducing the acid-gas partial pressure without the application of heat. Common commercial processes are: the Selexol (Union Cabide) and the Rectisol (Lurgi) process [29].

Contaminants removal

The producer gas produced by gasification contains contaminants; typically organic impurities such as, condensable tars (large hydrocarbons) and BTX (benzene, toluene and xylenes), inorganic impurities like H_2S, HCl, NH_3, HCN, and volatile metals, dust and soot. Before using the producer gas for other processes, it is therefore important to control the level of impurities, because they poison the catalyst and reduce the synthesis productivity. The most common mechanisms of catalyst deactivation are: sintering, carbon deposition, chemical poisoning and conversion of the active metal site into an inactive oxide site. Sulfur is an irreversible poison for cobalt and iron catalysts and to a lower extent for shift and reformer catalysts, because it can stick to active sites. Furthermore, condensing tars can foul downstream equipments, coat surfaces or enter pores in filters and sorbents. This can be avoided by removing tars by thermal cracking, catalytic cracking and scrubbing. At temperatures above 1000-1200^oC, tars are destroyed without a catalyst by addition of air or oxygen. Catalytic cracking (dolomite or Ni based) has higher thermal efficiency, however the catalysts costs are high and the technology isn't fully proven yet. Oil scrubbing can also remove tars which are subsequently stripped from the oil and reburned in the gasifier [16, 34].

The concentration of contaminants in the producer gas is influenced by the nature of the biomass feedstock and their contaminant concentration (Cl, N, S). The typical impurities in wood gasification gases and the cleanness requirements for the different synthesis processes are displayed in appendix B.5 in table B.3 [25, 35, 36].

Gas cleaning technologies

For gas cleaning, two main routes can be distinguished (figure 3.8 [25, 29]):

- 'wet' low temperature cleaning (i.e. cold gas cleaning) (figure 3.8 (top)) consisting of various successive operations: cyclones for recirculation of the bed material, gas cooling to 200^oC, bag filters to remove solid particles and partially tars, scrubbers using water, sulfuric or nitric acid as medium to remove NH_3 at $100 - 250^oC$, metals and tars, and finally ZnO guard beds for the oxidation of hydrogen sulfide. Wet gas cleaning removes particulates completely and its effectiveness is proven for coal gasification and FT synthesis applications. Optionally, a tar cracker can be introduced for removing the tar; the heat for the cracking reaction (1300^oC) being supplied by partial combustion of the fuel with pure oxygen.

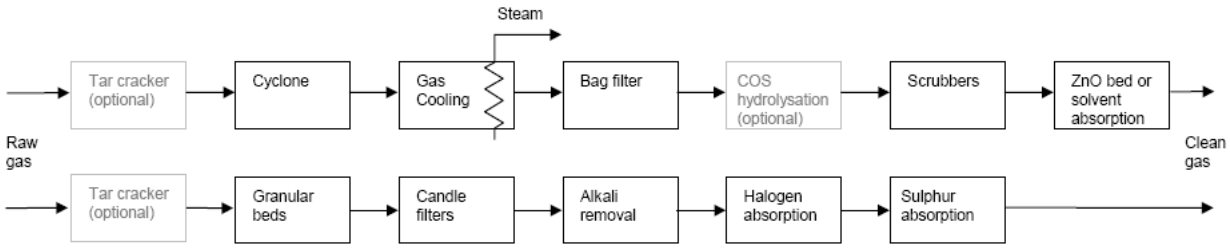

Figure 3.8: Conventional low temperature wet gas cleaning (top) and advanced high temperature dry gas cleaning (bottom) [29]

- 'dry' high temperature cleaning (i.e. hot gas cleaning) (figure 3.8 (bottom)) in which the residual contaminants are removed by using ceramic filters and reagents at 350-800^oC. Particles are removed above 400^oC by using bed filters instead of cyclones and final dust cleaning is done by ceramic candle filters. Alkalis are removed in the 750-900^oC range by passing the stream through a fixed bed of sorbents, absorbing preferentially alkalis via physical adsorption or chemisorption. Below 600^oC alkali metals condense and are removed by filters. Halogens are removed by sodium (Na) and calcium (Ca) based powdered absorbents and hot gas desulfurization is done by chemical absorption. A tar cracker can be optionally introduced or the tars can be decomposed catalytically. Many of these technologies for hot gas cleaning are still under development and not commercially available yet. Hot gas cleaning would only be of benefit, if the further process steps require high temperature or pressure.

3.3 Synthesis and Upgrading

3.3.1 Fischer-Tropsch Fuel

The original Fischer-Tropsch process discovered by Franz Fischer and Hans Tropsch in 1920, is a catalytic non-selective reaction in which syngas is converted into different hydrocarbons ranging from 1 to over 100 carbon atoms. The purpose of this process is to produce from coal, natural gas or biomass, a synthetic petroleum substitute for use as synthetic lubrication oil or as synthetic fuel, such as gasoline and diesel fuel.

In the Second World War, this process supplied Germany with fuel. Since 1955, South Africa has applied the Fischer-Tropsch synthesis (from coal derived syngas) in the SASOL plants with the objective to supply fuel and base chemicals to make the country less dependent on imported oil. Moreover, the FT process (from natural gas derived syngas) is operated commercially at Shell Malaysia [17]. Nowadays, the FT process has attracted renewed interest due to the environmental demands, since it can be regarded as an alternative to produce fuel from renewable resources when oil resources are depleted. Another advantage are the lower emissions (e.g. NO_x and particulates) from FT liquids used in internal combustion engines (compared to conventional diesel or gasoline) resulting from the absence of sulfur and the very low aromatic content. In a more futuristic scenario, CO and H_2 produced by photo-catalytic dissociation of CO_2 and water could even be regarded as feedstock for this process.

Multiple publications covering the different topics: reaction mechanism, reactor technology and overall process exist. Useful information about the FT process are regrouped in the Fischer-Tropsch Archive: [37], other references used in this work are [14, 24, 38, 39, 40, 41].

FT reactions

The FT synthesis producing hydrocarbons of different lengths can be summarized by the following simple reaction:

$$CO + 2H_2 \quad \rightarrow \quad -CH_2- + H_2O \qquad \Delta\tilde{h}_r^o = -165kJ/mol \tag{3.10}$$

where $-CH_2-$ is the methylene group which is the building block for the polymerization into longer hydrocarbons. The water can react in a side water-gas shift reaction to form CO_2 and H_2.

In general, the production of hydrocarbons in the FT synthesis can be summarized by:

$$2nH_2 + nCO \quad \rightarrow \quad C_nH_{2n} + nH_2O \tag{3.11}$$
$$(2n+1)H_2 + nCO \quad \rightarrow \quad C_nH_{2n+2} + nH_2O \tag{3.12}$$
$$nCO + 2nH_2 \quad \rightarrow \quad C_nH_{2n+1}OH + (n-1)H_2O \tag{3.13}$$

Where the first reaction represents the formation of olefins (alkenes), the second the formation of alkanes (paraffins) and the third the formation of alcohols. Depending on the nature of the catalyst and the reaction conditions, the hydrocarbons' distribution ranges from methane up to heavy waxes.

The FT synthesis reaction is expected to be a catalytic polymerization reaction, illustrated in figure 3.9 [14, 40]. The basic steps are [34]:

1. CO adsorption on the catalyst surface
2. Chain initiation by CO dissociation and subsequent hydrogenation (formation of chemisorbed methyl species)
3. Chain growth by insertion of additional CO molecules followed by hydrogenation
4. Chain termination to yield α-olefin or n-paraffin
5. Desorption of the product from the catalyst surface

The FT product selectivity is determined by the ability of the catalyst to catalyze chain propagation versus chain termination. The selectivity is influenced by different factors: either catalyst dependent ones, such as type of metal (Fe or Co), support, preparation, pre-conditioning and age of the catalyst or non-catalyst dependent ones, such as H_2/CO ratio in the feed, temperature, pressure and reactor type and size.

In a FT reactor, high catalyst selectivity towards long hydrocarbons (i.e. few methane) should be combined with a high conversion. To get a high fraction of heavy paraffins the growth probability α, expressing the chance that a hydrocarbon chain grows with another CH_2 instead of terminating, should be close to 1. High α can be reached by high pressure, low temperature and low inlet ratio H_2/CO. In fact, a lower H_2/CO ratio in the reacting gas increases the selectivity by decreasing the termination rate. The selectivity is hence related to the consumption ratio of H_2 and CO_2. For $\alpha = 0$ the H_2/CO ratio is 3 and for $\alpha = 1$ the H_2/CO ratio is 2.

α depends also largely on the catalyst nature: Fe: $\alpha = 0.65 - 0.70$; Co: $\alpha = 0.78 - 0.82$ (classical catalyst); $\alpha = 0.8 - 0.94$ (new catalyst) [42] and on the use of promoters.

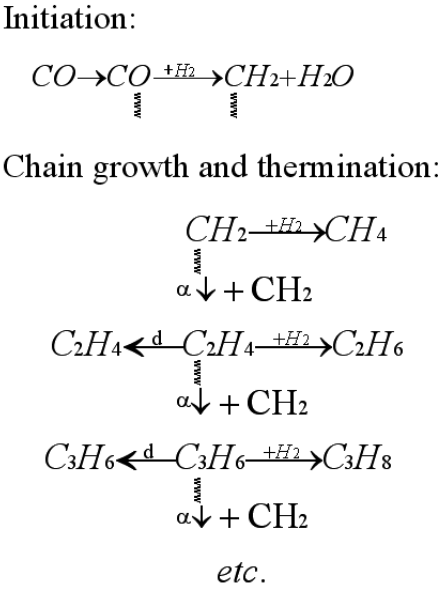

Figure 3.9: Fischer-Tropsch growth process (adapted from [40])

In general, the product distribution of the hydrocarbons having different chain lengths from C_5 to C_{20} is assumed to obey the Anderson-Schulz-Flory distribution (figure 3.10), expressed by:

$$P_n = \alpha^{n-1}(1-\alpha) \tag{3.14}$$

where P_n represents the mole fraction of hydrocarbon molecules containing n carbon atoms (i.e the n^{th} oligomer). Expressed in terms of the weight fractions W_n and in logarithmic form, the relation is given by:

$$log\frac{W_n}{n} = nlog\alpha + log\frac{(1-\alpha)^2}{\alpha} \tag{3.15}$$

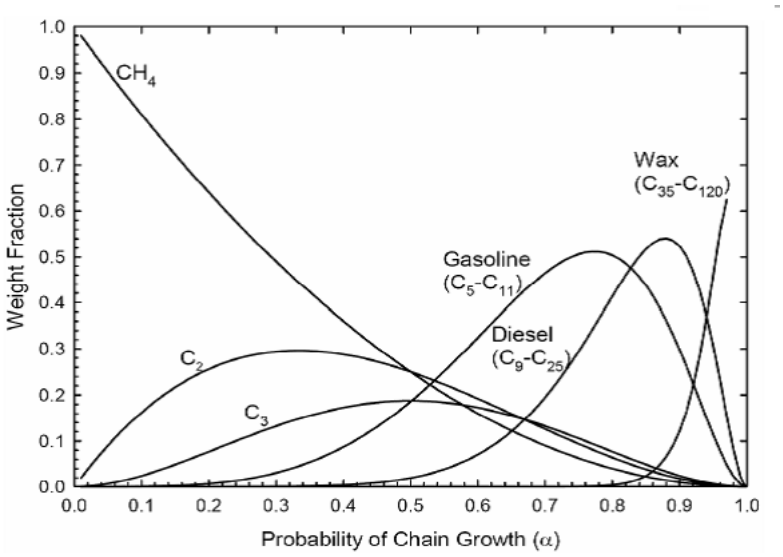

Figure 3.10: The Anderson-Schulz-Flory distribution [25]

The highest yield to diesel, the most promising FT-fuel because of its high cetane number achieved by the un-branched straight hydrocarbon chains, is attained by first making wax which is then hydrocracked into the diesel fraction. By this way shorter byproducts, especially CH_4 are minimized. For wax producing FT processes a common value of α is around 0.8-0.9 and of the molar usage ratio H_2/CO is about 2. However, the values depend on the catalyst nature, the stream composition and the process conditions. Figure 3.10 shows that in the range of high values of α, products with high molecular weight are prevalent; around $\alpha = 0.85$ diesel and gasoline fractions are predominant.

In literature, relations linking the selectivity to the process conditions and to the growth probability are found (eq.: 3.16) [16]. Qualitatively, the general tendency is that the selectivity decreases with temperature and increases with pressure.

The mass fraction of C_{5+} in the hydrocarbon product ($S_{C_{5+}}$) and the relation with α is given by [16]:

$$S_{C_{5+}} = 1.7 - 0.0024T - 0.088\frac{[H_2]}{[CO]} + 0.18([H_2] + [CO]) + 0.0078p_{total} \tag{3.16}$$

$$\alpha \approx 0.75 - 0.373\sqrt{-log(S_{C_{5+}})} + 0.25S_{C_{5+}} \tag{3.17}$$

where the concentrations are expressed as fraction of the feed gas, the temperature in K and the pressure in bar.

FT Technology

Different technologies were developed for the FT process. According to the process temperature a distinction is made between: low-temperature LTFT (T=$220 - 250^oC$ and P=25-45 bar) and high-temperature HTFT (T=$330 - 350^oC$ and P=25 bar) Fischer-Tropsch processes.

Different types of commercially applied FT reactors exist for the two alternatives (figure 3.11) [24, 34, 43]:

- Low-temperature FT reactors
  - The multitubular fixed-bed reactor (ARGE or FB) operated by SASOL and Shell. The catalyst is placed in the tubes and the syngas is passed downward through the bed and is catalytically converted to hydrocarbons.
  - The slurry bed reactor (SB) in which the syngas is bubbled through the slurry bed containing the solid phase catalyst suspended and dispersed in a high thermal capacity liquid (often FT-wax product). The syngas in contact with the catalyst is then converted to hydrocarbons. This reactor has the advantage to be simpler in construction, to be operated easily and isothermally, to have lower catalyst abrasion rates, to have a lower pressure drop and thus to lead to higher production rates and reduced operating costs.
- High-temperature FT reactors
  - The circulating fluidized-bed reactor (CFB) (Synthol reactor) in which the catalyst is circulated with the syngas through a complex system (reactor-hopper-standpipe)
  - The fixed fluidized-bed reactor (SAS (Sasol Advanced Synthol reactor)) where the syngas is bubbled through the catalyst bed where it is converted catalytically to hydrocarbons. The produced heat is removed by an internal heat exchanger immersed

in the catalyst bed. The advantage of this reactor, compared to the CFB reactor, is its simplicity, the lower operating cost due to the elimination of the catalyst maintenance, better temperature efficiency and greater product flexibility.

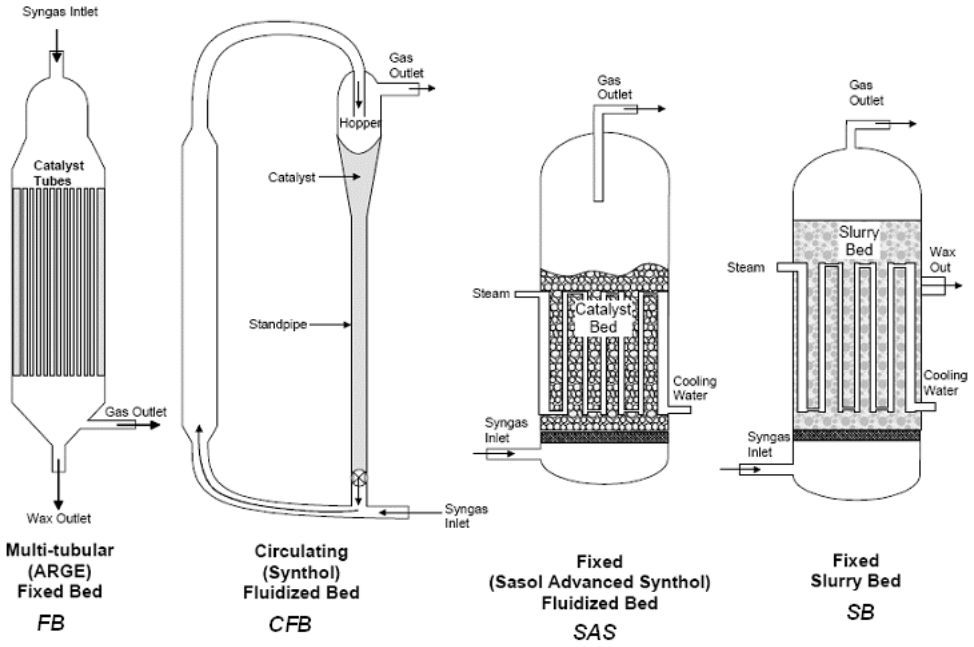

Figure 3.11: Different types of Fischer-Tropsch reactors [34]

LTFT reactors produce a large quantity of high molecular mass linear waxes and a minimum amount of methane. HTFT reactors on the other hand, produce less paraffins and more olefins, aromatic and oxygenated components.

Commonly used catalysts are based on supported iron or cobalt and to a lesser extent on nickel and ruthenium, with or without the presence of other metals as promoters. Good catalysts should have low selectivity for methane formation and high activity for water-gas shift reaction to ensure the utilization of the CO content of the feed.

Since the FT reactions are very exothermic: one mole of $-CH_2-$ generating 165kJ (e.q: 3.10), it is important to remove rapidly the heat to avoid catalyst deactivation by sintering and fouling. High rate of heat exchange is achieved by the different reactor designs described before, which all allow a good temperature control. A high heat exchange rate can be accomplished by forcing the syngas at high linear velocities through long narrow tubes packed with catalyst to achieve turbulent flow or by using a slurry reactor in which the catalyst is dispersed in the liquid product. Actually, the slurry phase reactor is the preferred choice when compared to a fixed bed reactor, because of the almost isothermal conditions achieved through the higher heat transfer coefficient on the slurry side. When high waxes are produced, fluidized beds cannot be used, due to the risk of heavy products deposition on the catalysts pellets [40, 43].

Depending on the synthesis process, the crude FT-fuel can be purified further and upgraded. Since the crude FT-fuel contains a large range of hydrocarbons, the product can be fractionated by distillation to yield the different parts which are further purified: C_1+C_2 (light gases), C_3+C_4

(LPG), naphta (C_5-C_{11}), kerosene (C_{12}-C_{18}) and waxes (C_{19+}). The hydrocarbon products in the gasoline boiling range ($50 - 180^oC$) are not directly suitable for gasoline, because straight chain structures predominate (i.e. no branching as for conventional petroleum fractions). The intermediate octane number of 55-65[1] has to be increased to meet the requirement for gasoline having an octane number of 87-95. The fraction that has a boiling point around $180 - 320^oC$ has a high cetane number (65-75) and consequently provides valuable diesel fuel with little additional refining.

In summary, the waxes produced by the LTFT process can be upgraded by hydrocracking to form diesel fuel and the olefins produced from the HTFT route can be processed by oligomerization, isomerization and hydrogenation into gasoline. These processes are similar to the one for petroleum refining [44].

3.3.2 DME

Dimethyl ether (DME), also called wood ether, is a colorless gaseous ether that can be used as refrigerant, aerosol, solvent, as well as, as fuel for applications in different sectors: residential and commercial, power generation and transportation (for example as fuel in diesel engines, petrol engines and gas turbines). Its high cetane number (55-60) makes DME a good fuel because of its efficient combustion properties and its physical properties similar to LPG (liquefied petroleum gas). Since DME can be made from natural gas, coal or biomass, it is considered as a clean-burning alternative to liquefied petroleum gas, liquefied natural gas, diesel and gasoline [45]. Moreover, it does contain any sulfur nor nitrogen and consequently, there are no SO_x emissions and lower NO_x emissions than from conventional diesel fuel during combustion. Another important environmental characteristic is, that it doesn't affect the ozone layer because of its rapid decomposition in the atmosphere (dozens of hours). This explains its use as a substitute propellant for spray cans for the ozone depleting chlorofluorocarbons being phased out [46].

DME reaction

The main reaction for the DME synthesis is the combination of two molecules of methanol to produce one DME molecule and one water molecule in an exothermic reaction.

$$2CH_3OH \rightleftharpoons CH_3OCH_3 + H_2O \qquad \Delta\tilde{h}_r^o = -23.4kJ/mol \tag{3.18}$$

Two different reaction routes are investigated by different companies. The classical two step route consisting of the formation of methanol followed by methanol dehydration proceeding according to this overall reaction (eq.: 3.21):

$$2CO + 4H_2 \rightleftharpoons 2CH_3OH \qquad \Delta\tilde{h}_r^o = -181.6kJ/mol \tag{3.19}$$
$$2CH_3OH \rightleftharpoons CH_3OCH_3 + H_2O \qquad \Delta\tilde{h}_r^o = -23.4kJ/mol \tag{3.20}$$
$$2CO + 4H_2 \rightleftharpoons CH_3OCH_3 + H_2O \qquad \Delta\tilde{h}_r^o = -205kJ/mol \tag{3.21}$$

The direct one-step synthesis (eq.: 3.25) of DME from syngas including virtually methanol synthesis, methanol dehydration and water-gas shift reaction:

$$2CO + 4H_2 \rightleftharpoons 2CH_3OH \qquad \Delta\tilde{h}_r^o = -181.6kJ/mol \tag{3.22}$$
$$2CH_3OH \rightleftharpoons CH_3OCH_3 + H_2O \qquad \Delta\tilde{h}_r^o = -23.4kJ/mol \tag{3.23}$$
$$CO + H_2O \rightleftharpoons H_2 + CO_2 \qquad \Delta\tilde{h}_r^o = -41.0kJ/mol \tag{3.24}$$
$$3CO + 3H_2 \rightleftharpoons CH_3OCH_3 + CO_2 \qquad \Delta\tilde{h}_r^o = -246kJ/mol \tag{3.25}$$

[1]The intermediate octane number is defined as the average of the research and the motor octane numbers

According to the preceding reactions the optimum H_2/CO ratio for the DME synthesis depends on the reaction pathway: 2 for the two step process and 1 for the one-step process.

Since the DME synthesis is very exothermic and since the catalyst is gradually deactivated at high temperature, it is important to remove the reaction heat and to control the temperature. Therefore, the reactor choice is crucial.

DME technology

Since the 80's, the Danish group Haldor Topsoe is involved in catalyst and technology development for the DME production. The Topsoe process occurs in two steps: first methanol synthesis in an autothermal reactor and then dehydration in an separated fixed bed reactor [47]. The first part takes place in a cooled reactor removing continuously the reaction heat and the second part being less exothermic is performed in an adiabatic fixed bed reactor.

Today direct DME synthesis technologies are developed and commercialized for the one-step production of DME in a single reactor stage. Companies exploring this route are mainly JFE Holding in Japan [48]. A general flowsheet of the DME process including the syngas production, DME synthesis and purification, as well as the potential recycling are represented in figure 3.12.

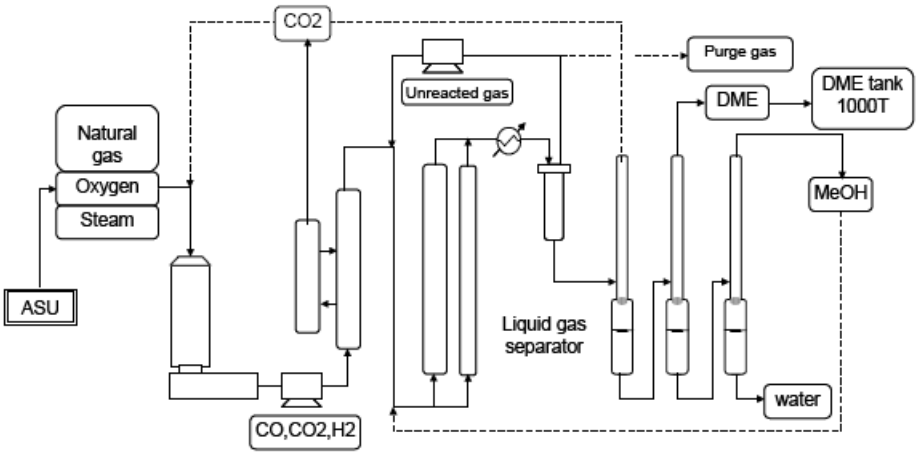

Figure 3.12: Process Flow Diagram of a DME synthesis plant located at Kushiro in the north of Japan [48]

The direct DME synthesis is performed in a slurry phase reactor (figure 3.13) in which the reactant syngas forms bubbles (T=260^oC, P=50 bar). The chemical reaction takes place when the bubbles rise through the slurry formed of solvent, often inert high-boiling-point oil, containing fine catalyst particles. This reactor avoids hot spot formation and controls the temperature of the very exothermic DME synthesis reaction through the homogeneous liquid phase mixing, homogenizing the temperature. This temperature control leading to higher conversion with longer catalyst life, is possible due to the large heat capacity and the high effective heat conductivity of the solvent [25, 45].

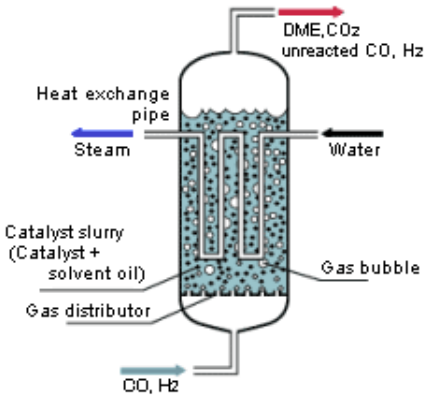

Figure 3.13: Slurry reactor for direct DME synthesis [48]

The crude DME is then separated and purified according to the demands of the product purity. Since the main impurities contained in the crude DME are methanol and water, the purification units consist primarily of different distillation steps. The DME purity reached in the JFE process is 99.8% and the international standards are 99.6% for diesel substitution.

Additional information on the technologies of the DME process are found in [46, 47, 48] and [6, 49, 50].

3.3.3 Methanol

Methanol is the simplest alcohol and is essentially used in industry as raw material to produce formaldehyde, MTBE (methyl tertiary butyl ether) and acetic acid. Methanol plays therefore an important role in the production of plastics, paints and explosives. Moreover, methanol is used as a general solvent and as fuel in internal combustion engines or in fuel cell vehicles.

The main emerging field of application for pure methanol is the use in Direct Methanol Fuel Cells (DMFC)[25] where methanol is oxidized at the anode to yield hydrogen:

$$CH_3OH + H_2O \quad \leftrightarrow \quad 3H_2 + CO_2 \tag{3.26}$$

Moreover, methanol could be efficiently transformed into $C_2 - C_{10}$ hydrocarbons via the MTG (methanol-to-gasoline) process converting methanol first into propylene followed by olefin oligomerization, product separation and hydrogenation, however the methanol-propylene step is still under development [29]. This process would yield near-zero sulfur gasoline having commercial octane ratings.

Methanol is naturally produced via the anaerobic metabolism of many varieties of bacteria and in some vegetation or synthetically through a process converting syngas into methanol.

Methanol reaction

Originally methanol was produced by the distillation of wood, therefore it is also known as wood alcohol. However, nowadays it is produced synthetically by a catalytic reaction involving hydrogen, carbon dioxide and carbon monoxide at 50-100bar and 500-550K and a catalyst $Cu/ZnO/Al_2O_3$.

The formation of methanol from syngas can be described by the following catalytic equilibrium reactions involving the conversion of carbon oxides and hydrogen:

$$CO_2 + 3H_2 \rightleftharpoons CH_3OH + H_2O \qquad \Delta\tilde{h}_r^o = -49.16kJ/mol \tag{3.27}$$

$$CO + 2H_2 \rightleftharpoons CH_3OH \qquad \Delta\tilde{h}_r^o = -90.77kJ/mol \tag{3.28}$$

Both reactions being exothermic, the yield decreases with increasing temperature. To achieve a high rate and a significant conversion, the reactions are performed at high pressure. However, the conversion is still limited by the equilibrium and therefore unconverted reactants are recovered and recycled to be economically profitable.

The combination of the syngas production reaction and the methanol synthesis yields the stoichiometry for the methanol production from syngas: $\frac{H_2-CO_2}{CO+CO_2} = 2$. Values above two indicate an excess of hydrogen and values below two a hydrogen deficiency. The ratio can be adapted by influencing the equilibrium reactions or by purging the reactants in excess from the synthesis loop and valorizing it [51, 52].

Methanol technology

The synthetic methanol production first began in 1923 at BASF's Leuna (Germany) plant with a high pressure process. Later ICI and Lurgi developed more active catalysts for higher selectivities and stability at low pressure. The low pressure process revolutionized the industry, allowing more energy-efficient and cost-effective plants. Figure 3.14 illustrates the overall ICI low-pressure methanol process, including the synthesis and separation as well as potential recycling.

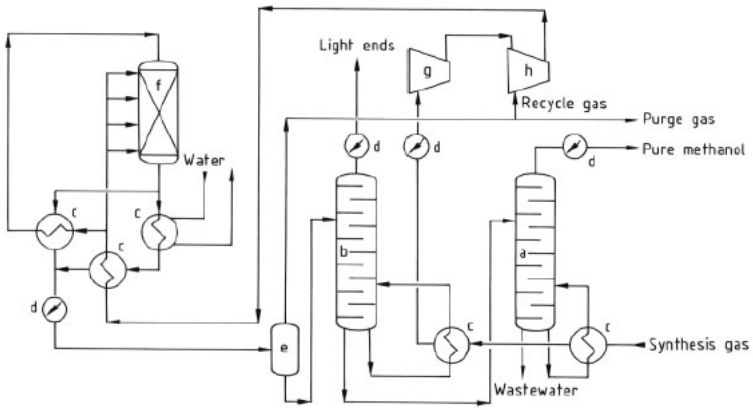

Figure 3.14: ICI low-pressure process: a) Pure methanol column, b) Light ends column, c) Heat exchanger, d) Cooler, e) Separator, f) Reactor, g) Compressor, h) Compressor recycle stage [51]

Current industrial processes for methanol production differ primarily in reactor design. Conventional reactors use fixed beds of catalyst pellets and are operated in the gas phase. Two types are predominant (figure 3.15) [25, 34, 51, 53]:

- Adiabatic reactor (ICI Process): reactor with catalytic beds (typically 3-6 beds) containing the catalyst and being operated around T=270^oC and P=50-100 bar. A portion of the mixed synthesis and recycle gas bypasses the loop interchanger, which provides the quench fractions for the intermediate catalyst beds. The temperature is controlled by quenching the synthesis reaction by adding a cooled mixture of fresh and recycled syngas between

the catalyst beds ($Cu/ZnO/Al_2O_3$). The injection of the quench gas cools the reactant mixture and adds more reactants prior to entering the next bed. Alternatively, heat exchangers can be used rather than quench gas for interbed cooling.

- Quasi-isothermal reactor (Lurgi Process): shell tube design, indirectly cooled, operating at T=230-265^oC and P=50-100 bar. The tubes containing the catalyst ($Cu/ZnO/Cr_2O_3$ + promoter) are surrounded by boiling water for heat removal. The near isothermal temperature is controlled by adjusting the water pressure and thereby the boiling temperature. The advantage of this converter is the reduced catalyst volume.

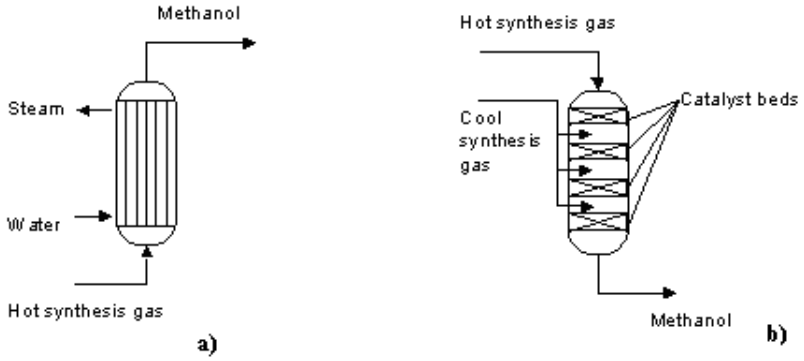

Figure 3.15: Reactors for the MeOH synthesis: a) Lurgi shell tube methanol converter (isothermal steam raising) b) ICI low pressure quench converter (adiabatic quench) [29]

Nowadays, processes under development focus on shifting the equilibrium to the product side to achieve higher conversions per pass. Examples are the gas/solid/solid trickle flow reactor and liquid phase methanol processes. For the liquid phase process, possible reactor types are: fluidized beds and slurry bubble column reactors [29].

After the synthesis, the crude methanol is separated by condensation and purified by different distillation steps. The purity requirement for methanol used as solvent is 99.85% (according to the specifications from General Services Administration for governmental purchase of methanol and ASTM D1152 [53]). As fuel, methanol can be used pure, however a better fuel seems to be 85% methanol + 15% gasoline [25].

3.4 Environmental Concerns

The processes converting biomass to fuel generate gaseous, liquid and solid effluents. According to the laws in vigor, these wastes have to be treated before being released in the environment. By recycling part of the streams and by reusing the offgases of one process for another one, the emissions as well as the energy losses can be reduced. According to the concept of industrial ecology, this integration shouldn't only be restrained to the process or the plant itself, instead cooperations/synergies between industries should be investigated. However, it is still impossible, to reuse and valorize everything. Therefore some equipments for the waste treatment have to be integrated in the plant design technologies. The waste management or pollution control usually represents an important contribution to the production costs [14].

3.4.1 Atmospheric Pollutants

The offgases of the process can't be released in the atmosphere due to environmental concerns. If no recycling is possible, the stream can be combusted to exploit the remaining energy potential. Atmospheric pollutants arise from burning coal, from fuel gases gasification, and from fuel refining. The combustion-generated pollutants from the steam and utility plant are particulates, sulfur dioxide, nitrogen oxides and volatile organic compounds. Common technologies for controlling the pollution created from the combustion are flue gas desulfurization units, electrostatic precipitators and bag houses for removing sulfur dioxide and particulates. In the refinery and natural gas industry hydrogen sulfide is removed by the Claus process converting it into residual sulfur being removed by the Shell Claus offgas treating process. Compared to processes based on fossil resources, the biofuel producing processes emit less air pollutants.

3.4.2 Aqueous Effluents

Wastewater mainly arises from steam plant blowdowns, gasification wash waters, Fischer-Tropsch wastewater and wastewater from the distillations of the MeOH and DME upgrading. The gasification wastewater can contain dissolved acid gas, organic acids, tar components, phenols and traces of ammonia. When the phenol and ammonia are removed by special processes, for example by solvent extraction or adsorption, the wastewater can be treated biologically by activated sludge. Once the alcohols and other oxygen compounds have been removed, the wastewater can undergo activated sludge biotreatment. After the treatment, the water can be discharged or be reused as cooling water.

3.4.3 Solid Wastes

Solid wastes include gasification residues such as ash, slag and char, wastes generated by steam plant wastes (ash and flue-gas desulfurization residues), biosludges from wastewater treatment, salts from blowdowns and spent catalysts.

The quantity of these wastes depends largely on the characteristics of the feed and the gasification process as mentioned in chapter 3.2 (gas cleaning). The wastes from the coal gasification (ashes, slags) and boiler plants are considered as nonhazardous by the RCRA (Resource Conservation and Recovery Act) and can be simply disposed of in nonhazardous landfills or settling lagoons. The sludge from the wastewater treatment is generally incinerated and active carbon regenerated. The inorganic salts from cooling tower blowdowns are hazardous and have to be disposed in lined landfills.

The fixed-bed gasification system represents the worst-case environmental scenario because it produces tars, oils, phenols and large quantities of wastewaters. However, for advanced entrained flow gasification systems the pollution control is greatly simplified. In fact, the Shell system produces mainly carbon monoxide and hydrogen without tars, oils or phenols.

Chapter 4

Process Modeling

For each process step, some representative technological alternatives have been considered in the modeling. The different process options including upstream and downstream transformations are summarized in figures 4.1 and 4.2.

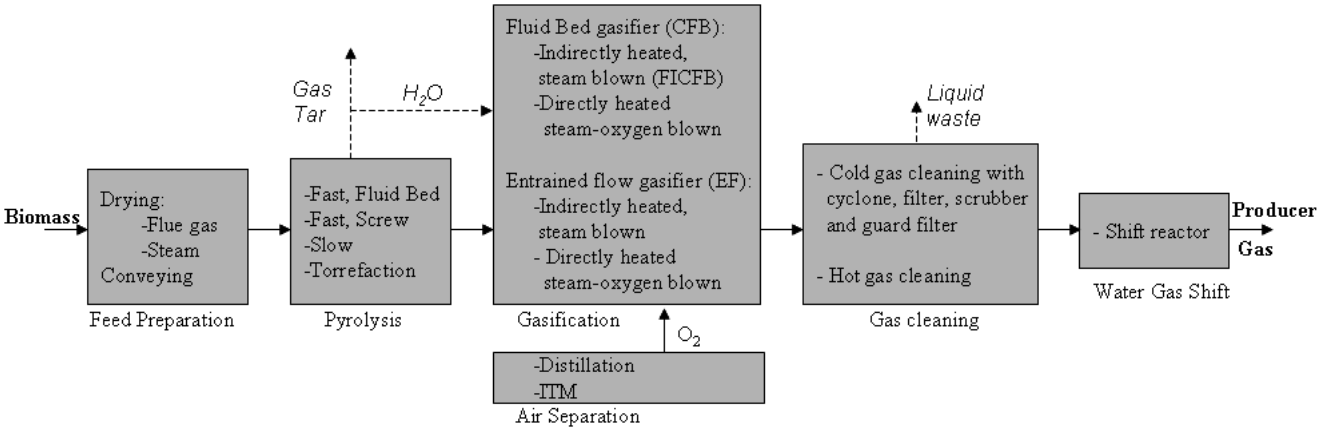

Figure 4.1: Process options for the producer gas synthesis (upstream processing)

The general approach applied to model the different sections is outlined here, while the details and numerical values are reported in appendix B. Parts of the models for the syngas production are adopted from the one developed in [5, 54] and for the DME production from [6]. The other units are modeled based on data from literature.

For the modeling, the choice of the appropriate thermodynamic model is crucial to simulate the exact liquid and vapor phase behavior and the corresponding properties of the compounds. The details of the thermodynamic models are reported in appendix A.

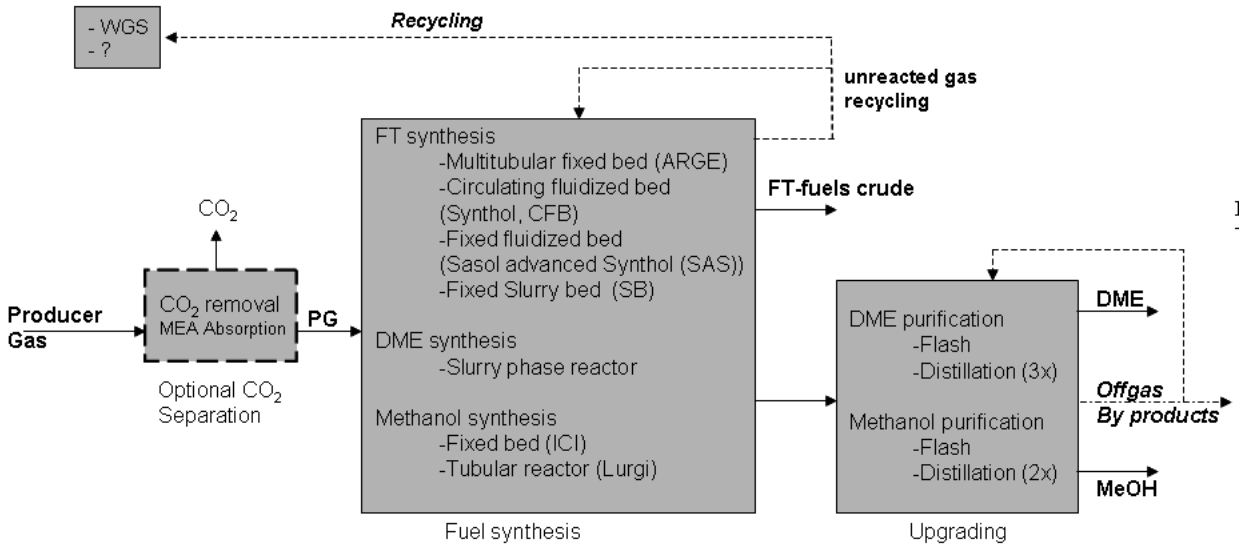

Figure 4.2: Process options for the fuel synthesis and upgrading

4.1 Initial Conditions

For the different biomass conversion processes wood is used as feedstock. The inlet wood humidity is expected to be $\Phi_w = 50\%$ and the composition, expressed as weight fraction of dry biomass, is given by the values in table 4.1 [5, 55]:

Compound	$wt\%$
C	51.09
H	5.75
O	42.97
N	0.19

Table 4.1: Characteristics of woody biomass [55]

4.2 Producer Gas Production

4.2.1 Drying

The drying section is not modeled in detail and is based on the assumptions reported in [54]. To provide a conservative estimate, it is assumed that the latent heat of vaporization corresponding to an initial moisture content of 50% needs to be supplied at 120^oC.

Two options are considered: flue gas drying and steam drying. Drying takes place at ambient pressure and the drying medium's temperature is fixed in each case at 200^oC. Key factors for modeling this process are the humidity Φ, as well as the mass and heat transfer coefficient as explained in [54].

4.2.2 Pyrolysis

For the pyrolysis four options can be considered: fast pyrolysis in a fluidized bed or a screw reactor, slow pyrolysis and torrefaction. Only the torrefaction option is modeled in this work.

The torrefaction is designed based on data from [56]. The process temperature is set to 260^oC and the wood humidity to 25%. As exact kinetics modeling is very complex (eq: 3.1), the outlet composition is determined based on the atomic balances. The solid conversion is fixed by the following relations based on the relative mass flow rates for a fixed temperature:

$$\frac{\dot{m_{i,out}}}{\dot{m_{,in}}} = cste \tag{4.1}$$

$$\Leftrightarrow \frac{x_{i,out}}{x_{i,in}} \cdot \frac{\dot{m_{tot,out}}}{\dot{m_{tot,in}}} = cste \tag{4.2}$$

where i corresponds to the species: H, C and O and x represents the weight fraction and $\dot{m}$ the mass flow rate.

The gas phase composition is specified in terms of the elementary composition (H and O) expressed by the fraction of hydrogen in methane over the gasified hydrogen, respectively the fraction of oxygen in carbon monoxide over the gasified oxygen:

$$\frac{\text{H in } CH_4}{\text{gasified H}} = cste \tag{4.3}$$

$$\frac{\text{O in CO}}{\text{gasified O}} = cste \tag{4.4}$$

In a first attempt, external heating was considered to reach the torrefaction temperature, however according to the information on the available equipments (Wyssmont's Turbo-Dryer®, [22]) internal heating is more accurate. For modeling the internal heating, one part of the vapor phase is recycled to be used as fuel for the heating and a pressure drop of 0.1 bar inducing a power consumption of 190kW for an inlet biomass mass flow of 1kg/s is introduced (appendix B, figure B.1). The liquid phase stream is sent to the gasification and the dried torrified gas can be combusted.

4.2.3 Gasification

The modeling of the different gasification options is based on the choice of the gasifier type. In this work entrained flow reactors or fluidized bed reactors either directly or indirectly heated are considered. However, as only few information on the technology and the industrial applications of entrained flow gasification are found and as the fluidized bed gasifiers seems to be the most suitable for large-scale syngas production from biomass (chapter 3.2.2), different options around this type of gasifier (indirect (FICFB) or direct (CFB)) are essentially considered.

Modeling the kinetics of this process to predict the exact outlet composition is far too complex for flowsheet calculations, therefore different simplified approaches are adopted.

Fluidized Bed Gasifier

The fluidized bed gasifiers (FICFB and CFB) performance is generally modeled based on equilibrium relationships. However, as kinetics modeling is complex and depends on the reactor design, artificial temperature differences to the actual gasification temperature are introduced

in the equilibrium relationships as mentioned in [5, 54]. This approach allows to obtain correct gas compositions and energy balances, as well as representative temperature and pressure dependencies around the nominal operating point.

The outlet stream composition (H_2, CO, CO_2, CH_4, C_2H_4, H_2O, N_2 and $C_{(s)}$) is specified by the atomic balances of C, H, O and N and by four additional equations: the corrected equilibrium relationships of the hydrogenating gasification (eq.: 4.5) and the water-gas-shift reaction (eq.: 4.6, the relation between the partial pressure of C_2H_4 and CH_4 (k_p) (eq.: 4.7) and the constant carbon conversion efficiency ϵ_{cc} determining the amount of solid carbon reformed in the gas phase (eq.: 4.8).

$$C(s) + 2H_2 \rightleftharpoons CH_4 \quad \Delta T_1 \tag{4.5}$$

$$CO + H_2O \rightleftharpoons CO_2 + H_2 \quad \Delta T_2 \tag{4.6}$$

$$p_{C2H4} = k_p \cdot p_{CH4} \quad k_p \tag{4.7}$$

$$\dot{m}_{rc} = (1 - \epsilon_{cc})\dot{m}_c \quad \epsilon_{cc} \tag{4.8}$$

A detailed description of the modeling of the indirectly heated fluidized bed gasifier (FICFB) and the directly heated fluidized bed gasifier (CFB Lurgi) is found in [5, 54]. The important modeling parameters are summarized in appendix B.3 in table B.2.

The flowsheet of a fluidized bed gasification either indirectly (f_2_315 off) or directly heated (qr_2_301 off) is represented in figure 4.3.

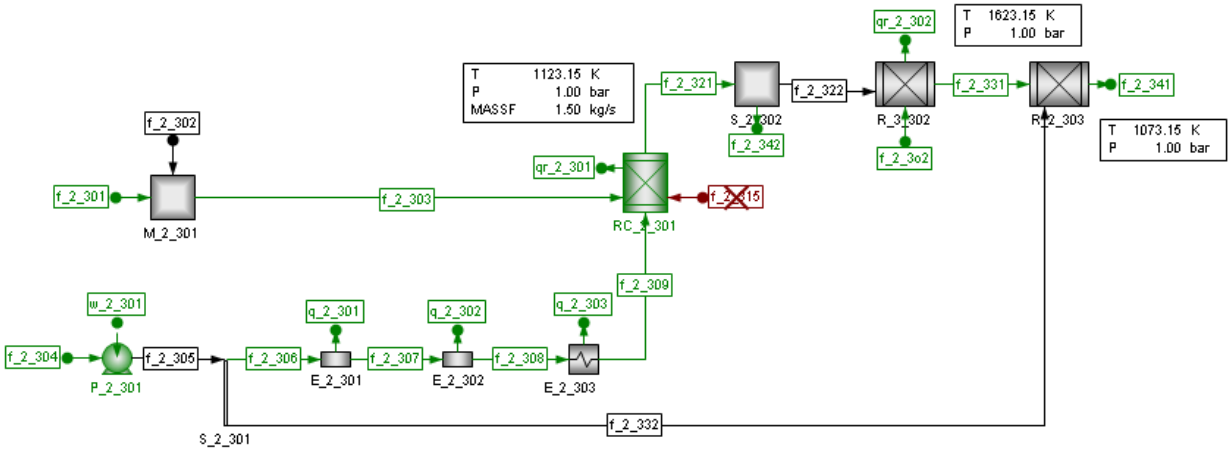

Figure 4.3: Flowsheet for the fluidized bed gasification

The first reactor (Rc_2_301) models the gasification reaction itself at T=850^oC, while the second one (R_3_302) represents a high temperature stage (T=1350^oC), improving the conversion of the synthesis reaction by steam methane reforming and water-gas shift reactions and the third one (Rc_2_303) represents a water quencher, cooling the producer gas down to T=800^oC. Because of the high temperature in the quencher a water-gas shift reaction takes place. The amount of H_2O that reacts in the WGS reaction is fixed to 20%. The separator (S_2_302) after the gasification reactor models the separation of the solid residues (char).

Entrained flow Gasifier

The entrained flow gasifiers is designed based on equilibrium considerations and atomic balances. The reactions are expected to be at equilibrium and the ratios of steam and oxygen (only for directly heated gasification) to biomass are fixed.

$$\frac{\dot{m_{H_2O}}}{\dot{m_{BM}}} = cste \tag{4.9}$$

$$\frac{\dot{m_{O_2}}}{\dot{m_{BM}}} = cste \tag{4.10}$$

The corresponding values are given in appendix B.3 in table B.2.

The flowsheet of a indirectly heated entrained flow gasification is represented in figure 4.4.

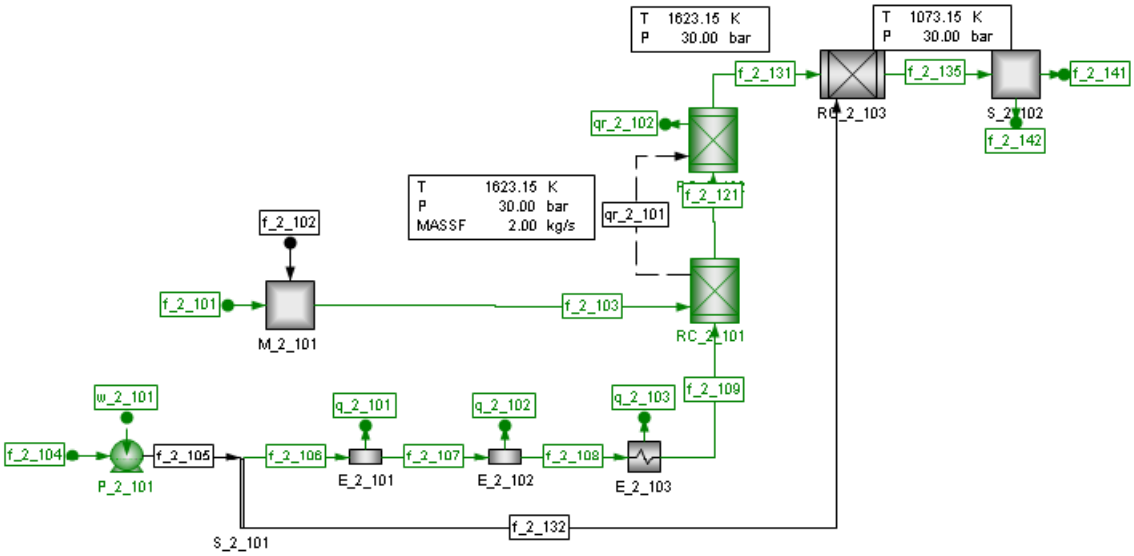

Figure 4.4: Flowsheet for the indirectly heated entrained flow gasification

The first and the second reactor (Rc_2_101 & Rc_2_102) model the gasification reaction, taking place at T=1350^oC. The second reactor increases the conversion. Again, the third reactor (Rc_2_103) is a quencher, cooling the producer gas down to T=800^oC and the H_2O conversion is fixed at 20%. A separator (S_2_102) is also introduced to remove the char.

Summary of the gasifier modeling options

The different parameters fixed to model the base cases of the indirectly and directly heated entrained flow and fluidized bed gasification are summarized in appendix B.3 (table B.2). In addition to these four base-cases, some other options are added after preliminary results, to increase the process efficiency, especially with fluidized bed gasification. The different alternatives are the indirect and direct heating of the high temperature stage, the absence of the high temperature stage reforming and the quencher, or the reforming at lower temperature in absence of the quencher (figure 4.3: R_2_303 & S_2_303). These options are modeled in the same way as the corresponding base-case (FICFB or CFB) operated at atmospheric pressure. To summarize, the following options are considered for the gasification; the abbreviations used for each technology choice being indicated in brackets:

1. steam blown, indirectly heated entrained flow (EF) gasifier with quencher [gas1]
2. oxygen-steam blown, directly heated entrained flow gasifier with quencher [gas2]
3. steam blown, indirectly heated fluidized bed (FICFB) gasifier with HT stage (directly or indirectly heated) and quencher [gas3direct/gas3indirect]
4. oxygen-steam blown, directly heated fluidized bed (CFB) gasifier with HT stage (directly or indirectly heated) and quencher [gas4direct/gas4indirect]
5. directly or indirectly heated fluidized bed gasifier with steam methane reforming at lower temperature (directly or indirectly heated) and without quencher [gas5dind (directly heated gasifier, indirectly heated reformer)]
6. directly or indirectly heated fluidized bed gasifier without steam methane reforming (no HT-stage) and without quencher [gas6direct/gas6indirect]

4.2.4 Steam Methane Reforming

The high temperature stage or the reforming at lower temperature performed optionally after the gasification, are modeled by considering a reactor taking into account the atomic and the energy balance. All the reactions taking place in the reactor are considered to be at equilibrium and specified by the corresponding equations. The reactions being taken into account, are the steam methane reforming reaction (eq.: 3.6), the water-gas shift reaction (eq.: 3.5) and the ethene reaction (eq.: 4.11).

$$\text{Ethene equilibrium}: \quad 2C + 2H_2 \rightleftharpoons C_2H_4 \tag{4.11}$$

The reactions are operated at the same pressure as the gasification. The optimal value of the reforming temperature and pressure is defined by the producer gas composition required for the synthesis reaction.

4.2.5 Air Separation

The oxygen used as medium in the directly heated gasification and/or reforming options is obtained by air separation through ion transfer membranes.

In this work air separation by ion transfer membranes isn't modeled in detail. However, a simplified model (appendix B.4, figure B.2) contains a compressor, an heat exchanger, a separator (representing the membrane) and a turbine. The problem consists in modeling accurately the pressure difference that is the driving force of the separation. It is accounted for the heat demand and the power consumption in the energy integration and for the costs in the economic analysis. In literature [30], a value in the order of 150kWh/ton O_2 corresponding to 530kW for an output of 1kg O_2/s is given for the total specific power consumption. With the simplified model and this flow of 1kg O_2/s, the compression power is 4'726.5kW, while the turbine's power is 4'196.97kW. This power relation allows to adapt the values for other flow rates and hence to calculate the corresponding costs.

4.2.6 Gas Cleaning

For gas cleaning two options are considered: cold and hot gas cleaning. Since wood is used as feedstock the amount of impurities is quite low. The modeling isn't done in detail, nevertheless the main steps, as well as the heat exchangers are considered. The costs of the different equipments are also included in the economic analysis.

Cold Gas cleaning

The cold gas cleaning model contains different units. First an heat exchanger reduces the gasifier outlet stream temperature to 150^oC, then two artificial units are introduced to model a filter with the associated pressure drop and heat losses. The stream is then flashed to remove the gaseous phase, containing the syngas, from the water being collected and removed from the process. The syngas is further treated in a compressor (isentropic efficiency 0.8) and heat exchanger to meet the operating conditions for the subsequent processes (i.e. 400^oC and 25 bar). The power used for the compression is accounted for in the power of the synthesis unit, because the pressure is increased to approach the synthesis pressure. The flowsheet and the different modeling parameters are given in appendix B.5.

Hot Gas cleaning

The hot gas cleaning is represented simply by a heat exchanger that models the cooling of the gasifier outlet flow from T=800^oC to T=400^oC. Since it is operated at the gasification pressure and a compressor is introduced before the synthesis reactor to reach the required synthesis pressure.

Water-gas shift

The water-gas shift reactor is introduced to adapt the H_2/CO ratio to the needs of the further processes. It is modeled by mixing, at T=400^oC, the producer gas coming out from the cleaning units with steam. The mass flow rate of the incoming water is chosen so that the equilibrium can be shifted to reach the desired ratio and that the remaining amount of unreacted water is small. The reactor is modeled by considering the water-gas shift reaction at equilibrium $\Delta T = 0^oC$ and by fixing the H_2/CO ratio. A heat exchanger is introduced after the reactor, to adapt the temperature to the value required for the chosen synthesis reaction.

CO_2 removal

Before the synthesis the option of CO_2 removal is considered to increase the conversion efficiency by meeting the optimal synthesis conditions. The CO_2 removal isn't modeled in detail in this work. It is modeled simply as a black box, removing part of the CO_2, as pure CO_2, according to the specified conditions. For the energy integration and the economic analysis, the values for the energy consumption for the CO_2 removal are taken from [57]. For the MEA absorption unit, the numerical values given for a 95% CO_2 separation efficiency are: thermal load: 3.7MJ/kg CO_2 (steam at 150^oC with a temperature of 110^oC in the condenser of the regeneration column) and electric power: 1.0MJ/kg CO_2.

4.3 Synthesis and Upgrading

Three different options for the synthesis of biofuels from producer gas are investigated, namely Fischer-Tropsch fuel, DME and MeOH. The operating conditions for the three different synthesis options are summarized in appendix B.10.

4.3.1 FT-Fuel

To model the FT synthesis, only the formation of olefins and paraffins is considered. The distribution between olefinic and paraffinic compounds is adjusted by the fraction of olefins in the different hydrocarbons ranges. The distribution of the hydrocarbons depends on the process operating conditions and on the reactor type. Fluidized bed technology (Sasol Advanced Synthol (SAS) fluidized bed) and cobalt-catalysis are considered for the base-case. The parameters for the growth probability and the fraction of olefins in the different hydrocarbon ranges are adjusted from data from [14, 42] (appendix B.6, table B.5). The value of the growth probability α is adjusted from the reported data. Figure 4.5 illustrates the difference between the reported distribution of hydrocarbons and the values calculated with the reconciliated α.

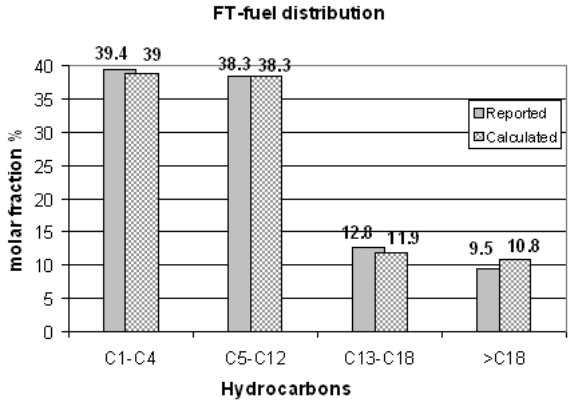

Figure 4.5: Illustration of the reported and calculated FT distribution

Since some hydrocarbons do not exist in the Belsim Vali database (i.e. C_{17}), an equal distribution between the hydrocarbons containing one carbon more and one carbon less than the missing compound is assumed for the modeling.

The process operating conditions are: FT reaction temperature 340^oC and pressure 25 bar. In a first attempt the CO-conversion defining the productivity (eq.: 3.10) is fixed at 85% [14]. In literature, values ranging from 70 to 90% CO-conversion are found for one-pass processes [16]. Different sensitivity analysis (studied in section 7.3.1) show the impact of this parameter on the efficiency.

The flowsheet of the FT synthesis unit is represented in figure 4.6.

The process is modeled by four reactors in parallel, since each reactor can only account for a restraint number of reactions. Because of the high amount of compounds that are synthesized, each reactor produces only one range of hydrocarbons: $C_1 - C_4$, $C_5 - C_{12}$, $C_{13} - C_{18}$ or higher

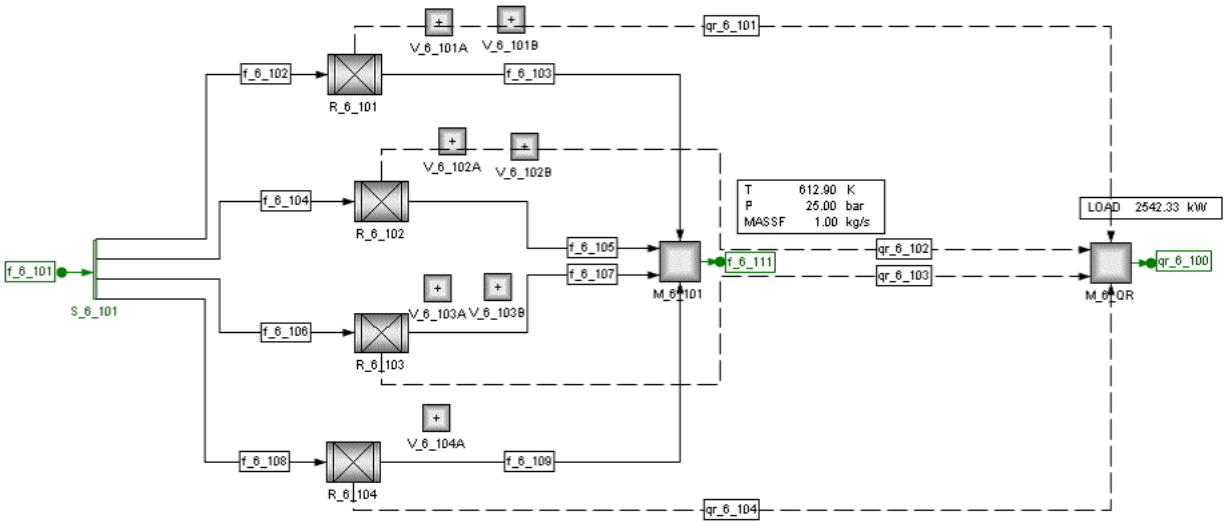

Figure 4.6: Flowsheet for the Fischer-Tropsch synthesis

hydrocarbons $> C_{18}$. The split of the inlet stream (S_6_101) is defined in such a way that the fixed carbon conversion is reached in every reactor and that the CO molar flow rate at the outlet of every reactor is the same.

FT upgrading

Upgrading of crude FT-fuels usually consists in a combination of hydrotreating, hydrocracking, hydroisomerization in addition to product separation.

In this work it is focused only on the crude FT-fuel production; consequently the purification of the different fractions by distillation isn't investigated. Only a flash drum removing part of the unreacted gases followed by a separator removing part of the water are introduced to recover the crude FT-fuel.

4.3.2 DME

The DME synthesis is modeled based on the one-step process developed by the JFE Corporation [48]. The process temperature is 277^oC and the pressure 50 bar. Some parts of the model are adapted and ameliorated from the one developed in [6].

DME synthesis

The flowsheet of the DME synthesis process is presented in figure 4.7.

Before entering the DME synthesis reactor (R_6_301), the producer gas has to be treated to meet the best conditions for the DME synthesis. Therefore, CO_2 has to be removed and the gas has to be compressed (compressor efficiency 0.8). CO_2 removal by scrubbing with MEA is modeled as artificial black box (B_6_301), removing one part of the CO_2 to reach a high DME productivty.

The kinetics of the DME synthesis are modeled by the following reaction scheme:

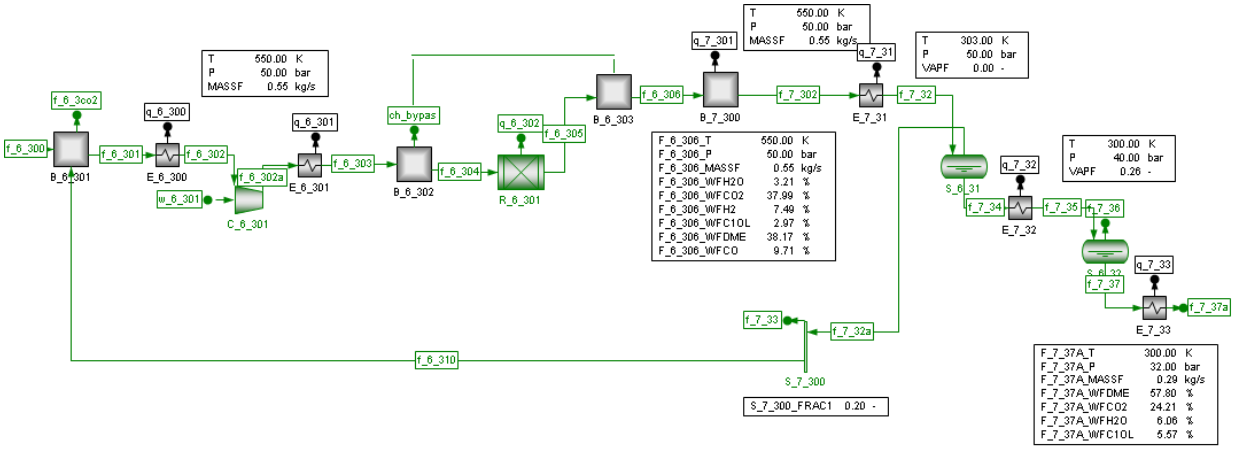

Figure 4.7: Flowsheet for the DME synthesis

Water-gas shift reaction ($\Delta\tilde{h}_r^o = -41.2kJ/mol$)

$$CO + H_2O \quad \rightleftharpoons \quad CO_2 + H_2 \tag{4.12}$$

Methanol synthesis from syngas ($\Delta\tilde{h}_r^o = -90.2kJ/mol$)

$$CO + 2H_2 \quad \rightleftharpoons \quad CH_3OH \tag{4.13}$$

Methanol dehydration ($\Delta\tilde{h}_r^o = -24.5kJ/mol$)

$$2CH_3OH \quad \rightleftharpoons \quad CH_3OCH_3 + H_2O \tag{4.14}$$

All these reactions are favored at moderate temperature since they are exothermic.

To optimize the production, the H_2/CO ratio should be close to 1, in accordance with the stoichiometry of the overall one-step reaction (vs. 2 for the two step process). After the gasification section the ratio is around 1.5 and has hence to be decreased by reverse WGS (section 7.2).

The methanol dehydration reaction (eq.: 4.14) is modeled as equilibrium reaction. An artificial temperature difference ΔT is introduced to take into account the deviation from equilibrium. The ΔT value was determined from Belsim Vali by preliminary flowsheet calculations based on a deviation of 95% from equilibrium conversion. First the equilibrium conversion was determined by setting ΔT to zero, then the conversion is fixed at 95% of the value of the equilibrium conversion and the temperature difference from equilibrium is computed. A value of $\Delta T = 43^oC$ was obtained for the methanol dehydration reaction at 277^oC and 50bar.

The water-gas shift reaction (eq.: 4.12) is expected to be at equilibrium: $\Delta T = 0^oC$.

In contrast, the methanol reaction (eq.: 4.13) is considered as a conversion reaction in Belsim Vali and the reaction extent is specified with a relation setting the ratio between the extent of equations 4.14 and 4.13 to 47%.

Moreover, the assumption is made that methane and ethylene have an inert behavior towards the catalyst (ACZ and HZSM-5)[6]. Therefore, an artificial splitter (B_6_302) is introduced to allow these substances to bypass the reactor. At the reactor outlet they are simply added to the product through an artificial mixer.

Since the amount of unreacted gas released at the reactor outlet is important, the efficiency can be increased by recycling part of these gases towards the reactor. Therefore, a flash drum (S_6_31) is introduced to remove part of the gases from the product stream. The gases are then sent to the CO_2 removal unit. By this way the optimal ratio and amount of CO_2 isn't influenced by the recycling.

DME upgrading

After the synthesis, the part of DME in the product is only around 20-40%wt. This purity depends on the process configuration (i.e recycling, stoichiometric ratio, etc.). To obtain high purity DME, the unreacted gas is first separated consecutively by two flash drums (figure 4.7). The temperature and pressure of the flash drums are chosen in such a manner to remove most of the light gases without loosing too much product, as it is explained in detail in appendix B.9. The offgas could be recycled or combusted. After the separation of the offgas, the DME purity in the liquid stream is around 45-65%wt.

The purity is then further increased by three distillation steps (figure 4.8), removing the light gases, methanol and water. The first distillation column removes essentially CO_2 and other light gases. Clean DME comes out of the top of a second distillation column (99.87%wt). The remaining water-methanol mixture is separated in a third column. Methanol with a purity around 97%wt is recovered in the distillate and nearly pure water (99.9%wt) is released at the bottom. Both streams could be used for different applications after some treatements. During the whole purification process, some DME is entrained in the offgas streams and hence there are some losses of the product, decreasing the efficiency.

The modeling of the DME upgrading is based on the purity requirement of 99.8% DME [48].

The characteristics of the distillations, such as number of stages, feed stage, reflux, etc., are determined by the following procedure. First, Belsim simulations units (SIMU) were used to make a good model on the basis of the targeted purities. With these results a simplified model is set up as VALI PFD, by specifying the inlet temperature and pressure, as well as the bottom stream (composition and % of inlet mass flow). This transformation is required, as only these units can be used in the energy integration model. A detailed description of the methodology used to model the distillations and to determine the characteristics, such as number of plates, feed plate and reflux is reported in appendix B.8.1. The numerical values of the DME purification characteristics are presented in appendix B.8.2.

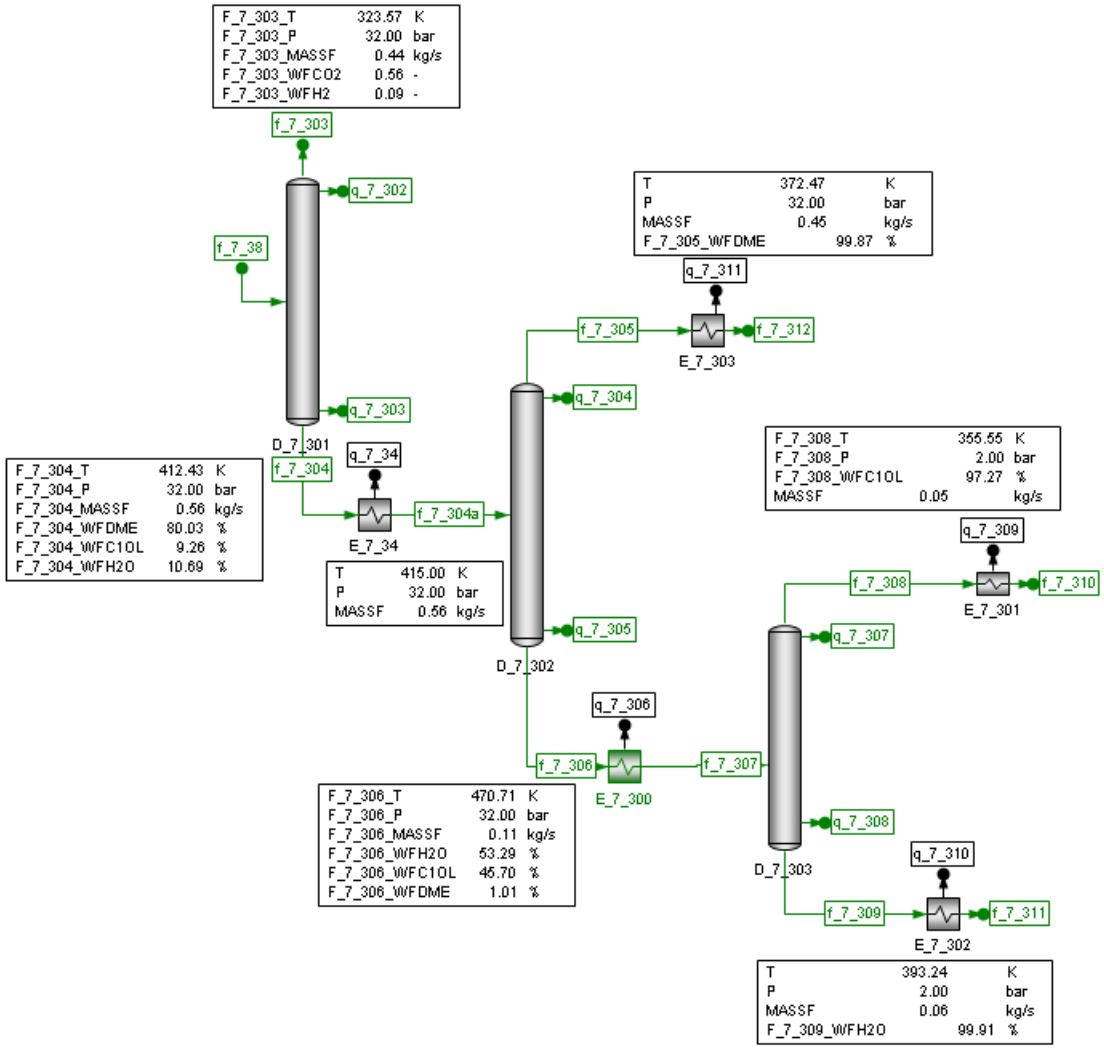

Figure 4.8: Flowsheet for the DME upgrading

4.3.3 Methanol

The modeling of the methanol synthesis and upgrading is done based on the data from [51, 52, 58].

Methanol synthesis

The different steps of the MeOH synthesis are shown in figure 4.9.

First the producer gas (F_6_200) is pre-treated to meet the reaction conditions (P=85bar and T=260^oC) and in the reactor methanol is produced. The product flow (F_6_218) containing methanol, by-products and unreacted gas is then introduced into a flash (S_6_202) to remove the gas from the liquid product. One part of the gas (90%) is recycled (F_6_225) after being compressed and cooled to the synthesis conditions. The other part has to be treated before being released in the atmosphere and can be used as combustible.

As explained in [52, 59], the reactor being a multistage reactor (4 beds) is modeled as four reactors in series. The syngas is divided into four parts (60/12/14/14%), the first part is

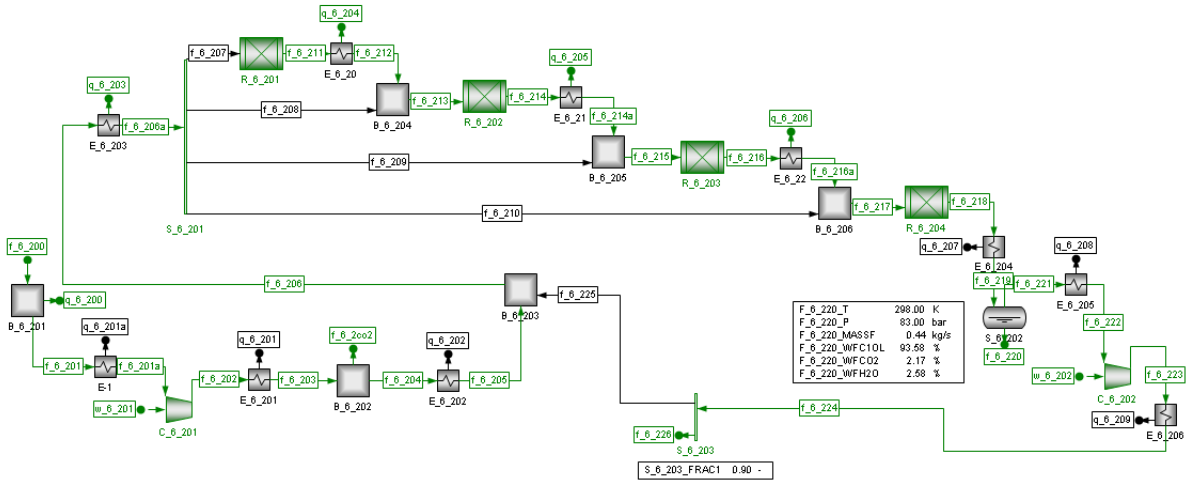

Figure 4.9: Flowsheet for the methanol synthesis

heated up and feeds the first reactor (R_6_201). The outlet stream, being hotter because of the exothermic reaction, is then mixed with the second part of the feed (being colder) cooling it down. The stream (f_6_213) is then fed to the second reactor (R_6_202) and the whole procedure is repeated for the next stage. This procedure allows to cool the outlet stream and to preheat the feed for the next reactor. Consequently, the energy integration is improved. The process pressure is 85 bar and the four beds are characterized by the relative flow rate and the inlet and outlet temperatures (appendix B.7, table B.6)

The reactor is modeled based on the kinetics of the following reaction scheme; involving the reverse water-gas shift reaction and the methanol synthesis from syngas:

$$CO_2 + H_2 \rightleftharpoons CO + H_2O \tag{4.15}$$
$$CO_2 + 3H_2 \rightleftharpoons CH_3OH + H_2O \tag{4.16}$$

and the by-products (DME and ethanol) formation:

$$2CH_3OH \rightleftharpoons CH_3OCH_3 + H_2O \tag{4.17}$$
$$2CH_3OH \rightleftharpoons C_2H_5OH + H_2O \tag{4.18}$$

The modeling follows the same approach as explained for the DME reactor, the water-gas shift reaction is expected to be at equilibrium: $\Delta T = 0^oC$ and for the methanol production the value of $\Delta T = 3.6^oC$ was determined.

For the byproducts formation the reaction type used in Belsim Vali is conversion and the reaction extent is specified by the selectivity. The data are fitted from [58, 59] and the selectivity determined for ethanol and DME production is 0.8%.

The optimal stoichiometric synthesis ratio is defined as $\frac{H_2 - CO_2}{CO + CO_2}$ and should be around 2 or slightly above. However after the gasification and cleaning the ratio is lower. To reach the targeted ratio, CO_2 is removed before the synthesis reactor.

Methanol upgrading

After the synthesis the methanol purity is, depending on the process configuration, around 90-96%wt. To increase the purity some purification steps are required. Since the product stream contains still a lot of gases (CO, CO_2, H_2), it is first flashed at a temperature of 25^oC and a pressure of 8 bar. A first distillation separates DME and light gases from water, methanol and ethanol. From a second distillation nearly pure methanol (99.9%wt) comes off as distillate and the bottom fraction is wastewater containing the heavier components (H_2O, EtOH) and residues of MeOH. The purity of water depends on the producer gas composition. The characteristics of the distillation columns are determined by the same methodology as for DME purification and reported in appendix B.8.2 (table B.10). The corresponding flowsheet of the methanol purification section is illustrated in appendix B.8.2 in figure B.6.

Figure 4.10 displays the composition profile of the liquid phase stream through the second distillation column for every plate for an optimal separation in the MeOH purification. MeOH is the light compound and prevalent in the distillate, while the bottom fraction contains the heavy compounds, water and ethanol. The purity of bottom fraction depends on the separation quality.

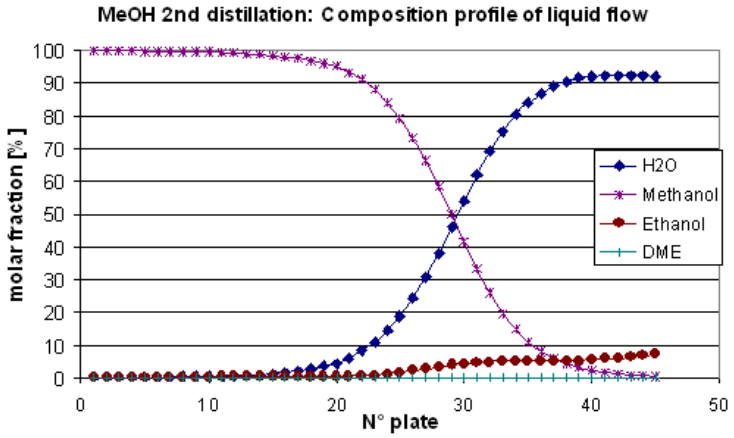

Figure 4.10: Composition profile of the liquid phase stream through the second distillation column of the MeOH purification section, yielding pure MeOH

Chapter 5

Energy Integration

5.1 Energy Integration Concept

Energy integration, also known as Pinch analysis, Pinch technology, heat integration or process integration is a methodology for minimizing the energy consumption of a process by calculating thermodynamically feasible energy targets and achieving them by optimizing heat recovery systems, energy supply methods and operating conditions. The process integration consists of two steps. The first step is the identification of the minimum energy requirement (MER) by revealing the possible energy recovery from the hot and cold streams. The second step is the implementation of the heat exchange network in a way to reach the targeted energy recovery.

The basis of the model is the definition and identification of the hot and cold streams and their correction with the minimum approach temperature to allow a heat transfer; $\Delta T_{min}/2$. By definition a hot stream needs to be cooled down and since its inlet enthalpy is greater than its outlet one, it is a heat producer. On the contrary, a cold stream has to be heated up and as the enthalpy at the inlet is smaller than at the outlet, it is a heat consumer. The heat required by the cold streams is usually supplied by primary energy sources and by recovering heat from the hot streams in the heat exchangers.

The temperature and the heat demand of the different streams are given by the flowsheet modeling calculations and are introduced in the energy integration software Easy2 integrating the process with regard to operating costs. A Pinch analysis of the proposed process is done based on these heat stream data.

The composite curves are calculated by assembling the hot and cold streams. The hot composite curve characterized by an enthalpy-temperature diagram represents the heat available in the process and the cold composite curve the heat demands of the process. The pinch point is the point where the temperature difference between the hot and cold curve is minimal and therefore the place where heat exchange is the most constrained. The maximum heat recovery is determined by considering, that heat exchange can only take place, if the temperature difference between the composites is superior to ΔT_{min}. The representation of the curves in corrected temperature scale gives the global or grand composite curve (GCC), depicting for each temperature the difference between the enthalpy of the hot and cold curve. The pinch point appears where the curve touches the temperature axis. Globally, the process needs energy above the pinch point (heat sink) and releases energy (heat source) below it.

Three heuristic rules are followed:

- No cold utility used above the pinch point
- No hot utility used below the pinch point

- No exchanger can transfer heat across the pinch point

The minimum approach temperatures $\Delta T_{min}/2$ depend on the physical properties of the stream. The numerical values that are used, are given in table 5.1.

State	$\Delta T_{min}/2$
Phase change	2
Liquid	4
Gas	8
Heat exchanger	25

Table 5.1: $\Delta T_{min}/2$ factors used for the different streams in the energy integration

The heat that has to be supplied to and to be evacuated from the system is computed by the heat balances. In integrated systems, the energy requirements are satisfied by using energy conversion units, that are modeled for a reference flow rate $\dot{n_w}$ for which the hot and cold streams are established. The optimal flow rate of each unit is determined by considering a multiplication factor f_w, that is computed to maximize the energy conversion efficiency, while satisfying the constraints of the heat exchange. The multiplication factor is determined by minimizing the following objective [60]:

$$min_{f_w} \sum (f_w \cdot \dot{n_w} \cdot LHV_w) + \frac{1}{\eta_{el}}(EL_i - EL_o) \tag{5.1}$$

where EL_i and EL_o stand for imported and exported electricity and η_{el} for the grid efficiency. A detailed explanation of this approach is found in [60].

The overall energy model of the process results hence from different building blocks: the heat exchanger network accounting for the hot and cold streams, the steam network and the mechanical power effects defining the electricity export and import constraints.

5.2 Minimum Energy Requirement

In a first stage, the energy integration is set up based on the preliminary models described in chapter 4 and the results are computed for a plant capacity of $20 MW_{th}$ nominal power based on LHV.

The minimum energy requirement is computed for different gasification and synthesis options from the definition of the hot and cold streams and the correction with the minimum approach temperature assuring heat transfer. From the results, giving a first picture of the overall performance of the process, the heat consuming steps and the potential improvements increasing the efficiency are identified.

In the biomass conversion processes, the characteristic heat demanding and consuming steps are the same. Heat is supplied from the hot streams after the gasification, the reforming and the purification section, where the gas stream is cooled down. Moreover, heat is released by the exothermic synthesis reaction. On the contrary, heat must be provided to perform the endothermic pyrolysis reaction, to heat the water prior to evaporation and to reheat the steam for gasification. An elevated amount is also consumed at low temperature for wood drying. There is hence a steam demand from the dryer, the gasifier, the reformer and the shift reactor.

The MER curves for different gasification options of the FT process are illustrated in figure 5.1. The curves are characterized by isothermal plateaus standing for the heat load for the evaporation of the steam required for gasification (461K), the FT synthesis (588K), the wood gasification (CFB: 1148K and EF: 1648K) and the high temperature stage (i.e. reforming) for the fluidized bed gasification (1648K). The line between 1148K and 631K represents the gas treatment, i.e. the producer gas cooling. The pinch point is determined by the heat demand of the gasification due to the important amount of energy that needs to be supplied to the reactor at high temperature.

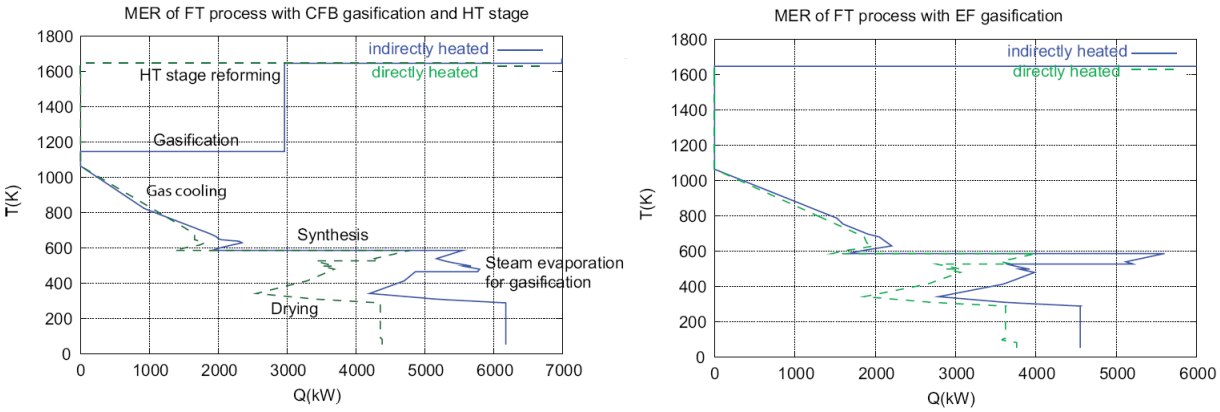

Figure 5.1: MER of the FT synthesis process for different gasification options

The comparison of the MER curves (figure 5.1) identifies the different minimum energy requirements below and above the pinch point and the characteristics resulting from the different gasification options. The directly heated gasification requires no energy for the gasification, since the thermal energy is supplied internally by oxidation and does not represent a heat demand of the process. This explains the disappearance of the plateau representing the endothermic gasification reaction (at 1148K for CFB and at 1648K for EF). However, for the CFB gasification there is still a heat demand at 1648K by the HT-stage. The differences in the composite curves below the pinch point are due to the different reaction heats (i.e. length of the plateau around 588K) resulting from the different reactants compositions. For each gasification option, the producer gas composition is different and consequently the value of the specific heat capacity and the reaction heat are different. This explains also the slight difference in the slope of the line representing the gas cooling.

For the other synthesis processes the tendencies are the same for the indirectly heated gasification (figure 5.2)[1]. Below the pinch point, the influence of the synthesis reaction can be clearly seen, as well as the impact of including the purification in the MeOH and DME process compared to the FT process. The difference in the energy requirement below the pinch point can induce a potential shift of the pinch point for the process streams from gasification to wood drying.

[1]At this stage, CO_2 removal isn't included in the energy integration (MEA in figure 8.12)

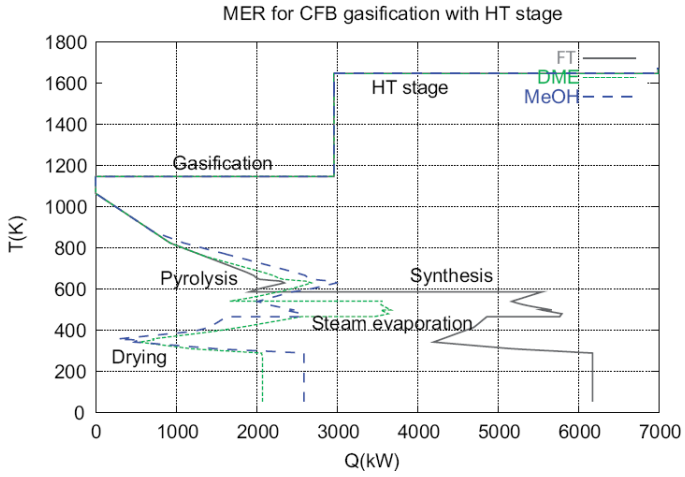

Figure 5.2: MER of the different synthesis processes with indirectly heated CFB gasification

5.3 Utilities

5.3.1 Hot Utility

The heat that has to be supplied above the pinch point, is supplied by the combustion of different fuels available from the overall process. The different depleted streams (i.e. dried torrified gas, offgas from the flash drums or distillation columns) can be used as fuel. In the case of indirectly heated gasification, where the heat transfer is achieved through circulating bed material, part of the heat demand can be satisfied by burning the residual char that enters the combustion chamber with the circulating bed material. If the combustibles from the waste streams are not sufficient to satisfy the whole demand, other sources have to be identified. Possible solutions are the process streams from the different process stages or the wood available on the production site. Since the goal is an efficient fuel production minimizing the energy consumption, it is aspired to withdraw the necessary fuel from the main stream at an early stage. Therefore, either producer gas at high temperature after the gasification (hot PG) or at lower temperature after the gas cleaning are considered as combustibles (cold PG). In general, the best choice is determined by assembling the potential fuels in a superstructure, integrating the possibilities and computing the optimal solution with regard to capital and operating costs [5].

5.3.2 Cold Utility

The cooling demand is satisfied by conventional cooling by river water, since the process temperatures are not below ambient temperature. However, in the case where oxygen is produced by cryogenic air distillation performed at around -180^oC a special refrigeration equipment would be required.

5.3.3 Cogeneration

Cogeneration or combined heat and power (CHP) designs the simultaneous generation of electricity and useful heat. These technologies provide greater conversion efficiencies by recovering heat that would be wasted otherwise. In fact, the excess heat that is released from the process can be used to produce high and low level steam that can be used either as heat source for industrial purposes or in steam turbines to generate additional electricity. For cogeneration different features can be distinguished: gas turbine, combined cycle and steam turbine.

A Rankine cycle (thermodynamic steam cycle) can be integrated to transform low grade

energy into mechanical power by using a steam turbine extracting the thermal energy from pressurized steam and converting it into useful mechanical work. The integration of a Rankine cycle decreases consequently the exergetic losses. Therefore, a steam network including the different headers, linking the hot and cold streams and the mechanical power production is implemented in the models. The Rankine cycle is characterized by the temperature and/or pressure of the steam production level, the condensation level and the bleeding levels. For the first experiences arbitrary values are used (appendix table E.8) and then the values are optimized successively in accordance with the different process heat demands and supplies in order to increase the overall efficiency, as it is explained in chapter 7.5.

In cases where more offgas than required for satisfying the MER is available, it is potentially advantageous not only to expand the offgas to atmospheric pressure and convert the excess heat of the combustion into power by means of a Rankine cycle, but to use it at least partially in a gas turbine. In such a combined gas turbine-Rankine cycle (model in appendix B.11), more electric power is generated from the process wastes due to the better overall electric efficiency.

5.3.4 Heat Pump

Another option to improve the energy integration is to include a heat pump or refrigeration cycle. Heat pumps upgrade heat available from a lower temperature to a higher one by using a small amount of electricity. The introduction of a heat pump valorizing heat available at low temperature is potentially interesting in cases where the pinch shifts from high to low temperature, as for example in the case mentioned before (section 5.2) with the potential pinch shift from gasification to drying (figure 5.2).

The heat pump unit contains a condenser, an expansion valve, an evaporator and a compressor. The key parameters are the refrigerant type, the temperature of the evaporator and the temperature of the condenser.

5.4 Typical Composite Curve

The integrated composite curve of the FT process with FICFB gasification at 1123K and steam methane reforming at 1050K is represented in figure 5.3. The different characteristics of the curve related to the main process steps are identified. For all the other processes the typical plateaus corresponding to the representative process steps are similar.

In comparison with the MER curve (figure 5.2), it can be seen how process modifications and the introduction of the hot and cold utilities and the cogeneration system affects the energy integration. The heat demand above the pinch point is satisfied by the combustion of waste streams (FT offgas (40.1%), char (21%), dried torrified gas (19.4%)) and process streams (hot producer gas (19.5%)). Since the flow rate after the gasification is decreased by the combustion of part of the producer gas, the heat demands below the pinch point get smaller. Valuable excess heat is available and converted to mechanical power by a steam Ranking cycle characterized by two production levels (80 and 120 bar) and three consumption levels (473, 433 and 293 K). The waste heat from this cycle is removed by cooling water.

The subsequent comparisons of the energy integration efficiency are based on the analysis of these composite curves. In some cases where two process composite curves are superposed for comparison, the steam network is omitted in the figure for clarity.

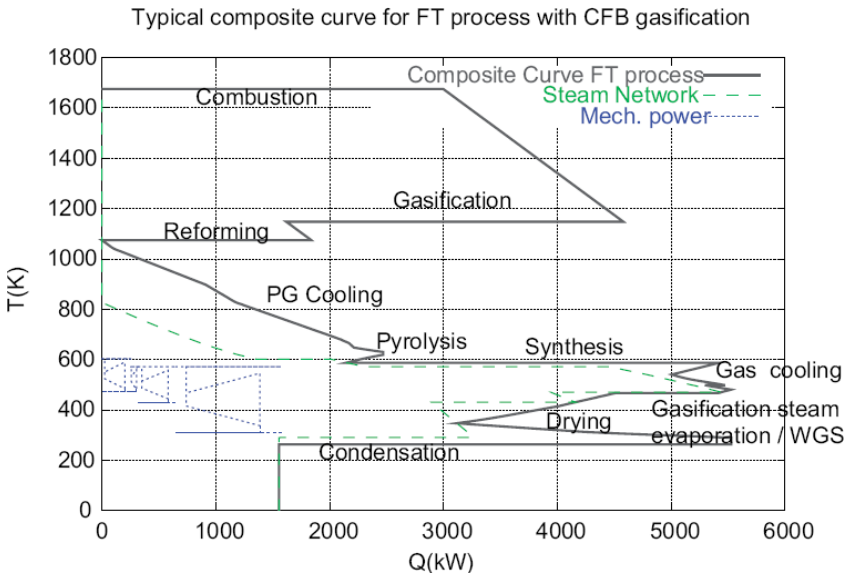

Figure 5.3: Typical integrated composite curve for the FT process with FICFB gasification including a steam network

Chapter 6

Process Economics

6.1 Economic Evaluation Methodology

Besides the efficiency of the energy integration, the economic performance expressed by the production costs determines the process thermo-economic performance. The production costs are defined by the total annual costs of the system divided by the produced amount of fuel. The total annual production costs consist of annual capital investments, operating and maintenance costs, biomass feedstock expenses and electricity costs. The economic evaluation is based on the size of the different equipments determined by the process productivity defined by the different decision variables and operating conditions. The different assumptions made for the economic analysis are specified in appendix C.1 in table C.1.

6.1.1 Capital Costs

The capital costs of the different processes are estimated based on the general approach outlined in [61, 62] and described in appendix C.2. The major process equipments, i.e. reactors, distillation columns, vessels, pumps, compressors, turbines and heat exchangers, are roughly sized and the corresponding purchase costs are estimated by using the correlations available from literature. If not otherwise stated, the correlations for the cost estimations of the different equipments are taken from [61, 62].

If no correlations are found, an alternative approach for the purchase cost estimation is the scaling from a known cost and size:

$$C_1 = C_0 \cdot \left(\frac{S_1}{S_0}\right)^R \tag{6.1}$$

where S_0 and C_0 are the known size and cost and S_1 and C_1 the desired ones respectively. R is the scaling exponent. The uncertainty range of such estimates is up to 30% [16]. For the biomass gasification, syngas cleaning and FT or MeOH synthesis relevant data are found in [16, 29, 17].

A summary of all the major process equipments for the different options of feed preparation, pyrolysis, gasification, gas cleaning, synthesis and upgrading is provided in appendix C.3. Depending on the considered options and the process conditions, not all equipments will be needed. The operating pressure and construction material are indicated for each unit. In general, the less expensive material, i.e. carbon steel, is used, however for the reactors a more resistant material: nickel-alloy is used.

6.1.2 General Approach for Sizing

To estimate the costs of the equipments the size has to be known. The physical quantities needed for the sizing are computed from the flowsheet models. The general methodology used to determined the size of the main process equipments is outlined in this chapter. The details of the dimensioning of each unit and the corresponding sizing parameters are reported in appendix C.4.

Reactor Sizing

The reactor diameter can be estimated by knowing the average velocity u_{mean} [m/s] and the volumetric flow rate $\dot{V}$ (or mass flow rate $\dot{m}$ and density ρ) by eq.: 6.2 by assuming that the mean gas velocity remains constant during upscaling:

$$d = 2\sqrt{\frac{\dot{V}}{\Pi u_{mean}}} \tag{6.2}$$

For vessels the height is determined either by an exponential relation between the height and the volumetric flow rate, fitted to data from existing plants or either by the ratio between the height and the diameter available for commercial equipments.

$$h = h_o \dot{V}^n \tag{6.3}$$

$$\frac{h}{d} = cste \tag{6.4}$$

The volume is then given by the following expression (eq.: 6.5) by assuming a cylindrical shape:

$$V = \pi h \frac{d^2}{4} \tag{6.5}$$

Flash Drum Sizing

Alternatively, the volume can be assessed directly from the volumetric flow rate by knowing the residence time $\tau[s^{-1}]$.

This method is used to determine the size and costs of a flash drum, by assuming a solvent residence time, τ, of 10 minutes and a height to diameter ratio of 3 [62]. The dimensions of a flash drum are related to the liquid volume flow by:

$$d = \left(\frac{2}{\pi}\tau \dot{V}_l\right)^{1/3} \tag{6.6}$$

$$h = 3d \tag{6.7}$$

Since the vessels are limited in size due to construction constraints, a condition is introduced to use multiple equipment units if the diameter exceeds a certain limit.

Distillation Column Dimensioning

A general approach to evaluate the size and costs of the distillation columns is given by the following steps.

First the diameter is determined by:

$$d = 2\sqrt{\frac{\dot{m}}{\Pi G}} \tag{6.8}$$

where G is the superficial gas mass flow [kg/sm^2].

The HETP (height equivalent of a theoretical plate) is assessed by:

$$HETP = 0.5 \cdot d^{0.3}/\epsilon_{Murphey} \quad if \quad d \geq 1m \tag{6.9}$$

$$\text{for Tray Towers} : HETP = 0.5/\epsilon_{Murphey} \quad if \quad d < 1m \tag{6.10}$$

$$\text{for Packed Towers} : HETP = 0.4 \cdot d/\epsilon_{Murphey} \quad if \quad d < 1m \tag{6.11}$$

where $\epsilon_{Murphey}$, Murphey efficiency, is the overall efficiency per plate. By knowing the number of plates N, the height is then given by:

$$h = N \cdot HETP \tag{6.12}$$

With these quantities the costs are estimated by using the correlations for vessels and tower packings or sieve trays.

Heat Exchanger Dimensioning

The capital cost estimation of the heat exchanger network is based on the average surface area and the number of units necessary to satisfy the minimum energy requirements computed by the energy integration. Since this approach does not include the actual heat exchanger network design, the cost estimation is not based on the proper sizing of each equipment and therefore the costs are overestimated because the minimum energy requirement generally results in a greater number of units having smaller surface areas.

The disadvantage of this method is, that it does not account for the specific process conditions. However, for heat exchangers operating in the range of 1-50bar, this doesn't affect much the cost estimation.

The costs of the heat exchangers are given by the correlation for a fixed tube sheet heat exchanger. The overall costs are assessed by the average value of the costs of a heat exchanger operating at high pressure P=30bar (construction material nickel alloy) and one at low pressure P=5bar (construction material carbon steel) multiplied by the minimal number of heat exchangers.

6.1.3 Production Costs

The costs of manufacturing (COM) of a chemical product comprise the cost of raw materials, utilities, labor, maintenance, contingencies, taxes and others. A general correlation is given by [61]:

$$COM = a_0 C_{GR} + a_2 C_{OL} + a_3 (C_{UT} + C_{RM}) \tag{6.13}$$

where C_{GR}, C_{OL}, C_{UT} and C_{RM} represent respectively the grass roots costs, operating labor, utilities and raw materials, and the factors a_i relate other costs to these expenses. In this work, no factoring is applied ($a_i = 1$) because the manufacturing costs are only related to the costs arising from the consumption of resources. By using this method, it is possible to study the balance between the costs arising from the initial investment and the performance of the equipment with regard to the consumption of resources.

The sum of the raw material, labor, electricity and maintenance costs is also sometimes called operating costs. The annual maintenance costs are estimated as 5% of the annual total grass roots costs.

The total annual costs take into account the technical and economic lifetime of the installation and the interest rate. The depreciation costs are estimated by dividing the total annual grass roots costs by the present worth of annuity defined as:

$$\text{present worth of annuity} = \frac{(1+IR)^t - 1}{IR \cdot (1+IR)^t} \tag{6.14}$$

where IR represents the interest rate and t the lifetime.

The total production costs [USD/MWh] are then calculated for a given annual production by summing the annual operating and depreciation costs.

Raw material

The only raw material that is considered is the wood used for gasification. For the different calculations wood chips having a moisture content of 50% and being available at a price of 50CHF/MWh are used [63].

Utilities

The only utilities consumed are cooling water and electricity. Since the cooling capacity can be supplied by river water and as these costs are low compared to the other manufacturing costs, the cooling water costs are neglected. The electricity price of $270 CHF/MW_h$ is based on green electricity and the costs for imported or exported electricity are assumed to be the same [63].

6.2 Economic Evaluation

Based on the final model of the FT process with FICFB gasification (appendix E), the results of the economic evaluation are analyzed and the main contributions to the capital and production costs are identified. The influence of the different process options and technologies on the economic performance is studied more in detail in chapter 8.2.

6.2.1 Capital Costs

For this FT-process the total grass root costs are in the range of 24.7MUSD for a plant capacity of $20MW_{th}$ nominal power. The analysis of the capital costs split-up (figure 6.1) reveals that, the upstream processing comprising the pretreatment, the gasification, the steam methane reforming, the producer gas cleaning and the WGS, represents more than half of the investment, followed by the synthesis itself (around one quarter) and the heat exchanger network. The upstream investment costs are formed by over 70% from the gasification costs. Consequently, advances in the gasification technology and commercialization have the potential to decrease the costs.

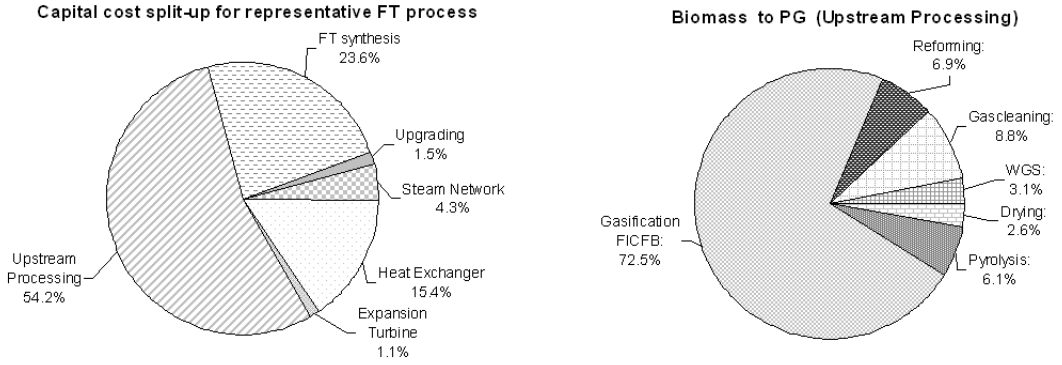

Figure 6.1: Capital cost buildup (left) and upstream processing cost split-up (right) for the representative FT process

Since the investment costs for the different equipments are estimated based on different correlations and scaling relations, the accuracy of the estimation could be increased by the availability of real market prices. However, as some technologies are still under development and not commercialized yet, the costs can't be evaluated exactly. Some costs are hence overestimated, while others are underestimated. Nevertheless, these cost estimations allow to compare the different options and to identify the key factors influencing the profitability.

6.2.2 Production Costs

The overall production costs are in the range of 126.6 USD/MWh for the selected FT process. The production costs comprise the operating costs including raw materials, labor, maintenance and electricity, as well as the depreciation costs. A detailed analysis shows that the raw material, wood in the present case, represents about half of the production costs (figure 6.2). In this case, not enough electricity is produced by cogeneration to cover the process power demand, consequently additional electricity has to be imported. Relative to this amount, part of the production cost are related to the electricity purchase. In cases, where more electricity is produced

than consumed, the surplus of electricity can be sold and electricity is then a benefit, that is favorable for the production costs.

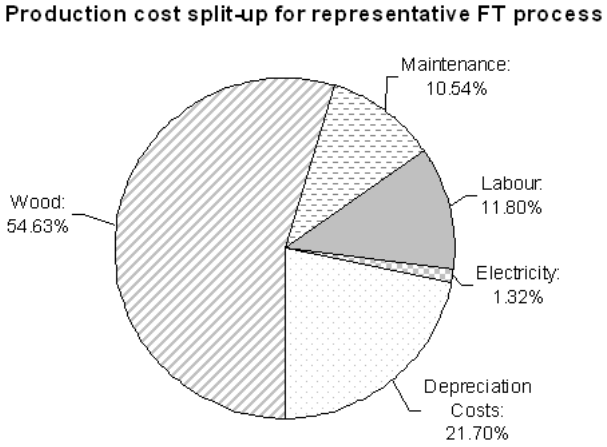

Figure 6.2: Production cost split-up for the representative FT process

The estimation of the production costs allows to make a relative comparison between the different processes by considering the same assumptions (table C.1). However, the value of the production cost depends highly on the different assumptions made, especially regarding the wood and electricity price (section 8.3.1). Consequently, absolute comparisons with literature data based on the production costs are quite problematic, while comparisons based on the investment costs for a given production scale are more appropriate.

6.2.3 FT reactor Technology

In the present work the FT-reactor modeling is based on the Sasol Advanced Synthol reactor. However, by using another type of reactor the efficiency is changed due to the different productivity and the economic performance. Since the price per unit for the different reactors is comparable, the influence for a small scale production with only one reactor per installation isn't relevant. The influence of the technology choice becomes more important at larger scale, because each reactor has another maximal capacity (table 6.1) and therefore the number of reactors to be installed for a given production would be different.

Capacity [bbl/day]	CFB	SAS	FB	SB
Capacity per reactor	6'500	11'000	500-700	2'500
Potential Capacity per reactor	7'500	20'000	3'000	20'000

Table 6.1: Sasol FT commercial reactors capacities [bbl/day] [64]

Chapter 7

Unit Performance

The overall process performance depends mainly on the synthesis performance quantified by the fuel efficiency and on the characteristics of the utility and cogeneration system. Several sensitivity analysis are made to see the influence of different key parameters on the productivity and on the total efficiency. Based on the preliminary set-up of the flowsheets (chapter 4) and on the preliminary choices of the design parameters, the thermo-economic performance of the processes is increased step by step by optimizing the main influencing factors. Decisive parameters of the energy integration efficiency are the steam network, the type of available combustible (offgas, producer gas, char, dried torrified gas, wood, etc.), as well as the introduction of a gas turbine or a heat pump.

The influence of some key parameters is studied in this chapter and some general tendencies are exposed for different representative options. From these results the best values for the key parameters are determined and the models are improved by adding different modifications and by defining the best design of the energy integration.

For the different comparisons, only the relevant choices for the different process options and the parameters that are varied are specified. The detailed process layout and the values of the important decision variables of each scenario are reported in appendix D. To see directly the influence of one parameter, only one parameter is varied at a time, the other ones remaining constant. Each analysis is done for an installation having a nominal thermal capacity of $20 MW_{th}$ (LHV basis).

7.1 Efficiency Definition

In this work the process performance is expressed as energy efficiency based on the lower heating values.

The chemical efficiency ϵ_{chem}, also known as fuel efficiency, is defined as the ratio of the chemical energy available in the product outlet stream (i.e. crude FT-fuel, MeOH or DME) to the energy available in the feedstock (i.e. woody biomass).

$$\epsilon_{chem} = \frac{LHV_{Fuel,out} \cdot \dot{m}_{Fuel,out}}{LHV_{wood,in} \cdot \dot{m}_{wood,in}} \tag{7.1}$$

The total energetic efficiency ϵ_{tot} including the electricity, is defined by eq.: 7.2 by assuming that 1 thermal kW is equivalent to 1 mechanical kW.

$$\epsilon_{tot} = \frac{LHV_{Fuel,out} \cdot \dot{m_{Fuel,out}} + \dot{E}^{-}}{LHV_{wood,in} \cdot \dot{m_{wood,in}} + \dot{E}^{+}} \tag{7.2}$$

where $\dot{E}^{-}$ refers to the overall produced mechanical power [1] and $\dot{E}^{+}$ to the overall consumed mechanical power.

In these efficiency calculations, $LHV_{wood,in}$ could either refer to the LHV of wet or dry wood. In this work, all the reported efficiencies are expressed on the dry wood basis.

The energy content of the different streams characterized by the lower heating value is directly computed from the flowsheet calculations done in Belsim Vali.

7.2 Composition - Stoichiometry

Each process needs an optimal stoichiometric ratio of the reactants for the synthesis of the product. Consequently, the efficiency of the synthesis process depends on the relative compositions of the inlet streams. The composition of a stream can essentially be changed by:

- Separation processes, removing some compounds
- Recycling, changing the relative composition by mixing a stream with a different composition to the main stream
- Chemical reactions, consuming some compounds and producing others

7.2.1 Ternary Diagrams

The composition variation can be studied by analyzing the composition change of the fuel stream in terms of the main energy elements: carbon (C), hydrogen (H) and oxygen (O). The fuel composition-conversion diagram, a ternary CHO-diagram (figure 7.1), based on the molar composition (i.e. giving similar weight to carbon and hydrogen as fuel components), can explain the composition and conversion processes for biomass and reveal the relationship between hydrocarbons, biomass and other fuels [65]. The products of combustion, CO_2 and H_2O, and the products of gasification, CO and H_2, lie on parallel vertical lines. The H-CO axis is the locus of syngas made from other fuels and used to make diesel and alcohol fuels, and of carbohydrates CH_2O, the source of all fossil and renewable fuels. The C-H axis contains the important fossil fuel hydrocarbons: oil and aromatics. The arrows indicate the directions for possible conversions of biomass to other fuels by addition of oxygen or air, steam, hydrogen and by fast or slow pyrolysis.

In general, composition change according to different reactions can be interpreted as follows. The addition of a substance A (e.g. O_2, H_2O or H_2) to one compound B displaces the dot representing the composition of B on a straight line towards A, while the removal of A displaces B in the opposed direction. A CHO-diagram displaying the compositions of the producer gas after gasification and of the target products reveals hence by which processes, such as water-gas shift and/or CO_2 removal the appropriate synthesis reactants composition can be reached.

[1] The net electricity output defined by (-1)·$\dot{E}$ is positive, if the amount of power that is produced is higher than the one that is consumed; electricity is generated by the overall process

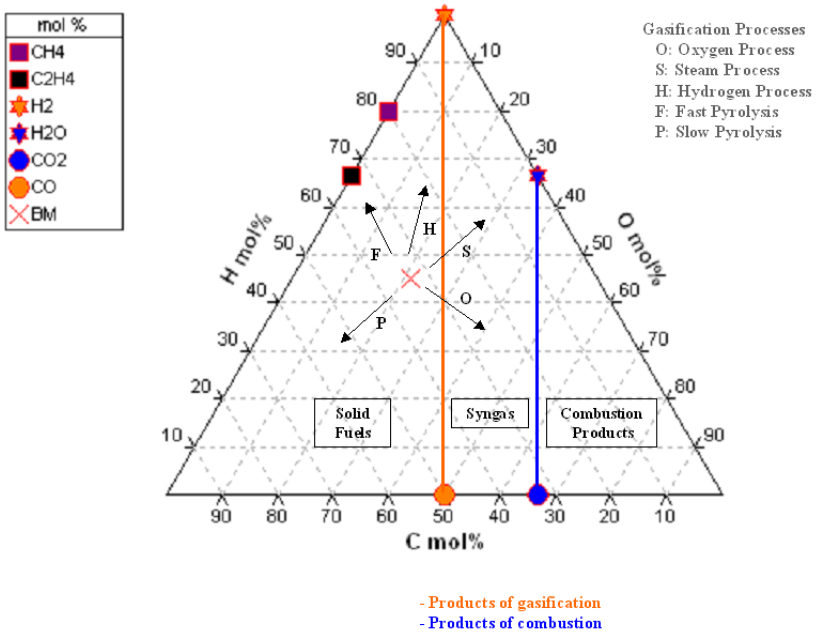

Figure 7.1: Diagram of the composition and conversion routes of fuels (adapted from [65])

The producer gas is situated near the $H - CO_2$ axis (figure 7.2)[2], as it was predicted. Methanol has a lower oxygen and higher hydrogen content than the hot or cold producer gas, whereas for DME the oxygen content is even lower (i.e. carbon content higher). This shows that in any case the relative oxygen content has to be reduced, whereas the hydrogen content has to be increased slightly. Consequently, it seems that CO_2 removal after a preliminary water-gas shift reaction is appropriate before the MeOH and DME synthesis.

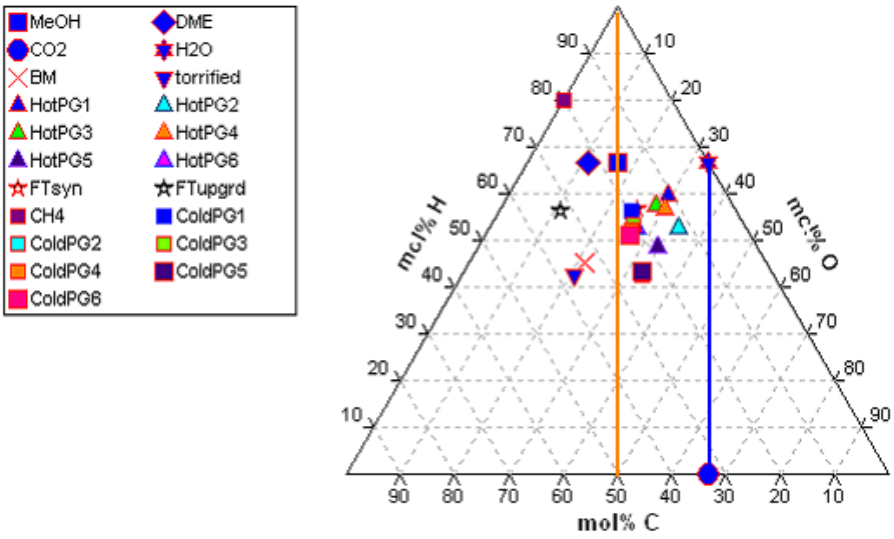

Figure 7.2: CHO-ternary plot representing the elementary composition [mol%] of the different fuels and the producer gas after different types of gasification

[2]Hot and cold producer gas are considered and the numbers refer to the gasification type

The straight comparison of the decisive stoichiometric ratios in the different streams highlights these trends also (table 7.1). The H_2/CO ratio can be increased to the target value of 2 by adding water to displace the water-gas shift reaction equilibrium towards the formation of hydrogen (i.e. consumption of CO). For the DME synthesis the ratio can be decreased by a reverse water-gas shift reaction (i.e. no water addition). A water-gas shift reaction can't however influence the $\frac{H_2-CO_2}{CO+CO_2}$ ratio since the overall the C, H, O composition doesn't change, because the relative differences remain constant. Only CO_2 removal or H_2 addition can alter this ratio.

Ratio	$\frac{H_2}{CO}$		$\frac{H_2-CO_2}{CO+CO_2}$	
FT-fuel	2		-	
Methanol	-		2	
DME	1 or 2		-	
Gasification	indirect	direct	indirect	direct
EF	1.97	1.31	1.02	0.31
CFB (+HTstage)	1.52	1.41	1.02	0.30
CFB (gas5)	1.30	1.26	1.02	0.53

Table 7.1: Comparison of the decisive stoichiometric ratios for the different synthesis and of the composition of the producer gas after different types of gasifications

From the composition analysis, the amount of water to be added to the water-gas shift reactor is determined in such a way to reach the targeted ratio and to minimize the amount of unreacted water. In directly heated gasification less hydrogen is produced, therefore more water has to be added to increase the $\frac{H_2}{CO}$ ratio up to 2. For a flow of 1kg/s of producer gas, the amount of water to be added before the WGS reactor is set to 0.08kg/s for directly heated and to 0.05kg/s for indirectly heated gasification followed by wet gas cleaning.

7.2.2 CO_2 Removal and Recycling

The influence of the stoichiometric ratio, the percentage of CO_2 removal before the reactor and the offgas recycling, on the process performance are studied and the best values are determined.

DME process

The effect of the stoichiometric synthesis ratio (H_2/CO) on the performance of the DME process is investigated for two different gasification options with 95% CO_2 removal and 80% recycling (scenario A). Ideally, the ratio should be one for the one-step process and two for the two-step process, as it can be seen from the synthesis equations (eq.: 3.22 and 3.19). Despite the fact that the reactor was modeled based on the one-step process, the value of the ratio fixed in the WGS reactor was initially set to 2, whilst the optimal value is 1. To reach a lower ratio, the ratio is adapted by a reverse water-gas shift reaction. The amount of CO_2 in the producer gas determines the equilibrium shift since H_2 is the reactant in excess and CO_2 the limiting reagent. Consequently, the ratio can't be decreased down to one for any composition (without CO_2 addition). Therefore, the ratio is fixed to 1.3, in accordance with the lowest ratios after the indirect gasification (table 7.1). For the cases where this ratio is already achieved after gasification, an alternative, that isn't investigated here, could be to completely remove the WGS reactor.

Table 7.2 shows how this ratio affects the chemical efficiency in the case of the directly heated entrained flow gasification (gas2) and the indirectly heated fluidized bed gasification (gas5) (scenario A). The efficiency is of course increased in both cases by approaching the

optimal stoichiometric ratio for the DME synthesis. Consequently, the H_2/CO ratio is fixed hereinafter to 1.3.

Ratio	$H_2/CO = 2$ ϵ_{chem} [%]	$H_2/CO = 1.3$ ϵ_{chem} [%]
Direct EF (gas2)	28.07	45.72
indirect FICFB (gas5ii)	37.95	41.94

Table 7.2: Comparison of the chemical efficiency of the DME process for different gasification options for a H_2/CO ratio of 2 and 1.3 in the synthesis reactants stream (scenario A)

The effect of the CO_2 removal and recycling on the performance of the DME synthesis is studied by analyzing the effect on the DME production, expressed as relative increase of the DME mass flow rate at the reactor outlet compared to the case with no CO_2 removal or no recycling (scenario B).

CO_2 removal before the synthesis reactor can increase the relative production of DME up to 5% compared to no CO_2 removal (figure 7.3), because the reactants stoichiometry is more appropriate for the synthesis. If the amount of produced DME is higher, the amount of purified DME is also higher and consequently the chemical and overall process performance are increased (table 7.3). For the subsequent analysis, CO_2 removal is fixed to 95% of the synthesis unit inlet stream (F_6_300 figure 4.7).

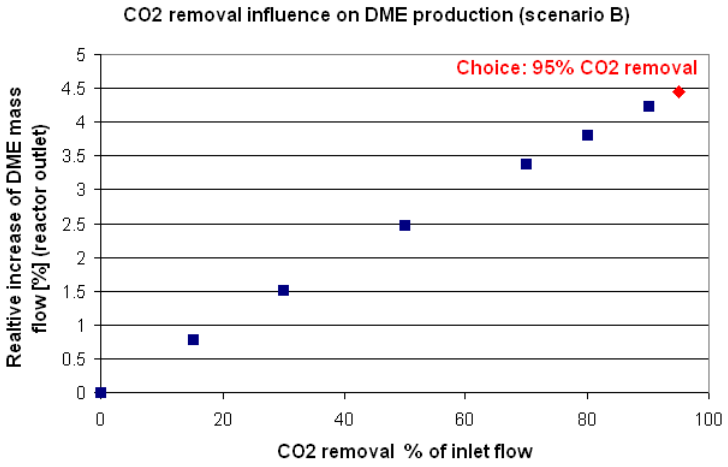

Figure 7.3: Effect of the CO_2 removal on the DME production (in the stream at the reactor outlet) with 80% recycling (scenario B)

Recycling the offgas of the first flash (S_6_301: figure 4.7) can increase the DME mass flow rate at the reactor outlet up to 25% compared to the one-pass model (figure 7.4). However, the increase of the DME flow rate after the two successive flash drums (f_7_37a: figure 4.7) is much less important and above a certain recycling rate any increase isn't observed. This can be explained by several facts. First, the recycling changes the composition of the stream and hence changes the stoichiometric ratio. Since, the recycled stream contains mainly H_2 (48%mol), CO (10%mol), CO_2 (34%mol) and a small fraction of DME (6%mol), the H_2/CO ratio of 4.7 deviates from the optimal value and consequently the production isn't anymore improved at high

recycling rates. Second, there is one part of DME that accumulates in the recycling loop, which explains why the amount of DME at the reactor outlet increases, while outside the loop the production isn't increased. If there is more DME produced, there is also more that is entrained with the gaseous phase in the flash drums. Therefore, an alternative (not investigated in this work) to increase the efficiency further, would be the recycling towards the gas-cleaning section or to adjust of the stoichiometric ratio by other means (e.g. addition of CO).

This trend is also reflected in terms of efficiency (table 7.3); the recycling improves slightly the chemical efficiency, while the total energetic efficiency remains nearly constant. Nevertheless, the value is fixed subsequently to 80% recycling and the non-recycled part of the offgas can be burned.

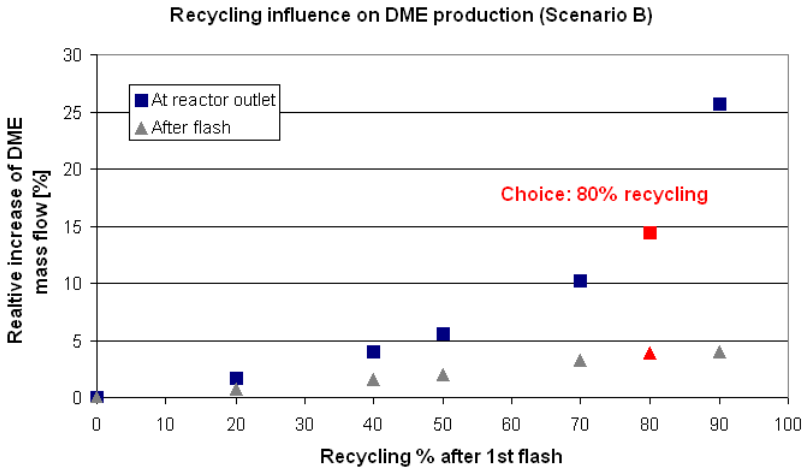

Figure 7.4: Effect of the recycling rate on the DME mass flow rate (with 95% CO_2 removal) in the stream at the reactor outlet, respectively after the flash drum (scenario B)

CO_2 removal [%]	95	95	0
Recycling %	80	0	0
ϵ_{chem} [%]	42.4	41.0	36.3
ϵ_{tot} [%]	40.2	40.4	35.5

Table 7.3: DME process performance for different percentages of CO_2 removal and recycling rates

Alternatively, the offgases of the second flash (f_7_38: figure 4.7) and of the first distillation column (f_7_303: figure 4.8), containing part of the unreacted gases, could be recycled. Even if these streams contain a lot of hydrogen, they are limited in carbon monoxide and the H_2/CO ratio exceeds the optimal ratio. Consequently, these streams have to be treated before being recycled (for example by H_2 and/or CO_2 removal and WGS). Since this recycling isn't ideal and induces additional treatment, it isn't investigated in this work.

Another option would be to inject the small amount of methanol, released at the bottom of the third distillation column, in the reactor to shift the reaction towards DME production.

MeOH process

The effect of the recycling on the MeOH production performance is studied for the process with FICFB gasification, in which the stoichiometric ratio $\frac{H_2-CO_2}{CO+CO_2}$ is fixed to the optimal value of 2 by CO_2 removal (scenario C). The recycling is expressed as percentage of the flow rate of the vapor phase of the flash drum (S_6_202: figure 4.9). The stream being recycled (f_6_224) contains mainly the unreacted gases: around 67%mol H_2, 29%mol CO and 3%mol CO_2. This composition corresponds still to the optimal ratio (around 2), since the reactants have reacted according to the stoichiometric ratio and hence the relative changes in composition were the same. Therefore, recycling (without CO_2 removal) towards the reactor inlet can increase the production.

Figure 7.5 illustrates for different recycling rates the differences in the performance expressed as relative MeOH mass flow rate increase at the reactor outlet (f_6_218: figure 4.9), compared to the one-pass synthesis. The production is increased drastically by recycling because more product is formed since more reactants in the optimal proportions are present. Recycling of 60%, produces already 2 times more product than the one-pass synthesis (i.e. 100% increase) and a recycling of 90% nearly 4 times more (i.e. 300% increase) .

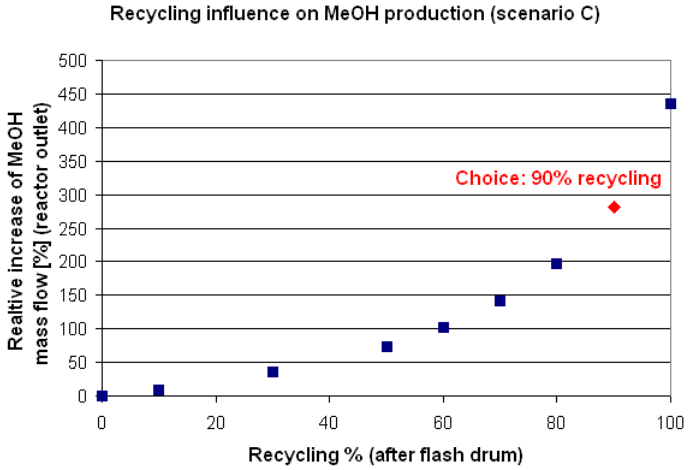

Figure 7.5: Influence of the recycling on the production of MeOH (scenario C)

Expressed in terms of chemical efficiency and overall energetic efficiency (table 7.4), recycling of 90% increases the chemical performance nearly three and a half times compared to the one-pass option. The overall performance is increased only around twofold; the difference being due to the different performance of the power generation system resulting from the different heat demands from the larger flow rates.

$\frac{H_2-CO_2}{CO+CO_2}$	2	2	1.5
Recycling %	0	90	90
ϵ_{chem} [%]	14.86	50.62	50.04
ϵ_{tot} [%]	22.27	47.06	47.17

Table 7.4: MeOH process performance for different recycling rates and stoichiometric ratios (scenario C)

The results of the thermo-economic analysis done for two different values of stoichiometric ratios $\frac{H_2-CO_2}{CO+CO_2}$; for 1.5 and for the optimal value of 2 with a recycling rate fixed at 90%, show that the chemical efficiency is only slowly higher for the optimal ratio (table 7.4). This can be explained by the fact that the reaction equilibriums occurring in the reactor are only slightly affected.

Consequently, the stoichiometric ratio influences for the MeOH process the performance in a lesser extent than the recycling rate. Recycling has a big potential to increase the performance, if the stoichiometric ratio of the considered stream approaches the optimal value. Based on these results, the CO_2 removal is fixed hereinafter in such a way to reach the optimal stoichiometric ratio of 2 and 90% of the offgases are recycled after the flash drum (in accordance with the purge of 10.25% in [59]). The non-recycled part of the stream can be combusted for heat and power generation.

FT process

For the Fischer-Tropsch process recycling can also be considered as an option. In this work, where the upgrading isn't modeled in detail; the possibility to recycle the offgas of the flash drum, separating the unreacted gases from the liquid fuel is considered for one FT process (scenario E) where the CO-conversion is fixed at 85%.

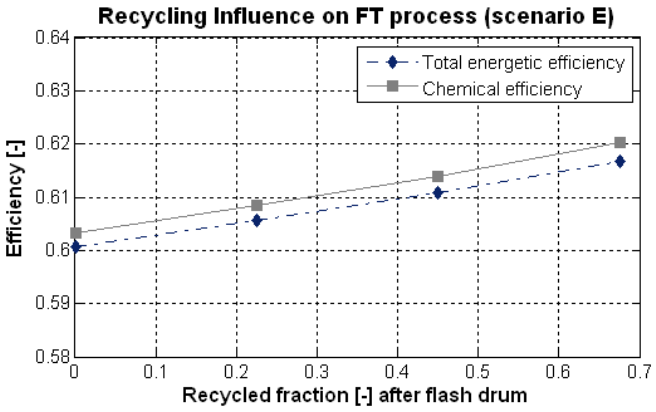

Figure 7.6: Effect of the recycling on the FT-fuel production (scenario E)

For the FT process, recycling doesn't improve the synthesis performance much (figure 7.6); recycling 65% of the offgas increases the efficiency less than 2%. In the one-pass synthesis the offgas contains mainly: CO_2 (41.7%mol), H_2 (34.7%mol), CO (19.8%mol) and methane (2%mol) and the H_2/CO ratio of 1.75 is close to the optimal value of 2. However, by increasing the recycling rate, the stoichiometric ratio decreases down to one and the methane fraction increases up to 5%mol and accumulates in the recycling loop. Depending on the gasifier and reformer set-up, the methane content can even become more important. In the presence of methane, the FT-fuel productivity decreases and fewer longer hydrocarbons are formed because the FT-catalyst can't catalyze methane reforming. Since the variation of the H_2/CO ratio does influence the performance in a lesser extent (i.e. for H_2/CO ratio 1.7-2.1 the efficiency variation is below 2%), the methane accumulation is the main reason why the short recycling towards the reactor doesn't increase the performance considerably.

The performance could hence be increased further by recycling the stream towards the reformer, removing part of the methane and subsequently to the WGS reactor adjusting the stoichiometric ratio to the optimal value or by introducing a reformer in the recycling loop before the reactor. Since the stoichiometric ratio can already be adjusted by a simple WGS reaction by adding a small amount of water (figure 7.2), the option of CO_2 removal isn't investigated in this case. The CO_2 removal could increase the chemical performance slightly, however due to the energy consumption and the investments associated with the MEA absorption unit, the thermo-economic performance would drop. These options of recycling and CO_2 removal could be investigated in further studies.

Since recycling doesn't improve the performance considerably, the one-pass FT process is considered for the subsequent comparisons.

7.2.3 MeOH process on Ternary Diagram

In order to visualize the composition changes occurring in the different steps of the MeOH process from the biomass, to the final product, MeOH, the different streams are represented on a ternary CHO-diagram (figure 7.7) for the process with FICFB gasification and with 90% recycling towards the synthesis reactor (scenario D).

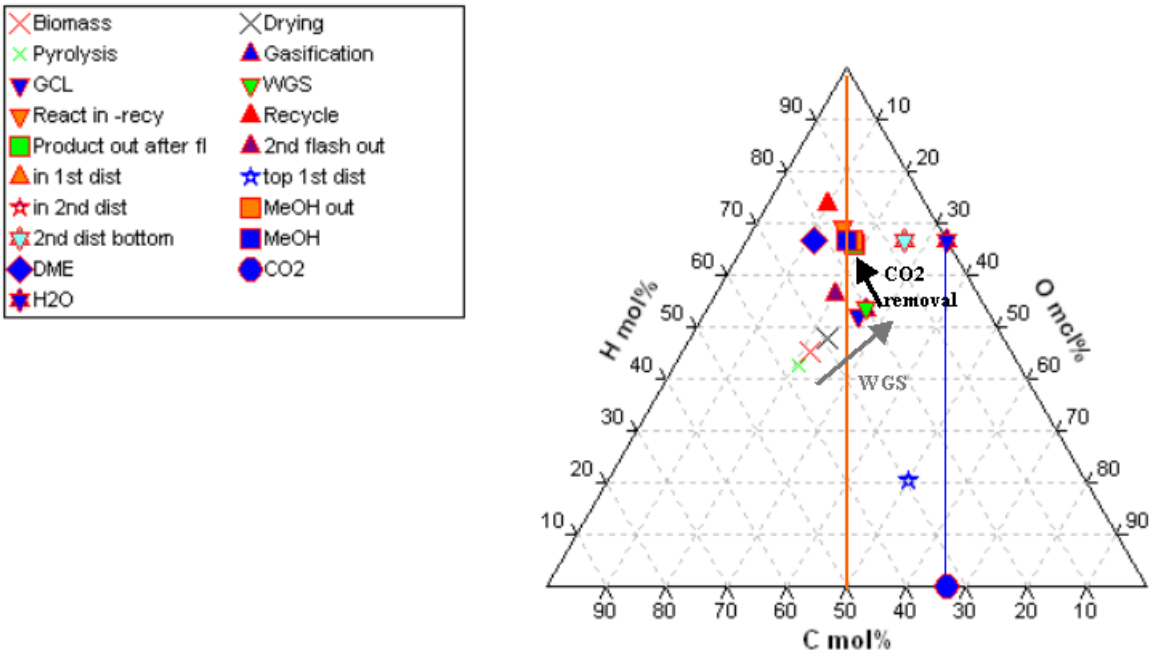

Figure 7.7: CHO-diagram representing the compositions of the different streams of the MeOH process (scenario D)

The CHO-diagram (figure 7.7) illustrates the different transformations taking place during the process. Torrefaction lowers the O/C ratio of biomass. Gasification and gas-cleaning increase the hydrogen content and decrease the oxygen and carbon amount by the addition of water, displacing the dot representing the biomass composition towards H_2O (WGS arrow). To reach the optimal product composition, the oxygen amount has to be decreased further. By drawing a line between the MeOH composition and the composition after the WGS reaction, it can be seen

that the CO_2 composition lies exactly on this line. This proves that the optimal stoichiometric ratio can be reached by CO_2 removal (leading to the composition represented by *react in -recy*). The methanol purity is increased further by removing traces of CO, CO_2, H_2O and EtOH by liquid-vapor separation and distillation.

This plot reveals also potential valorization options for the offgases. The offgas of the first flash drum (recycle) is in fact well suited for recycling because it has nearly the optimal composition. Therefore, the methanol production is increased by recycling this stream. The offgas of the second flash drum could also be recycled, however as it has not the optimal composition, it can't be recycled directly towards the reactor, but instead could be recycled to the WGS reactor. The addition of water followed by the CO_2 removal would optimize the composition. The offgas of the first distillation column containing mainly DME (35%mol), CO_2 (25%mol), CO, MeOH and H_2 and having a low mass flow rate (around 2% of the inlet flow rate) can't be recycled anywhere in the process without treatment and is therefore sent to the combustion chamber.

The wastewater being released at the bottom of the second distillation column containing mainly water and ethanol, has to be treated since the water can't be released simply in the groundwater due to environmental concerns. Besides water treatment, another solution could be to add a distillation column to separate ethanol and water. However, as these compounds form an azeotrope and as the flow rate is small, the economic concerns have to be considered and the most profitable treatment has to be chosen.

In this work, only the recycling of the offgas of the first flash drum is considered and the other offgas streams are sent to combustion.

7.3 Synthesis Parameters and Operating Conditions

The process productivity is determined by the operating pressures and temperatures and the conversion parameters related to the catalyst activity and selectivity. These parameters influence not only the reaction rate, the selectivity and consequently the productivity, but also the heat release/demand and so the energy integration.

7.3.1 CO-Conversion in the FT process

The FT synthesis reaction (eq. 3.10) shows that the FT-fuel production is essentially determined by the CO-conversion. A sensitivity analysis (figure 7.8) is done for the CO-conversion ranging from 65% to 90% to see the effect on the FT performance (scenario L).

Increasing the CO-conversion from 70% to 90%, increases the chemical efficiency by nearly 10% (figure 7.8) because higher CO-conversion goes in pair with higher product formation. In theory, total conversion would yield the best productivity. However, this can't be achieved in practical due to many factors, essentially related to the catalyst activity and selectivity. According to [14], a CO-conversion of 85% is realistic and therefore the value is fixed to 85% in the subsequent essays.

A detailed analysis of the chemical efficiencies of the different hydrocarbons fractions of the crude FT-fuel (appendix figure F.1) shows that by increasing the CO-conversion the efficiencies increase evenly. Consequently, the product distribution isn't affected, which is logical as only the product amount is influenced but not the composition specified by the polymerization probability.

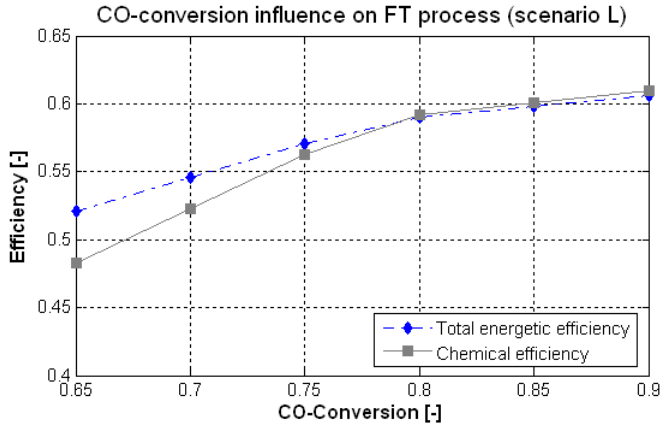

Figure 7.8: Effect of the CO-conversion on the performance of the FT process (scenario L)

7.3.2 Polymerization Probability

The value of the growth probability ($\alpha = 0.884$) was adapted from reported data [14]. A sensitivity analysis allows to see the impact of this parameter on the FT-fuel production and essentially on the hydrocarbon distribution for a CO-conversion of 85% (scenario E without recycling).

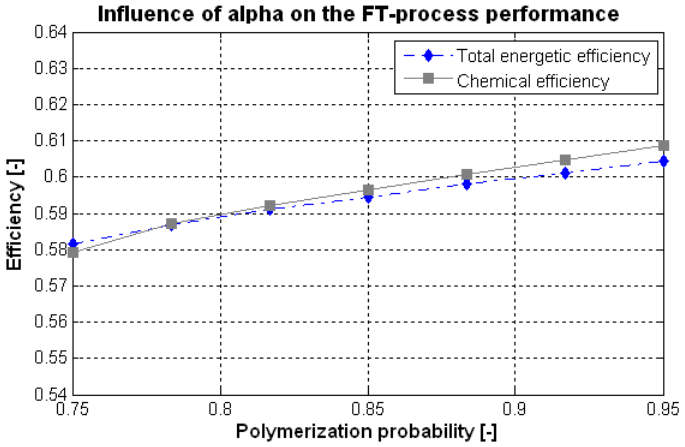

Figure 7.9: Influence of the polymerization probability on the FT process performance (scenario E)

The growth probability doesn't affect the chemical and total energetic efficiency much (around 3%)(figure 7.9); however the characteristics of the crude FT-fuel that is produced are influenced. By increasing α, the fuel efficiency of the longer hydrocarbons raises, since more larger hydrocarbons are formed. Another way to see this is based on the weight fractions of the different hydrocarbon ranges (normalized by omitting the non-hydrocarbons) (figure 7.10). For α greater than 0.9 the large hydrocarbons ($> C18$(diesel)) are prevalent, while for lower α the gasoline fraction becomes more important. The trends are in accordance with the Anderson-Schulz-Flory distribution (figure 3.10) and prove that the modeling of the FT synthesis is accurate.

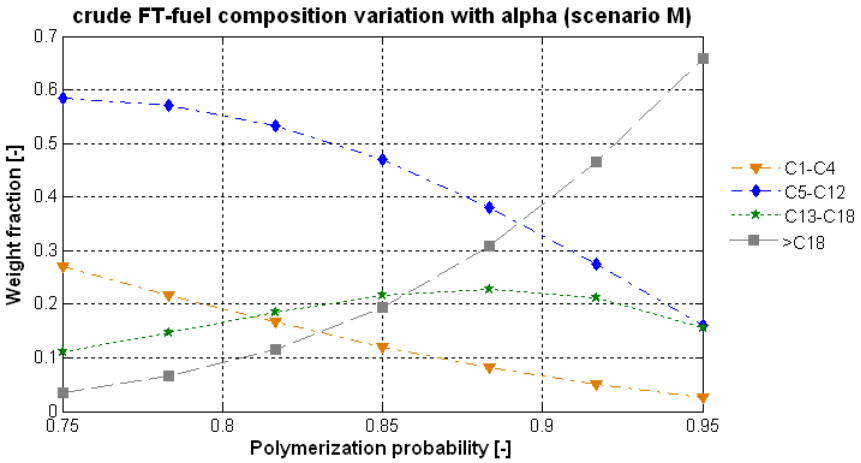

Figure 7.10: Crude FT-fuel composition change with α (scenario E)

7.3.3 Operating Conditions

Synthesis

The influence of the synthesis pressure and temperature variation on the performance is related to the modeling of the synthesis reaction.

In the FT synthesis, the operating pressure and temperature doesn't considerably affect the process performance of the developed models, since the product composition is fixed by the growth probability α, independently of the temperature or pressure. The productivity isn't affected because the conversion is fixed, however the energy integration and hence the overall energetic efficiency are slightly influenced.

The methanol synthesis on contrary is modeled by equilibrium reactions and consequently a pressure and/or temperature variation shifts the equilibrium and thus the product composition. To see the influence, the synthesis is performed for three different synthesis pressures without changing the distillation pressures to optimize the separation. By increasing the pressure of 10 bar, the chemical efficiency is increased by around 1.4% (table 7.5). The total energetic efficiency increase is lower due to the higher power consumption related to the compression. Slightly more product is formed at higher pressure because the equilibrium (eq. 4.18) is shifted, according to the Le Chatelier's Principle, to the methanol production.

Synthesis pressure [bar]	80	85	90
ϵ_{chem} [%]	56.3	57.0	57.7
ϵ_{tot} [%]	52.1	52.5	52.9

Table 7.5: MeOH process performance for different synthesis pressures (scenario D)

Similarly, a slight performance variation with the synthesis pressure is observed for the DME process modeled by equilibrium reactions.

A detailed analysis of the influence of the operating conditions on the performance isn't feasible without adapting the modeling and the fixed specifications. Depending on the modeling, no influence can be seen for conversions defined independently of the temperature or convergence problems (i.e. flash drum, recycling, distillation) related to the composition variation with the temperature can be encountered for the models based on equilibrium reactions. To investigate

the influence of these parameters in detail, additional experiments with modeling changes have to be performed.

Gasification

As already mentioned before (section 7.2), the gasification technology influences the producer gas composition and hence the performance. Beside the technological choice, other key factors are the gasification temperature and pressure. The influence of the gasification operating conditions on the producer gas composition was studied in [5] and isn't investigated in detail in this work. From the previous results, it can be seen that even if the composition changes, the determinant stoichiometric ratios (e.g. H_2/CO) remain constant. Besides the composition, the power balance and the energy integration are also influenced by the gasification operating conditions.

In general, an increase of the gasification pressure results in a lower power consumption in the synthesis section since the producer gas is already under pressure and hence the power needed to compress the gas to the synthesis pressure is lower. The amount of power needed to pressurize the gasification reactants is neglected because it is a solid/liquid state compression. A lower power consumption goes in pair with lower electricity costs and hence lower production costs. However, the production costs are also influenced by the investment costs variation which depends on how the influence of the density is taken into account in the sizing.

This influence of the gasification pressure variation is studied for the FT process with indirectly heated fluidized bed gasification followed by steam methane reforming operated at the same pressure and at different temperatures in the following chapter 7.4.

7.4 Steam Methane Reforming

The process performance is influenced by the operating conditions of the steam methane reforming step performed after the gasification. By changing the temperature or pressure, the equilibrium of the reactions is shifted. Consequently, the composition of the producer gas and the heat requirement of the reforming is changed. The reactions being considered in the reformer are the steam methane reforming (eq.: 3.6), the water-gas shift (eq.: 3.5) and the ethylene reaction (eq.: 4.11). Figure 7.11 illustrates the composition variation with the reforming temperature after a fluidized bed gasification at atmospheric pressure. Since the steam reforming reaction is endothermic, methane is formed at low temperature, while methane is consumed and carbon monoxide and hydrogen are formed at high temperature. The change of the equilibrium occurs between 1000-1100K. The kink at higher temperature can be probably explained by the fact that the range of validation is exceeded at such high temperatures. The optimal reforming temperature (at atmospheric pressure) is determined for different options through the best chemical efficiency and in a similar way the optimal temperature could be determined for other gasification and reforming pressures.

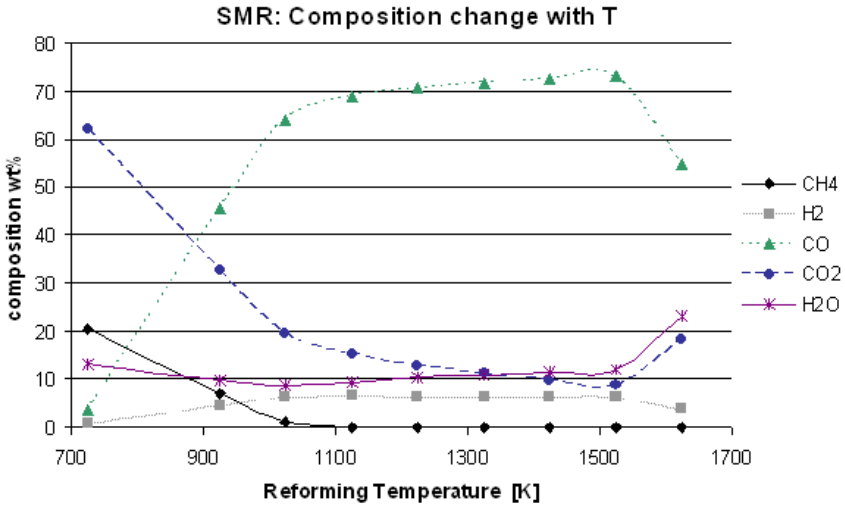

Figure 7.11: Effect of the reforming temperature [K] on the chemical composition [%wt] of the producer gas after FICFB gasification at atmospheric pressure

7.4.1 FT process

Chemical efficiency

A sensitivity analysis is done for different reforming temperatures for the fluidized bed gasification, either directly or indirectly heated followed by the FT synthesis (80% CO-conversion) (scenario F). The overall efficiency passes through a maximum in accordance with the composition change (figure 7.12). If too much methane is present (at lower temperature than the maximum value), the productivity of the FT process drops, since CH_4 cannot be reformed by the FT-catalyst and hence less larger hydrocarbons are formed. Due to the difference in composition, the maximum position (x axis), as well as the maximal value (y axis) is different for the directly and indirectly heated gasification. Above a certain temperature the efficiency isn't influenced anymore because methane is totally consumed and the composition remains constant. A good choice is a temperature slightly below or at the gasification temperature of 1123.15K.

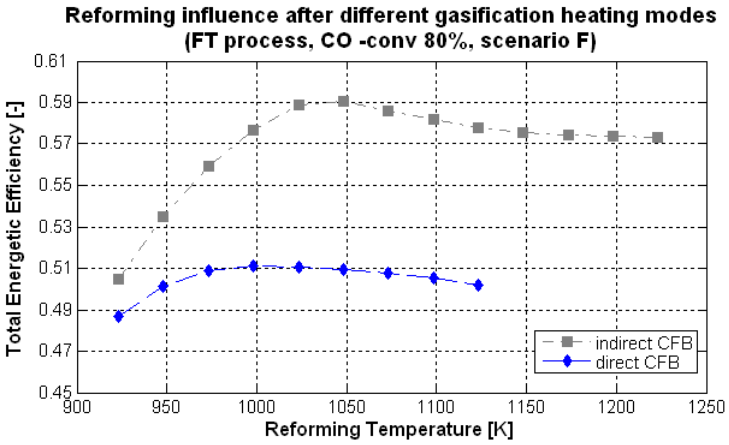

Figure 7.12: Effect of the reforming temperature [K] on the total energetic efficiency of the FT process for different heating modes of the CFB gasification at atmospheric pressure (scenario F)

As already seen before (section 7.3.1), the process performance increases with the CO-conversion. Since the composition changes, the equilibrium is affected and the optimal reforming temperature at which the efficiency is the highest changes (figure 7.13). At low CO-conversion, the highest efficiency is reached at a higher temperature compared to high CO-conversion because at higher temperature, there is slightly more CO that is formed (figure 7.11) (i.e. methane consumed) and hence the relative amount of converted CO is higher and more product is formed.

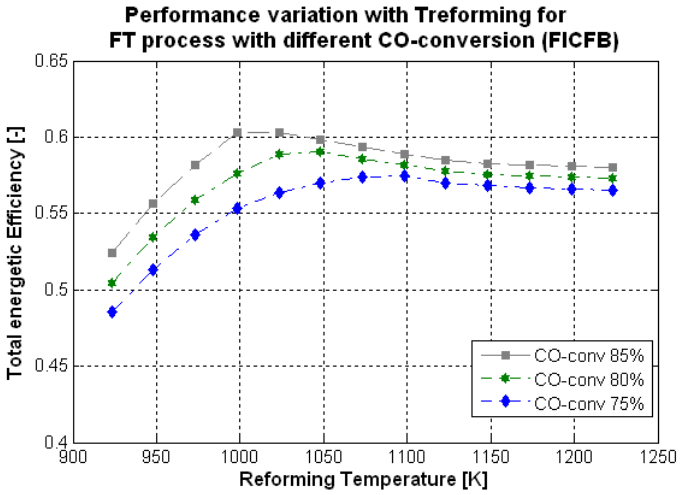

Figure 7.13: Effect of the reforming temperature [K] on the total energetic efficiency of the FT process with FICFB gasification (P=1bar) for different CO-conversions (scenario F (FICFB))

Another key parameter is the reforming pressure being equal to the gasification pressure. By increasing the pressure, the steam methane reforming equilibrium (eq.: 3.6) is shifted according to the Le Chatelier's Principle towards the formation of methane. Consequently, the optimal reforming temperature corresponding to no or few methane formation is higher in case of reforming at higher pressure, as it is seen from the fuel efficiency variation with the gasification/reforming pressure and the reforming temperature (figure 7.14).

At the optimal reforming temperature of 1050K (determined for 1bar), a pressure increase results in a fuel efficiency decrease because the FT-production yield is reduced, since more methane is formed at higher pressure (appendix F.1.2, figure F.3). At lower reforming temperature, the efficiency decrease is even more pronounced. By increasing the reforming temperature, the point where the equilibrium is shifted towards nearly complete consumption of methane can be reached and consequently the fuel efficiency isn't influenced anymore.

The pressure influence on the overall energetic efficiency is less pronounced because the decrease of the fuel production is outweigh partly by the reduced power consumption. This explains also the initial decrease of the production costs with increasing pressure (appendix F.1.2, figure F.2). At higher pressure the influence of the density on the size and hence on the investment is less important and consequently the production cost remain constant or increase.

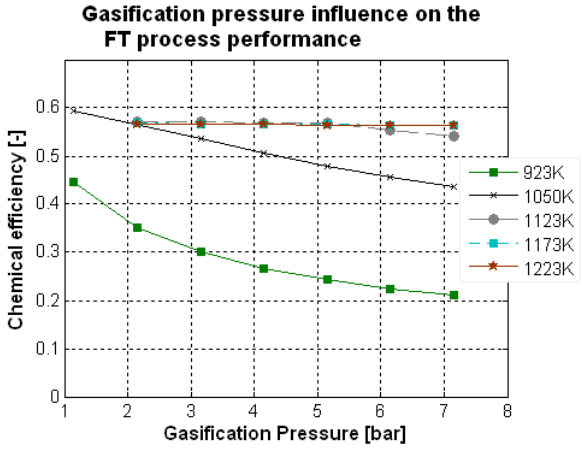

Figure 7.14: Gasification pressure influence on the chemical efficiency of the FT process (CO-conv 85%) with FICFB gasification (P=1bar) for different reforming temperatures (scenario O)

Hot utility consumption

The reforming temperature affects of course also the energy integration. The relative consumption of the process gas as combustible and the corresponding quantity in absolute terms changes, because the energy potential of the offgas and producer gas changes. Figure 7.15 illustrates the influence of the reforming temperature on the type and amount of fuel burned in the combustion chamber for the FT process (CO-conversion 80%) with indirectly heated fluidized bed gasification (scenario F (FICFB)). At low temperature no producer gas is burned due to the presence of methane. Since the offgas contains a large amount of methane, it is more advantageous to exploit the high energy potential of this stream by burning it. On contrary, at high temperature a small part of the producer gas has to be burned simultaneously to cover the heat demand because the energy potential of the offgas isn't sufficient. The relative energy supplied from the burning of the dried torrified gas and the char is almost not influenced. The total amount of the energy that has to be supplied by the combustion of producer gas and waste is also influenced by the reforming temperature and passes through a minimum at the optimal reforming temperature (around 1050K).

The efficiencies, as well as the energy supplied by the producer gas, offgas and waste combustion are compared for two temperatures situated below and above the optimal temperature: 948K and 1148K (table 7.6). The comparison between the two composite curves including a steam cycle (figure 7.16) reflects well this influence of the reforming temperature on the energy integration. The difference in the hot utility is illustrated by the length of the plateau at 1648K.

To summarize, it is more efficient for the FT-process to avoid the formation of methane reducing the FT-fuel yield and to perform therefore the reforming at a temperature slightly below the gasification temperature of 1123K.

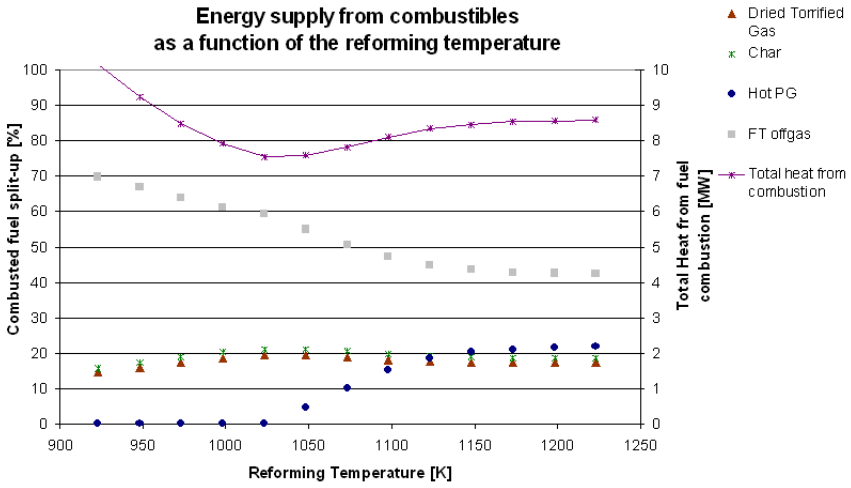

Figure 7.15: Relative [%] and absolute [MW] energy supplied from the combustion of producer gas, offgas and waste as a function of the reforming temperature (scenario F (FICFB))

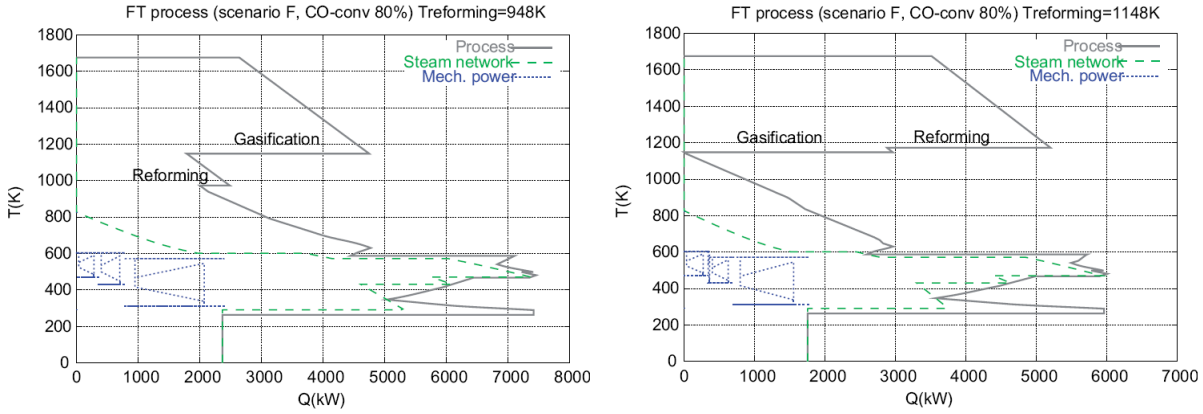

Figure 7.16: Comparison between the composite curves for two different reforming temperatures (left: 948K; right:1148K) for the FT process (scenario F (FICFB))

Parameter	Reforming at 948K	Reforming at 1148K
Combusted Fuel split-up	%	%
char	17.27	20.96
dried torrified gas	15.93	19.35
Hot producer gas	0	4.69
FT offgas	67.80	55.00
Total heat from combustion [MW]	9.24	7.60
ϵ_{chem} [%]	49.4	56.9
ϵ_{tot} [%]	53.5	57.6

Table 7.6: FT process: effect of the reforming temperature on the energy supply from producer gas, offgas and waste combustion and on the efficiency (scenario F)

Stepwise reforming

A detailed analysis of the composite curves at different reforming temperatures (figure 7.16), suggests that the energy integration could be improved by performing successive reformings at different temperatures. By performing a first steam methane reforming at lower temperature, the heat demand at high temperature is reduced. Consequently, the pinch point could be displaced to a lower temperature and the energy integration improved.

Different set-ups are considered, for the FT process (scenario G). First three reformers are operated successively at different temperatures between the inlet temperature of 1123K and the outlet high temperature reforming of 1623K (set-up1). Then the temperature of the first and second reformer are reduced, while the final temperature after the last reforming remains the HT-stage temperature of 1623K.

Performing the reforming in three steps without changing the inlet temperature (set-up 1) doesn't affect the energy integration and the total energetic efficiency compared to the case with one reformer (set-up 0) (table 7.7). This can be explained by the fact that the pinch isn't influenced and that the energy required at high temperature remains the same, as it can be seen on the composite curves (figure 7.17 (upper left and right)).

By varying the temperatures, the chemical efficiency and the total energetic efficiency are increased by a few % for one configuration (set-up 3) (table 7.7). The analysis and comparison of the corresponding composite curves (figure 7.17) shows that in this case, the pinch point occurs at a lower temperature. Set-up 2 is worse than the base case (set-up 1) because the temperatures of the different heat loads are changed but the pinch point is still determined by the gasification. The optimal configuration would be an intermediate case where two pinch points could be observed: one at the first reforming temperature and one at the gasification temperature. For the DME and MeOH process the same trend is observed; the performance is only slightly increased by performing the reforming in steps at different temperatures (appendix figure F.4).

Reforming set-up	0	1	2	3
Number of reformers	1	3	3	3
$T_{reform1}$ [K]	-	1123	923	973
$T_{reform2}$ [K]	-	1455	1223	1333
$T_{reform3}$ [K]	1623.15	1623.15	1623.15	1623.15
ϵ_{chem} [%]	50.3	51.0	49.3	53.4
ϵ_{tot} [%]	51.4	51.5	50.5	52.9

Table 7.7: Influence of the reforming modeling on the efficiency of the FT process (scenario G)

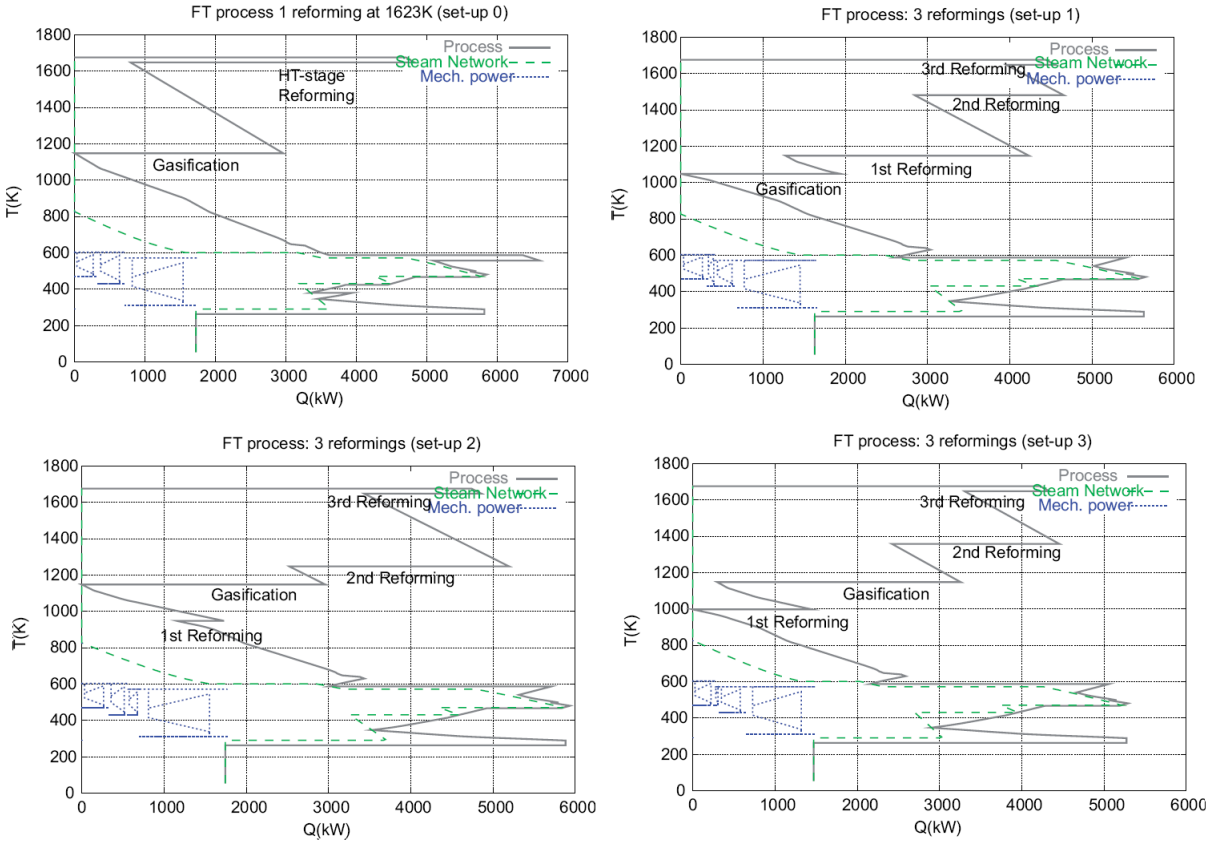

Figure 7.17: Comparison of the composite curves corresponding to different reforming temperatures and set-ups for the FT process (scenario G)

7.4.2 MeOH process

Since the optimal composition of the producer gas required for the methanol synthesis is different from the one for the FT synthesis, the best temperature to perform the reforming is also different. To find the optimal temperature, the chemical and total energetic efficiencies are computed for different reforming temperatures for the MeOH process with FICFB gasification (scenario H) (figure 7.18). As for the FT process, the efficiency passes through a maximum. In this case, the best reforming temperature is around 1223.15K.

Again a small improvement of the energy integration can be obtained by performing the reforming in two steps; the first reforming occurring at lower temperature. By performing the first reforming at 973.15K and the second one at 1223.15K, the total energetic efficiency is increased less than 1%. By decreasing the temperature of the first reforming to 923.15K, the total energetic efficiency increases by around 2.5%. This efficiency increase results from the improved energy integration related to the change of the heat demands at different temperatures.

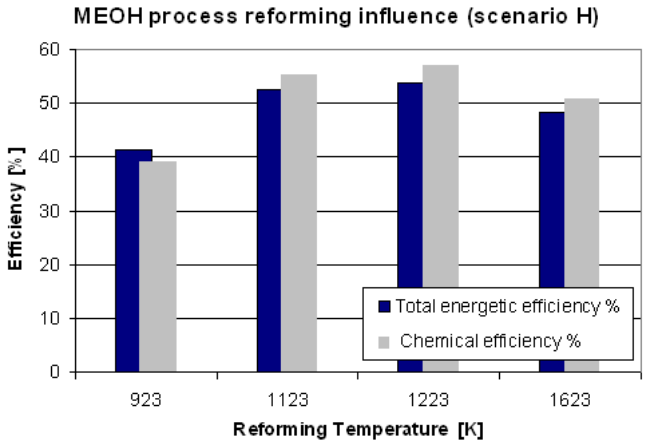

Figure 7.18: Reforming temperature influence on the MeOH process performance (P=1bar) (scenario H)

7.4.3 DME process

Similar essays for the DME process with FICFB gasification (scenario M), show that reforming slightly above the gasification temperature is advantageous. Increasing the temperature from 1123K to 1223K yields a large increase in the total energetic efficiency. The reforming temperature is therefore fixed at 1223K for the DME process for the subsequent essays (figure 7.19).

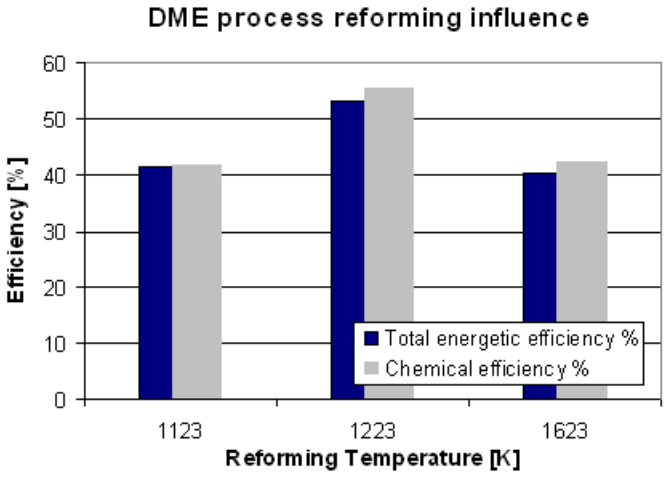

Figure 7.19: Reforming temperature influence on the DME process performance (P=1bar) (scenario M)

7.5 Energy Integration Optimization

After having analyzed the influence of some key parameters of the flowsheet modeling, the influence of the implementation and the characteristics of the energy integration are studied. The efficiency of the energy integration is determined mainly by the modeling of the energy system and the definition of the cogeneration system including the steam network, the hot utilities and the introduction or not of a gas turbine or a heat pump.

7.5.1 Steam Network

The process performance can be increased by introducing and optimizing a Rankine cycle producing the steam required by the process (e.g. gasification, drying, reforming, WGS), while producing mechanical power using back pressure and condensation turbines (table 7.8). The right choice of the number of production and utilization levels and of the associated pressure or temperature, can improve the energy integration, as it is seen on the basis of the DME process with directly heated fluidized bed gasification and reforming at 1123.15K (scenario I).

For steam networks characterized by different key parameters, table 7.8 compares the efficiencies and figure 7.20 illustrates the corresponding composite curves including the steam networks. The main characteristics of the steam network are identified: the steam superheating, the plateaus for the steam production, the preheating, and the plateaus for the steam condensation.

The integration of the steam network characterized by set-up 1 isn't optimal (figure 7.8 (left)), since the chosen values of the pressures and temperatures result in a pinch point between the process stream and the steam network. The system could be improved by increasing the temperature of the lowest utilization level (set-up 2) and by decreasing the pressure of the second steam production level (set-up 3).

In the optimal Rankine cycle, the utilization levels temperature corresponds to the temperature of the gasification steam evaporation, the steam requirement of the stripper of the MEA absorption unit and the cooling water.

For the DME process the set-up 3 is chosen for the steam network definition in the final model (appendix table E.9). Similar experiments allow to identify the optimal parameters for the steam cycle for the FT and MeOH process. The corresponding values for the different production and consumption levels are given in appendix table E.9.

Even if the investment costs are increased by introducing a steam network, the production costs are lower due to the better cogeneration, inducing a lower electricity demand.

As it will be explained in the following sections, the energy integration could further be improved by introducing a gas turbine using one part of the wasted energy potential.

Set-up	no steam network	1	2	3
Steam production pressure 1	-	80 bar	80 bar	50 bar
Steam production pressure 2	-	120 bar	120 bar	120 bar
Bleeding temperature (1)	-	423K	433K	433K
Bleeding temperature (2)	-	473K	473K	473K
Bleeding temperature (3)	-	293K	293K	293K
Condensation	-	292K	292K	292K
ϵ_{tot} [%]	40.13	42.79	43.02	43.32

Table 7.8: Optimization of the Steam Network of the DME process (scenario I)

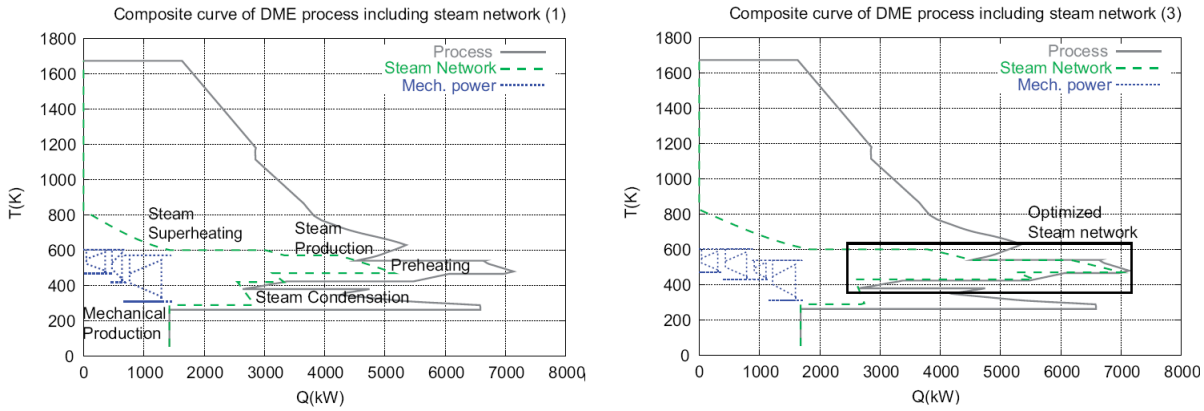

Figure 7.20: Composite curves including a steam network (not optimized (left), optimized (right)) for the DME process (scenario I)

7.5.2 Gas Turbine

The performance of the energy integration can be improved by introducing in some cases, notably for the MeOH and DME process, a gas turbine recovering the energy potential of the offgases. The impact on the performance is studied for the DME process with directly heated fluidized bed gasification (scenario I). A steam network having the optimal characteristics determined in the previous section is included. The comparison of the two composite curves (figure 7.21) shows that, by introducing a gas turbine, the excess energy contained in the offgas is converted at a higher efficiency to electrical power, and less excess heat is removed from the process.

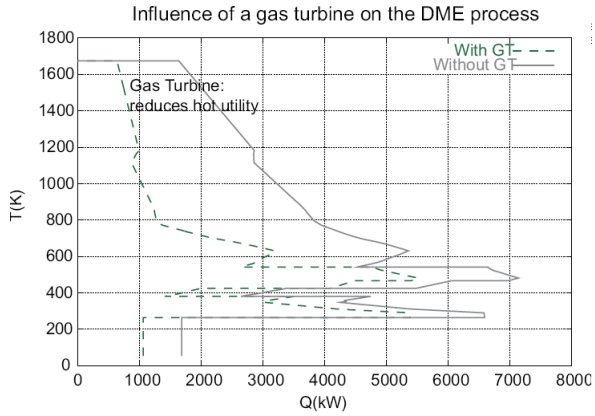

Figure 7.21: Composite curves including an optimized steam network (not shown) for the DME process: without and with gas turbine (scenario I)

A detailed analysis of the power balance (table 7.9) shows that more power is generated by introducing a gas turbine. Due to the higher conversion efficiency of the combined cycle, the overall power production is increased by 282.6kW, even if the power generated by only the steam turbine is lower. Less additional electricity has to be imported and consequently, the process performance, expressed by the total energetic efficiency is higher. The investment costs remain of the same magnitude, however the production costs are reduced due to the lower expenses for the electricity purchase.

Parameters		no GT	GT
Power Consumption [kW]	Process	2598.5	2598.5
Power Production [kW]	Steam Turbine	1633.7	1038.7
	Expansion Turbine	148.1	0
	Gas Turbine	0	1025.7
Net electricity [kW]	output	-816.7	-534.1
Performance [%]	ϵ_{chem}	45.1	45.1
	ϵ_{tot}	43.28	43.88

Table 7.9: DME process: mechanical power balance [kW] and efficiencies without and with gas turbine (scenario I)

The integration of a gas turbine decreases consequently the heat demand above the pinch point. The energy demand that has to be covered by the combustion of producer gas, offgas and waste (table 7.9) is decreased from 4.6MW to 1.25MW. Even with a gas turbine, there's still a small amount of energy that has to be supplied from the fuel combustion.

Combusted fuel split-up [%]	no GT	GT
dried torrified gas	31.86	100
1st Flash offgas	2.53	0
2nd Flash offgas	7.54	0
1st distillation offgas	58.07	0
Hot producer gas	0	0
Total Heat from combustion [MW]	4.62	1.47

Table 7.10: Relative [%] and absolute [MW] heat from waste combustion for the DME process without and with gas turbine (scenario I)

7.5.3 Hot Utility

The energy supply from the hot utility depends on the type of combustible that is burned in the combustion chamber. The effect on the performance is analyzed for one representative scenario of the FT synthesis with FICFB gasification (scenario J). Besides the FT-offgas, the dried torrified gas and the char, three different sources of combustibles are considered: dried wood, hot producer gas and cold producer gas. The solid waste (char) can be considered as potential fuel because the case of indirect gasification is considered.

Table 7.11 compares the relative energy supply from the combustion of the producer gas, offgas and waste and the corresponding efficiencies for the different options. The combustion of waste streams alone (i.e. dried torrified gas, FT offgas and char) isn't sufficient to cover the heat demand above the pinch point and therefore additional combustibles have to be used. For every option, the chosen additional fuel; that is to say hot or cold producer gas or wood, is the main energy source (38-45%). Besides this source, 23-30% of the heat is supplied by the combustion of the offgas from the FT separation. Even, if dried wood is the most efficient fuel for combustion, yielding the highest performance, it isn't used on a large scale in industry, because it isn't competitive with regard to operating and total costs, since the equipment for solid combustion is more expensive and complex than for gases. The burning of hot producer gas is more efficient, than the one of the cold producer gas, because the energy potential contained in the hot stream is higher. This influence can also be seen on the composite curves (reported in appendix F.1.4: figure F.5).

From these results it follows that only hot producer gas is chosen, besides the process waste streams (i.e. dried torrified gas, char and process offgas), as fuel for the combustion to supply energy in the subsequent scenarios.

Parameter	Hot PG	Cold PG	Dried wood
Combusted fuel split-up			
Dried torrified gas [%]	14.91	15.11	14.91
Char [%]	16.16	16.37	16.16
FT offgas [%]	24.15	23.68	30.08
Hot producer gas [%]	44.78	0	0
Cold producer gas [%]	0	44.84	0
Dried wood [%]	0	0	38.85
Total heat from combustion [MW]	9.87	9.74	8.23
Performance			
Net electricity output [kW]	-69.3	-234.5	67.6
ϵ_{chem} [%]	53.14	51.41	55.18
ϵ_{tot} [%]	52.95	50.81	55.52

Table 7.11: Effect of the combustible nature on the FT process performance (scenario J)

7.5.4 Heat Pump

In some cases where not enough excess energy is available to extract the exergy potential of the high temperature heat, the energy integration can be improved by introducing a heat pump transferring heat from a low temperature heat source to a higher temperature heat sink by using mechanical work. The influence of the integration of a heat pump is studied based on the methanol process (scenario K : steam drying and FICFB gasification). The introduction of a heat pump, characterized by an evaporation temperature of 378K, a condensation temperature of 428K and using water as refrigerant, increases the total efficiency by around 2% (table 7.12). More electricity can be produced by the Rankine cycle (i.e. less electricity has to be imported), since the exergy potential of the high temperature heat is made available for conversion into electricity by the heat transfer. Even if the investment costs increase due to the costs induced by the purchase of a heat pump, the production cost decrease, as less electricity is consumed due to the better cogeneration.

Parameter	No Heat Pump	Heat Pump
ϵ_{tot} [%]	51.32	53.25
Net electricity output [kW]	-2429.1	-1815.7
TGRC [MUSD]	36.0	38.1
Production costs [USD/MWh]	199.2	190.8

Table 7.12: Influence of the introduction of a heat pump on the MeOH process performance (scenario K)

The improvement of the energy integration can be seen on the corresponding composite curves (figures 7.22) including the steam network. The Rankine cycle can generate more electricity after the introduction of the heat pump because more excess heat is available. The optimization of the steam network, by choosing the right production and consumption levels, would increase the efficiency slightly. Figure 7.23, illustrates how the heat pump is integrated in the energy integration by removing heat at low temperature and releasing it at higher temperature. The heat that is transferred comes from the heat load of the MEA absorption unit (steam at 150^oC with a temperature of 110^oC in the condenser).

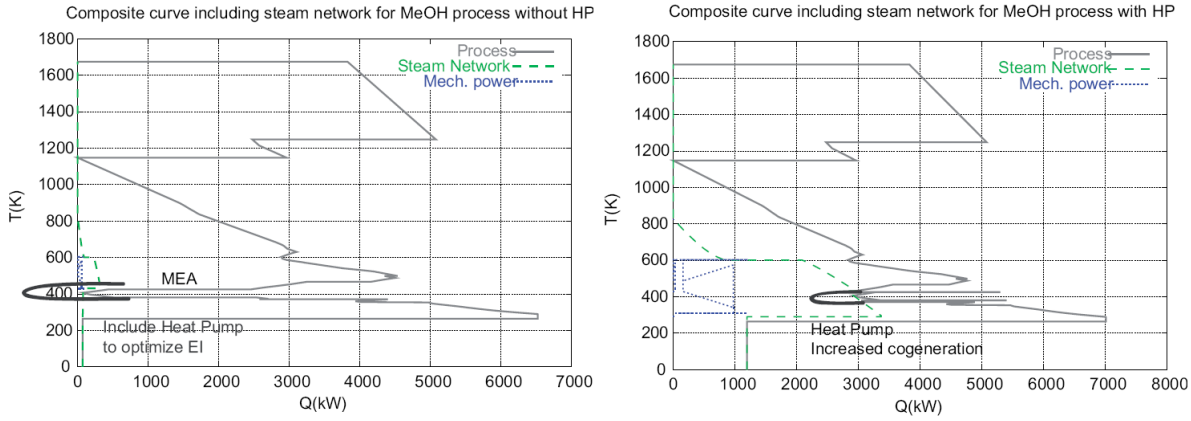

Figure 7.22: Composite curves comparison for the MeOH process (scenario K) without (left) and with the integration of a heat pump

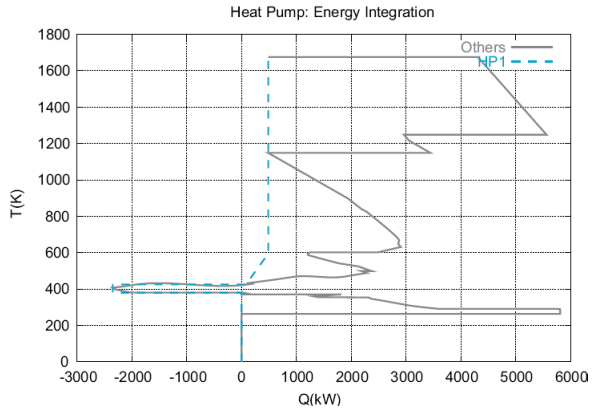

Figure 7.23: Effect of the introduction of a heat pump on the energy integration (scenario K)

7.5.5 Reactants Preheating

The modeling itself of the gasification or the synthesis reactor can also offer opportunities to increase the efficiency of the overall integrated system. By considering isothermal reactors, the contribution of the chemical reaction and the heat transfer can be decoupled. Reactants preheating before the isothermal reactor can improve the energy integration.

In the case of the indirectly heated entrained flow gasification (gas1) being performed at 1613.15K; the energy integration can be improved considerably by preheating the reactants up to 1123K before the gasification. This influence on the performance is analyzed for the FT process (scenario N) by comparing the composite curves (figure 7.24) and the numerical values of the process performance (table 7.13). The main reason for this improvement is the reduction of the heat demand at high temperature inducing a reduction of the hot utility and so of the energy to be supplied by the combustion of offgas and waste. Another advantage is that the contribution of the hot producer gas is decreased and the one of the waste stream (offgas) increased. One drawback is that, electricity isn't coproduced any longer and that instead electricity has to be imported; consequently the production costs are increased. The Rankine cycle for the cogeneration can't operate anymore as not enough supplementary heat below the pinch is available. In this case, the introduction of a heat pump could perhaps improve further the performance by moving heat from a low temperature to higher temperature, but only a few electricity can be expected as the pinch around 600K will be activated soon.

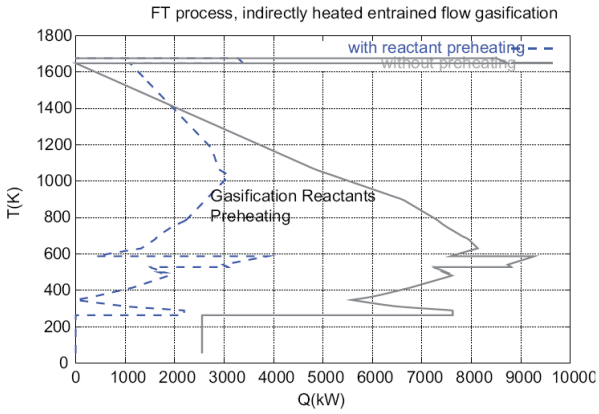

Figure 7.24: Composite curves comparison for the FT process with entrained flow gasification without/with reactants preheating (scenario N) (steam network not shown)

Parameter	No preheating	Preheating
ϵ_{chem} [%]	30.99	63.71
ϵ_{tot} [%]	41.8	63.5
Net electricity output [kW]	2356	-58.11
Combusted fuel split-up		
Dried torrified gas [%]	8.54	20.34
Char [%]	0.59	1.40
Hot producer gas [%]	82.87	39.24
Offgas FT [%]	8.01	39.02
Total heat from combustion [MW]	17.24	7.24

Table 7.13: FT process: effect of the reactant preheating on the efficiency and on the energy supplied from the combustion of producer gas, depleted streams and waste (scenario N)

7.6 Further Improvements

The previous studies showed that the performance of a process depends on many factors that can each one offer the opportunity to induce potential ameliorations by choosing the optimal values. These factors influence the two key elements defining the overall performance: the chemical productivity and the energy integration.

Besides the parameters studied here many other factors influence the chemical performance of the system and much more options could be envisioned to improve the energy integration and hence the overall performance. In this work, it was focused only on some important parameters due to time constraints. Some suggestions for further studies of potential improvements are listed below.

- Study the influence of other key factors, such as the wood humidity, the gasification agent preheat temperature, the WGS temperature, the amount of water added to WGS, etc.
- Study the influence of the synthesis temperature and pressure in detail.
- Study the influence of the synthesis temperature and pressure on the selectivity and conversion of the FT process (e.q.: 3.16).
- Study the influence of the catalyst activity and selectivity. In this work, the catalyst is chosen in accordance with the process operating conditions from literature.
- Study the effect of additional recycling from the purification section.
- Study the option to remove CO_2 before the FT-process.
- Study the option to remove the WGS section in the DME process after certain gasification technologies.
- Study the influence of the reforming temperature after other types of gasification.
- Study the influence of the gasification and reforming pressure for the other options.
- Study and improve the energy integration for other options.
- Etc.

Chapter 8

Process Performance Comparison

In the previous chapters, the key parameters affecting the chemical and overall efficiencies were discussed. With these results improved models are set up for different synthesis processes. The key parameters and the characteristics of the energy integration are summarized for three synthesis models in appendix E. Based on these final models, the thermo-economic performances of the different technological options for drying, gasification, gas cleaning and synthesis, are computed and compared between each other and with literature data. Literature comparison allows to determine the accurateness of the developed models and the comparison between the different options reveals some general trends regarding the competitiveness.

8.1 Comparison with Literature Data

The production of biofuels from biomass is investigated by different research centres. The ECN [10] and the University of Utrecht in the Netherlands have done many studies on biomass. The FT and MeOH process models developed in this work are compared with conceptual similar process layouts designed by the ECN.

8.1.1 FT Process

The ECN model of Fischer-Tropsch process is designed with the following key assumptions (ECN publication [16]):

- $400 MW_{HHV}$ input scale, dry biomass 72.4 tonnes/hour
- Steam drying
- Directly heated circulating fluidized bed gasification at 1.2 bar and 850^oC
- No reforming
- Wet gas cleaning
- Partial water-gas shift
- One-pass FT-synthesis, 70% CO-conversion
- Slurry FT reactor at 60 bar
- FT-fuel purification, fractionation, hydrocracking

This process layout corresponds to the model developed in this work with directly heated fluidized bed gasification and without steam reforming (gas6direct) (with the same values for the key parameters). The corresponding composite curve is represented in appendix F.2 (figure F.7).

One essential difference between both systems consists in the upgrading. In the ECN study, the FT crude fuel is purified by distillation separating the light and heavy compounds and by hydrocracking of the heavy compounds to increase to diesel fraction, while in this work the final product is the crude FT-fuel. Other differences are that, in the ECN model the pyrolysis step isn't considered separately and that a tar cracker is introduced before the wet gas cleaning section. Moreover, oxygen is produced by cryogenic air separation in the ECN study and by oxygen transfer membranes in this work. Despite these differences, the key assumptions are the same and both processes can be compared to highlight the differences and similarities. Table 8.1 summarizes the performances of both FT processes.

Parameter	Process from [16]	FT process
Overall balances		
Fuel output [MW]	131.2 (HHV)	119.8 (LHV)
Power Gas Turbine [MW_e]	38.2	9.5
Power Steam Turbine [MW_e]	32.6	72.4
Power Expansion Turbine [MW_e]	1.03	3.8
Power Needs [MW]	33.5	35.2
Power Output [MW_e]	38.2	50.5
Fuel Efficiency [%]	32.8	31.96
Total Efficiency [%]	42.4 (HHV)	45.4 (LHV)
Economic Analysis	M€	$M€_{2008}$
Pretreatment	46.0	45.4
Pyrolysis	-	9.2
Gasification	77.6	109.8
Air separation	34.3	45.96
Gas Cleaning	73.3	6.0
FT reactor	21.7	64.5
Compressor	37	-
Hydrocracker	24.9	2.5 (flash)
Steam Cycle + HEX	37.8	25.5
Gas Turbine	56.0	3.6
Expansion Turbine	2.3	2.0
Total Investment	410.9	314.5

Table 8.1: Performance comparison of the FT process with literature data [16]

The comparison shows that the fuel efficiency of both systems is similar (even if expressed on a different basis HHV versus LHV)[1]. The difference in the overall performance comes from the differences in the process layout mentioned before and from the implementation of the power generation system.

The total investment costs are of the same magnitude, but somewhat lower for the model developed here. The analysis of the investment costs distribution shows that, the main difference comes from the differences in the modeling of the gas cleaning, the upgrading and the cogeneration system. For another scenario, where an oil scrubber is used instead of the tar cracking, the related costs found in the ECN study are 6.8M€ which is in the range of the corresponding costs found in this work.

The introduction of the purification step separating the different fractions of the crude FT-fuel in the present model, would increase the costs and change the energy integration.

The estimation of the FT reactor costs, including the compressor costs, as well as the pretreatment costs (i.e. drying) evaluated in this work with the correlation from [61, 62] are

[1]The HHV being bigger than the LHV, the efficiency based on the HHV is lower

appropriate since the results are in the same range than the estimations from ECN based on the scaling method.

Despite all the differences, it seems that the results found in this work are quite realistic. A more accurate comparison could be made by introducing the crude FT-fuel upgrading and by implementing identical cogeneration systems.

8.1.2 MeOH Process

The methanol process performance is studied in the ECN publication [29] for several configurations differing mainly in the gasification type (indirectly or directly heated). The comparison with the model developed in this work is made based on the concept 6 from [29] having the following characteristics:

- $430 MW_{HHV}$ input scale (80 tonnes/hr biomass)
- Steam drying
- Indirectly heated fluidized bed gasifier at 1.2 bar and 860^oC
- Steam reforming at 890^oC
- Wet gas cleaning
- Partial water-gas shift
- Methanol reactor operating at 260^oC with recycling
- Refining to recover pure MeOH (i.e. 100%)
- Steam Cycle

The ECN process design is similar to the model developed in this work with indirectly heated fluidized bed gasification (gas5indind) followed by steam reforming at 890^oC (corresponding composite curve represented in appendix F.2 figure F.6). A conceptual difference between both models is the refining option. In the ECN model, the methanol is purified up to a purity of 100% by different separation steps: two flash drums, Selexol CO_2 removal, water separator and PSA membranes, whereas in this work purification is done by distillation to reach a purity around 99.95%. Another difference is that in the ECN process no separate pyrolysis step is included before the gasification.

The performances of both MeOH models are summarized in table 8.2.

The fuel efficiency and total efficiency of both models is similar, although the investment costs estimated in this work are two times higher. All in all, the model seems to be quite coherent, however the equipment costs are overestimated.

The slight difference in the energetic efficiency can be explained by differences in the modeling assumptions, mainly regarding the upgrading and the definition of the steam network.

The relative costs distribution analysis, reveals that the difference in the investment is essentially due to the overestimation of the gasification costs and the reactor costs. The costs for the gasifier are estimated based on the cost for a FICFB gasifier and a multiplication factor of 4 was introduced to take into account the special construction and the fact that the equipment is still under development; this value seems to be overestimated. Without this factor the costs

Parameter	Process from [29]	MeOH process
Production		
Fuel output [MW_{LHV}]	223.9	214.2
Production MeOH [tonne/hour]	40.5	38.9
Power output [MWe]	-17.3	-25.5
Fuel efficiency [%]	58.9	56.4
Total efficiency (LHV) [%]	53.9	52.8
Economic Analysis	$MUSD_{2001}$	$MUSD_{2008}$
Pretreatment	38.2	60.2
Pyrolysis	-	12.2
Gasification	30.4	201.91
Steam Reformer	43.3	27.5
Gas Cleaning	26.2	6.9
WGS	1.9	3.9
CO_2 removal	9.5	26.3
MeOH reactor	34.5	108.6
Compressor	16.5	-
Refining	19.5	5.9
Steam System + HEX	17.9	38.6
Expansion Turbine	-	3.1
Total Investment	237.9	495

Table 8.2: Performance comparison of the MeOH process with literature data [29]

would be in the same range. The costs of the methanol reactor including the compressor costs, are twice as high than for the estimations of the ECN study. This difference can be related to a different synthesis pressure, synthesis technology or sizing and cost estimation methodology. The difference in the refining costs comes from the different purification options chosen. To obtain totally pure methanol further treatment would be required to remove the traces of water and ethanol. This treatment would add additional costs because the costs increase with the degree of purity and would alter the energy integration.

Consequently, it seems that some costs are overestimated, while others are underestimated. More detailed information on the commercial available equipment at industrial scale could increase the reliability of the cost estimation. However, the modeling seems to be coherent.

8.2 Process Options Comparison

The thermo-economic performance of different process options is compared based on two key parameters: one for the thermodynamic performance; the total energetic efficiency referring to the overall process performance including the energy integration and one for the economic performance; the total grass roots costs. All the comparisons are done for an installation having a nominal thermal capacity of $20MW_{th}$ (based on the LHV).

Different process options for the producer gas production and treatment are compared based on the final FT process and the general trends remaining true for the other synthesis processes are identified. For one gasification technology the impact of the dryer type (drying agent: air or steam), the heating mode (indirect or direct) and the gas cleaning technology (hot or cold GCL) is analyzed (section 8.2.1). In another series of experiments the influence of the gasification technology is studied in detail (section 8.2.2). Then, the different synthesis options (section 8.2.3) are compared between each others for the most efficient options.

8.2.1 FT process options for CFB gasification

By following the general process layout, the different options are analyzed and the causes for the thermo-economic performance differences are revealed for the FT process (appendix table D.3: base-case 1).

The comparison of the different pretreatment options of the FT process with fluidized bed gasification (figure 8.1) reveals some general trends:

- The drying technology doesn't affect the process energetic efficiency, however steam drying is more expensive.
- Indirectly heated gasification has a higher thermo-economic performance than directly heated gasification.
- Hot gas cleaning doesn't influence the overall efficiency, but reduces the economic performance.

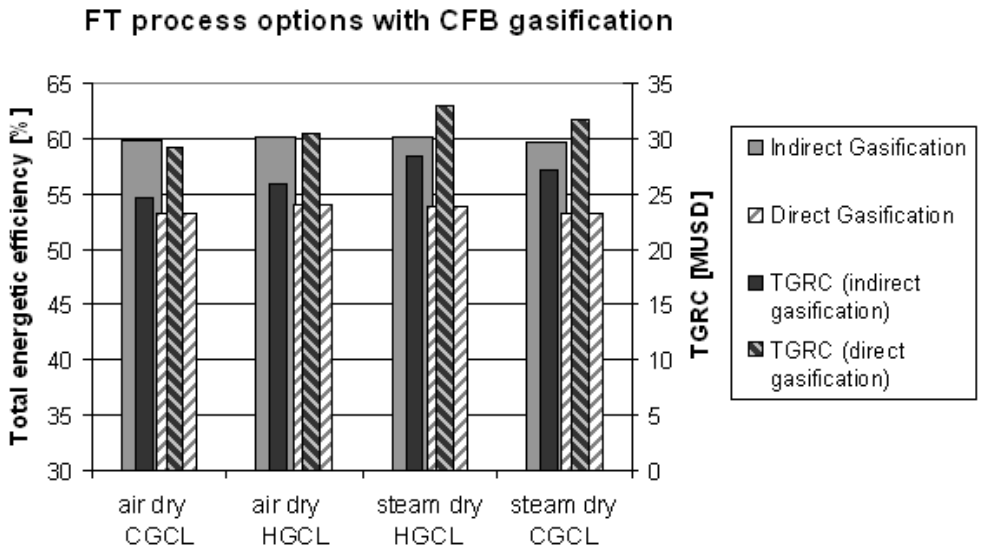

Figure 8.1: Thermo-economic performance for different FT process options with CFB gasification (base-case 1)

A detailed analysis of the power balances (figure 8.2) and the energy supplied by the various combustibles (figure 8.3) identifies the differences induced by the process alternatives. The economic competitiveness of the different options is compared based on the investment and production costs (figure 8.4).

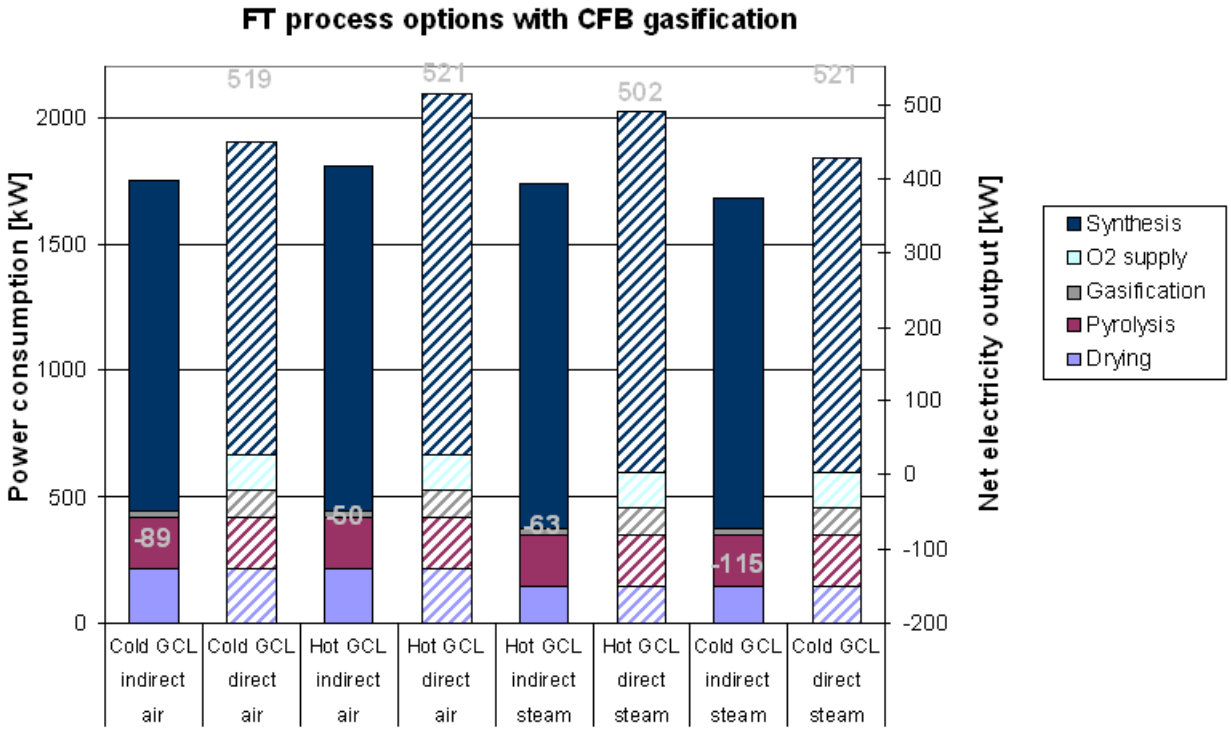

Figure 8.2: Power consumption split-up (represented by bars) and net electricity output [kW] (given by numbers) for the different options of the FT process with CFB gasification (base-case 1)

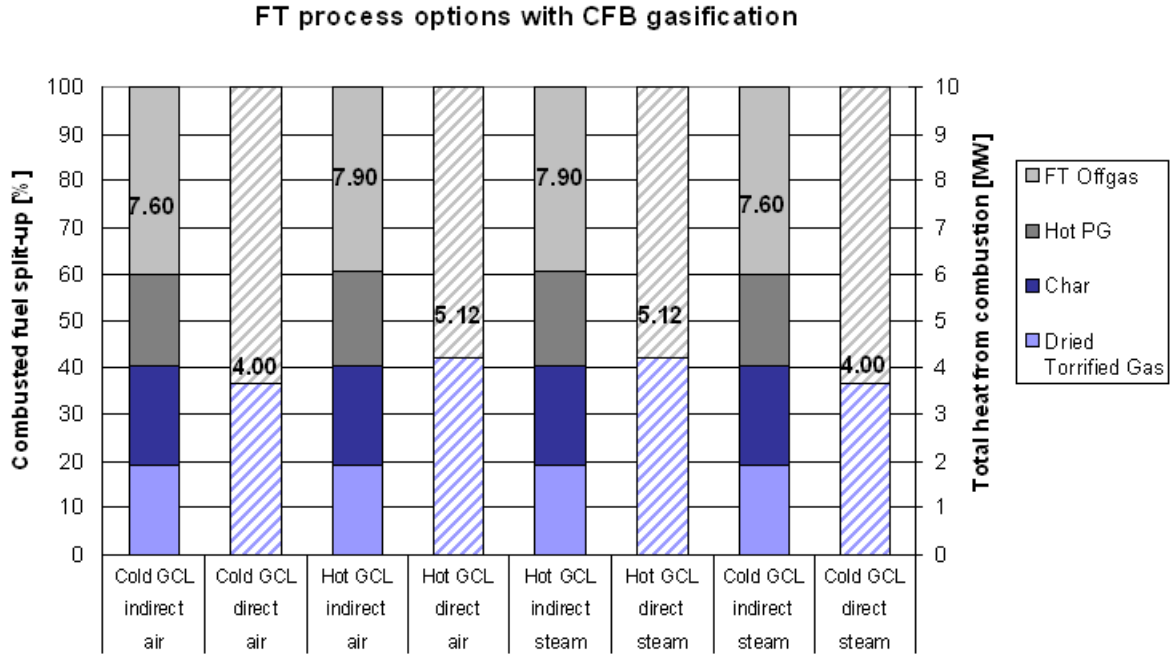

Figure 8.3: Relative and total energy supplied [MW] by the producer gas, offgas and waste combustion for the different options of the FT process with CFB gasification (base-case 1)

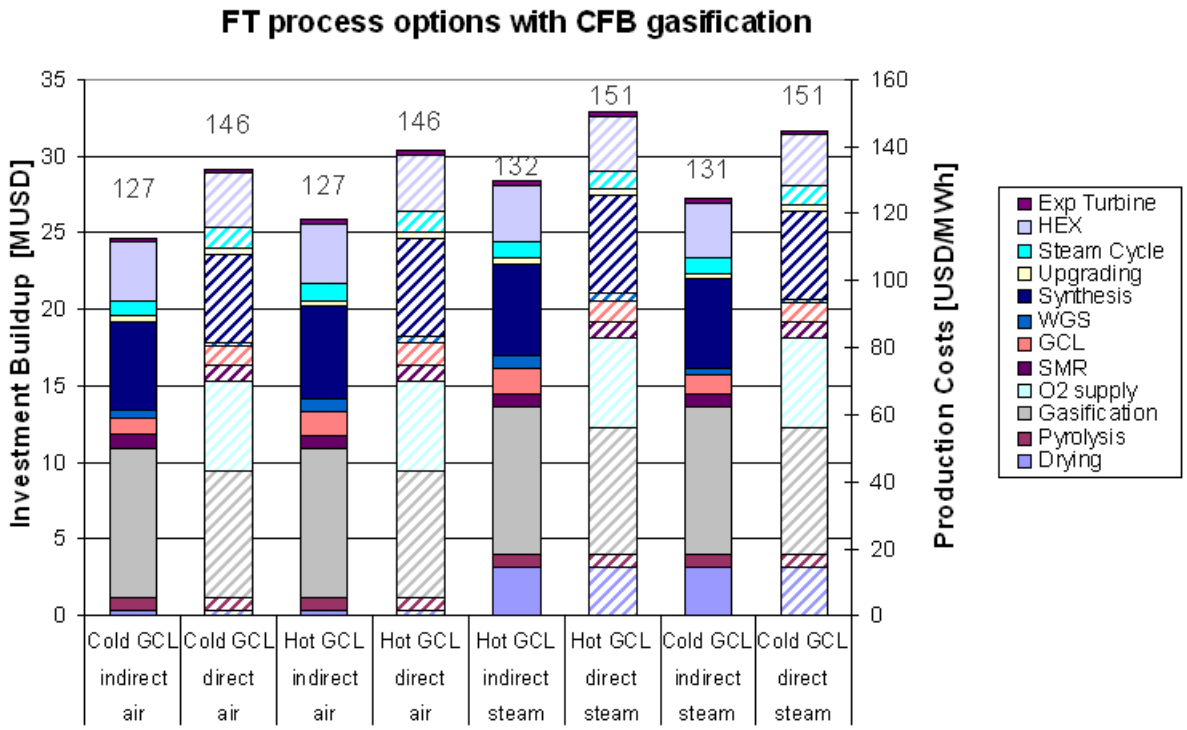

Figure 8.4: Investment buildup [MUSD] and production costs [USD/MWh] for the different options of the FT process with CFB gasification (base-case 1)

Air versus Steam drying

By changing the drying mode, all the other choices remaining the same, the efficiency isn't influenced. The drying technology doesn't interfere with the reactants elementary composition because the biomass humidity is specified. The power consumption by air drying is slightly higher and the net electricity produced is almost constant or slightly higher due to the influence on the cogeneration system. The overall energy supplied from the hot utilities, as well as the relative consumption of the different fuels isn't affected by the drying option since the heat demand above the pinch point isn't affected. From an economic point of view, air drying is more profitable due to the lower investment costs.

The comparison of the composite curves of air and steam drying (figure 8.5), emphasizes these findings. As a consequence of the modeling differences, the composite curve aspect changes in the range of the drying temperature. Air drying is represented by a cold stream representing the air preheating and a hot stream for air cooling (after dryer), while steam drying is characterized by a cold stream (vapor heating), a plateau representing the water condensation (hot stream) and a hot stream for water cooling.

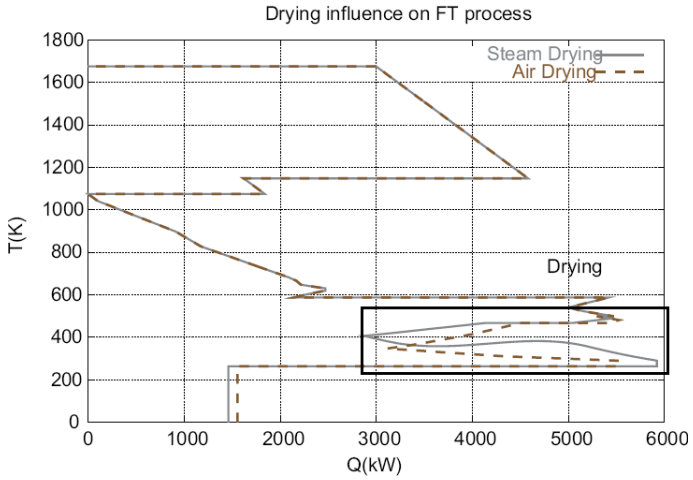

Figure 8.5: Composite curves for the different drying options of the FT process including a steam network (not shown)(base-case 1: indirectly heated, cold gas cleaning)

Gasification heating mode

The chemical and overall energetic efficiency of the process are determined by the heating mode of the gasifier. Indirectly heated gasification has a higher performance because the fuel efficiency is higher due to the more appropriate stoichiometry of the producer gas for the synthesis (i.e. higher hydrogen content)(section 7.2). Moreover, the heating mode of the gasifier and in a lesser extend of the reformer influences also the energy integration by the different specific heat capacity.

The most relevant thing to notice from the comparison of the corresponding composite curves, is the disappearance of the plateau corresponding to the gasification temperature (figure 8.6). In the case of directly heated gasification, the heat is supplied internally by oxidation and hence no external heating is required. However, it has to be accounted for the heat and power supply for the production of the oxygen needed for the oxidation in directly heated gasification.

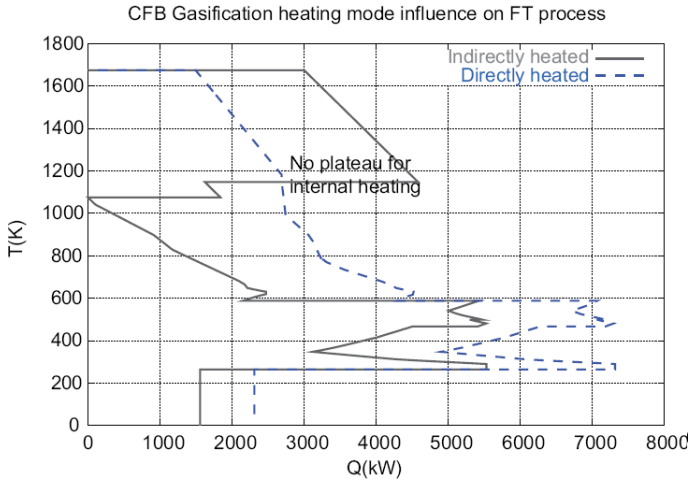

Figure 8.6: Composite curves for the different heating modes of FICFB gasification for the FT process including a steam network (not shown) (base-case 1: air drying, cold gas cleaning)

The comparison of the power balance, shows that in both cases the compression power consumed to reach the synthesis pressure is the largest contribution. The process with directly heated gasification consumes more power because additional power is needed to compress the oxygen up to the gasification pressure (if different from atmospheric pressure) and to produce the oxygen by the ion transfer membranes requiring a pressure difference (label: O_2 supply). Despite the larger power consumption, more electricity is generated by the process with directly heated gasification. The Rankine cycle coproduces more power because the specific heat capacity of the producer gas is increased by the partial oxidation and consequently more excess heat is available.

For the directly heated gasification, less energy has to be supplied above the pinch point by combustion, as it can be seen from the composite curves (figure 8.6) and from the numerical values. For the directly heated gasification, the energy is supplied exclusively by the combustion of FT offgas and the dried torrified gas and consequently the relative percentage of combusted offgas is higher. The combustion of the waste streams is sufficient to cover the demand and therefore no hot producer gas has to be burned. For the indirectly heated gasification in contrast, some producer gas has to combusted to cover the heat demand.

From an economic point of view directly heated gasification is also penalized. Even if, the costs of the gasifier itself are lower due to the simpler construction, the total investment is higher due to the additional costs for the oxygen production. Despite the better cogeneration, the earnings related to the electricity generation are not sufficient to outweigh the higher investment cost. Consequently, the production costs are higher for processes with directly heated gasification.

Cold versus Hot gas cleaning

After the gasification the producer gas has to be cleaned to remove the impurities. The cleaning technology and the degree of impurities influence therefore the process performance. Based on the simplified modeling of the cleaning section, the conclusion that the thermo-economic performance isn't influenced much is drawn. Despite the slightly higher investment induced by the higher gas cleaning and WGS costs, the production costs are of the same magnitude due to the reduced electricity costs. The Rankine cycle generates slightly more electricity in the case of hot gas cleaning because slightly more excess heat is available. Consequently, the net electricity output is somewhat larger, even if the power consumption is slightly higher. The energy supplied by combustion and the relative consumption of waste and process streams as combustible are nearly identical. These conclusions are confirmed by the shape of composite curves (appendix F.3, figure F.8).

The remaining drawback of hot gas cleaning is that this technology is still under development. The applicability at large scale isn't proven and the modeling and costs estimation are only based on assumptions.

Conclusion

For the different upstream process options, the choice of the gasification heating mode is crucial. The influence of the drying and gas cleaning technology is much less pronounced. The best combination, leading to a high efficiency and reduced investment and production costs, appears to be air drying, followed by indirectly heated gasification and cold gas cleaning (since hot gas cleaning isn't established yet) (figure 8.1).

8.2.2 FT process gasification options

The different gasification technologies; entrained flow (EF) and fluidized-bed gasification (CFB), the different heating modes; indirectly and directly heated and the different configurations; with or without high-temperature stage reforming and/or quencher are analyzed for the FT process with air drying and cold gas cleaning (appendix table D.3: base-case 2).

The thermo-economic performance of the different options is expressed by the total energetic efficiency and the investment or production costs (figure 8.7).

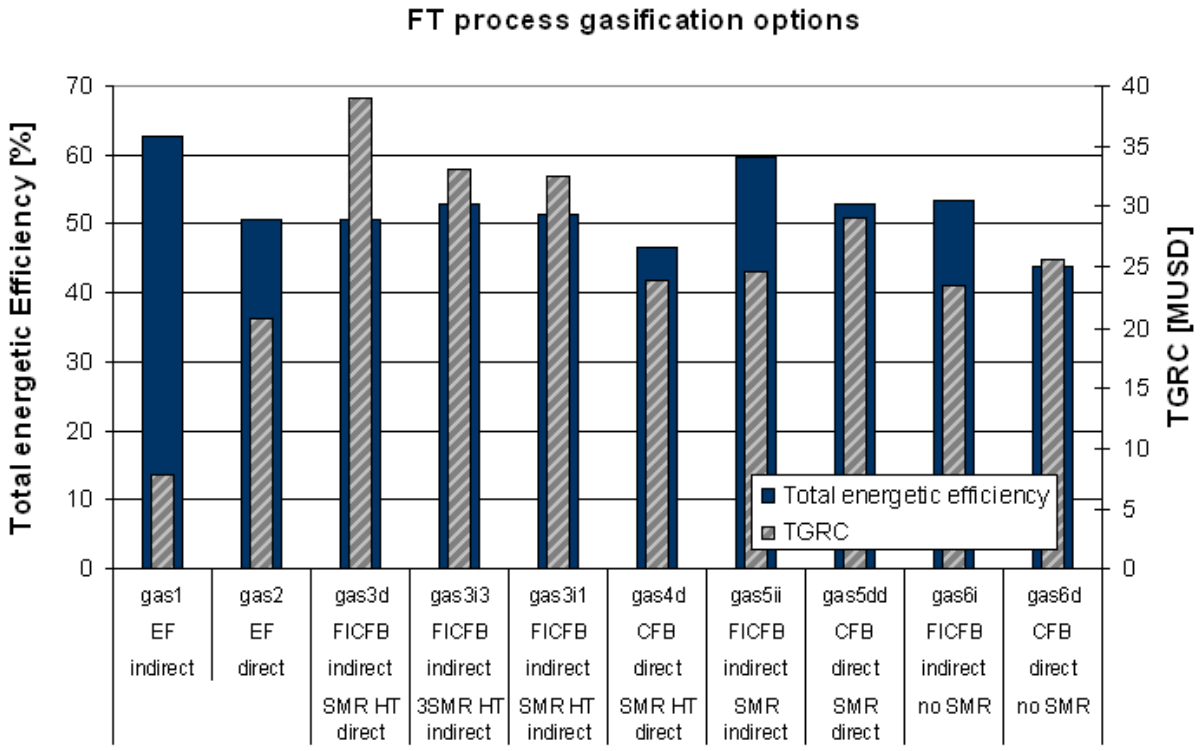

Figure 8.7: Total energetic efficiency [%] and total grass roots costs [MUSD] for the different gasification options of the FT process (base-case 2)

The main performance differences are assessed by a detailed analysis of the power balances (figure 8.8), the energy that has to be supplied by the combustibles (hot utility) (figure 8.9) and the investment buildup (figure 8.10).

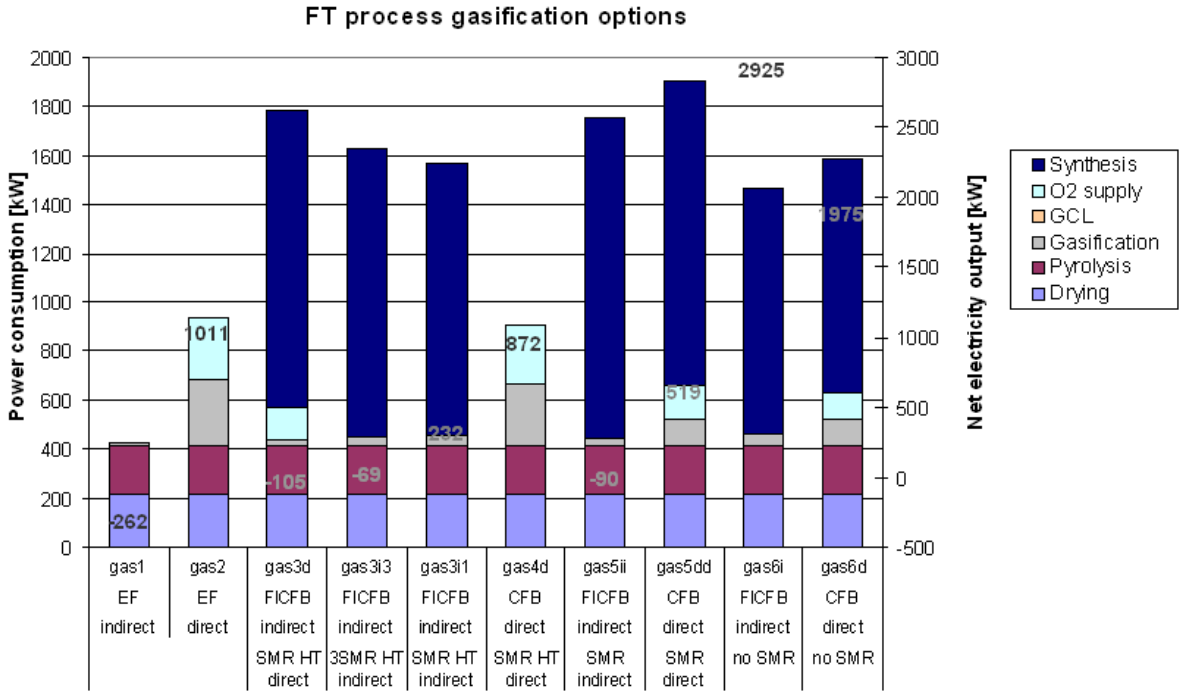

Figure 8.8: Power consumption buildup [kW] and net electricity output [kW] for the different gasification options of the FT process (base-case 2)

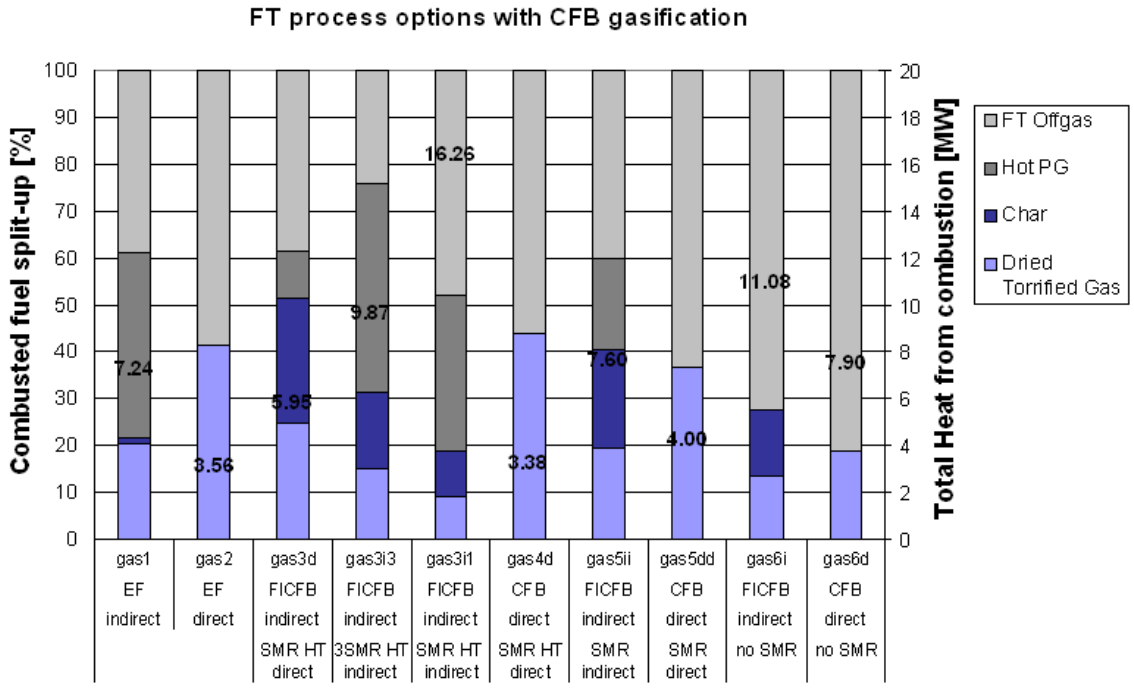

Figure 8.9: Relative and overall energy supply from the combustion of producer gas, offgas and waste for the different gasification options of the FT process (base-case 2)

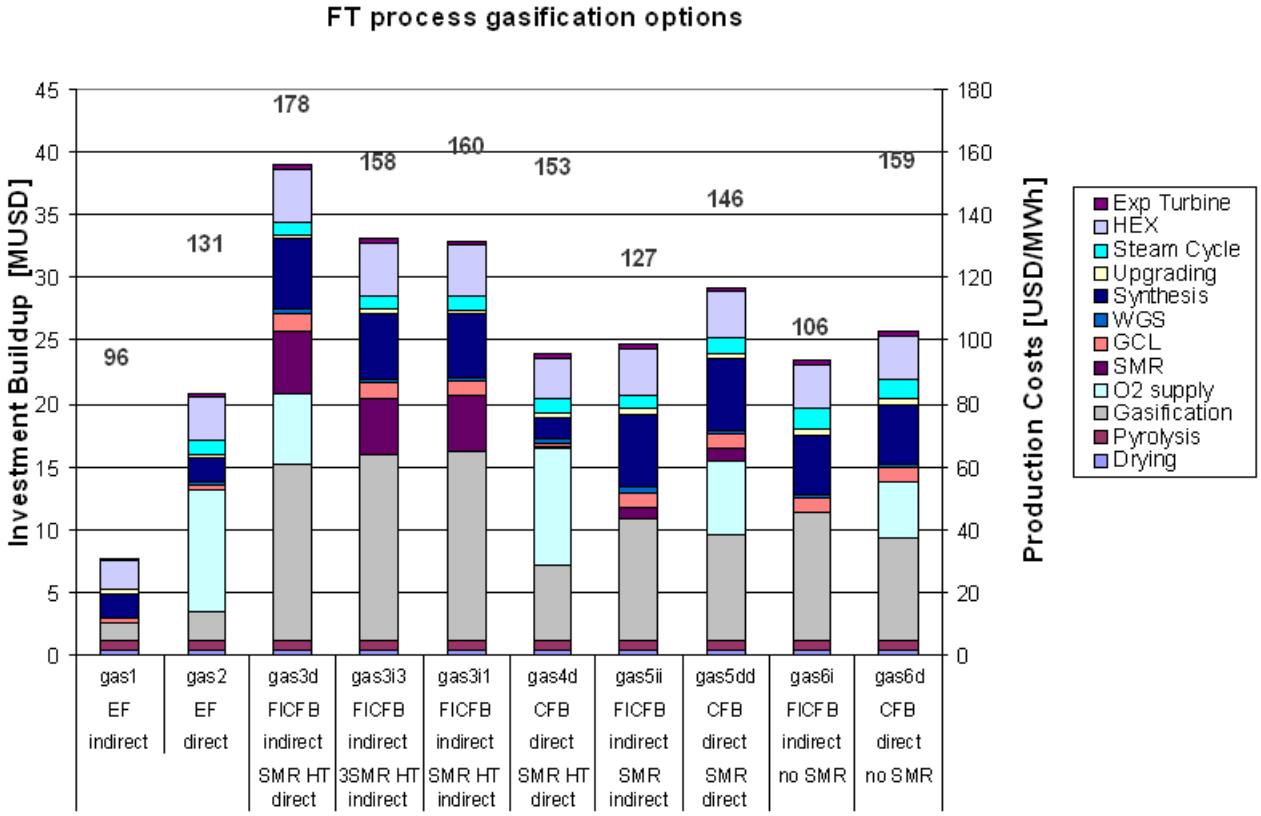

Figure 8.10: Investment buildup [MUSD] and production costs [USD/MWh] for the different gasification options of the FT process (base-case 2)

Gasification Technology

According to the results of the thermo-economic modeling, indirectly and directly heated entrained flow gasification (gas1, gas2) are more efficient than fluidized bed gasification. However, these results have to be considered with precaution. The high efficiency of the indirectly heated fluidized bed gasification is achieved with reactants preheating (section 7.5.5); without preheating the total energetic efficiency is reduced by half and worse than the CFB gasification. The problem associated with the indirectly heated EF gasification is the required very high temperature (1623K). Only few information about the technical realization of indirectly heated EF biomass gasification are found in literature. According to information from [26], the heat could be supplied by circulating hot synthetic olivine.

In the case of directly heated entrained flow gasification, the heat is supplied by oxidation and is hence less problematic. Nevertheless, this type of gasification has only few applications in biomass gasification due to the required reduced particle size (section 3.2.2). This problem can however be solved by introducing the torrefaction step prior to gasification, pulverizing the wood to small size particles.

Another important thing to notice is the low power consumption of the EF gasification which can be explained by the modeling. EF gasification is performed under pressure (30 bar) and consequently the producer gas is already under pressure and no gas compression is required to reach the FT-synthesis pressure of 25 bar. The power needed to pressurize the reactants before the gasification or pyrolysis is neglected since the reactants are in the solid/liquid state.

The comparison between directly heated EF (gas2) and CFB (gas4d) gasification, both

operated at 30 bar, shows that the efficiency is higher for the EF gasification, while the power consumption/generation and the amount of heat that has to be supplied by combustion are almost the same. These results are in accordance with [66], where it is stated that oxygen-blown EF gasification of torrified wood is an attractive alternative for high temperature gasification because it reduces the thermodynamic losses. However, the application in practice has to be proven.

Concerning the results of the economic evaluation, it is predicted that the costs for the EF gasifier are lower because of the much simpler construction. The reactor can be considered as a simple vessel. However, this costs might be underestimated.

For a more reliable comparison of both technologies for biomass gasification, additional information about the exact technical realization of EF gasification at small and large scale are required. Due to this lack of information on industrial applications of EF gasification, this option is studied in this work only on a theoretical basis and it focused more in detail on the CFB gasification. However, EF gasification could have a great potential in the perspective of biofuel production and therefore it is worth to investigate in the research and development of this option.

Gasification heating mode

The influence of the heating mode was studied in the previous chapter (8.2.1) based on the directly and indirectly CFB gasification with reforming around the gasification temperature (gas5ii, gas5dd). The trends that were pointed out can also be distinguished for the other configurations. In general, indirectly heated gasification has a higher thermo-economic performance. The directly heated gasification consumes more power due to the oxygen compression and generates more power through the Rankine cycle because of the larger excess heat.

The difference in synthesis power consumption between the two gasifications options with one-step reforming at high temperature (1623K): gas3i1 (indirectly heated) and gas4d (directly heated) (figure 8.8), is due to the different operating conditions. The indirectly heated gasification is performed at atmospheric pressure, while the directly heated gasification is operated under pressure (30bar). In the last case, the power for the compression is neglected, as it is performed before the gasification and hence no gas compression has to be considered.

Reforming

The introduction of a steam methane reformer and a quencher after the gasification affects the thermo-economic performance. The reforming at high temperature (1623K) after directly (gas4d) or indirectly heated gasification (gas3i1) increases the total energetic efficiency only slightly compared to the corresponding process without reforming (gas6d respectively gas6i), while the reforming at lower temperature increases the total energetic efficiency considerably (gas5dd respectively gas5ii). The reforming at the optimal temperature stimulates the production of more producer gas having the appropriate composition for the product synthesis and yields hence a higher productivity.

Altough the reforming stage increases the fuel efficiency, it also increases the power consumption and reduces the net electricity output.

Without reforming the heat that has to be supplied by the combustion is much higher, as it can be clearly seen from the numerical values and from the corresponding composite curves for the process with directly heated gasification (gas5dd, gas6d) (appendix F.3 figure F.9) and the relative consumption of offgas compared to dried torrified gas is also higher.

The purchase of the reformer increases the investment costs. However, the production costs variation is also related to the electricity generation (i.e. to the cogeneration quality).

For the heating mode of the reformer the influence is the same than for the gasification, as it can be seen by changing only the heating mode of the reformer without affecting the gasifications heating mode (gas3d and gas3i1 (indirectly heated gasification)). Indirectly heating has a better thermo-economic performance.

Process options: General Trends

Based on the thermo-economic performance some general trends can be identified for the upstream process options:

- Indirectly heated gasification has a higher thermo-economic performance than directly heated gasification (section 8.2.1).
- Directly heated entrained flow gasification is slightly more efficient than indirectly heated fluidized bed gasification and less expensive; but scarce information on large scale industrial applications
- Steam methane reforming increases the performance

According to these outcomes and the one from the previous chapter 8.2.2, the recommended process layout is:

- Air Drying
- Indirectly heated fluidized bed gasification
- Indirectly heated steam methane reforming around the gasification temperature
- Cold gas cleaning

8.2.3 Synthesis

The performance differences for the three fuel production processes are highlighted by comparing the results for the same upstream process options: air drying, indirectly heated fluidized bed gasification with one-step steam methane reforming and cold gas cleaning. The optimal reforming temperature is chosen for each case: FT 1050.15K, MeOH 1223.15K and DME 1223.15K (section 7.4). The key parameters of the models, as well as the characteristics of the different streams are summarized in appendix E. For each synthesis option, a Rankine cycle is included (appendix table E.9) and no gas turbine nor heat pump is introduced. The fuels available for combustion are waste streams (i.e. dried torrified gas, char, process offgases from the separation section (flash drums and distillation)) and if needed process streams (i.e. hot producer gas). For the analysis it is important to keep in mind that the three processes differ in the upgrading; for the FT process crude FT-fuel is the final product, while for the others pure MeOH or DME is obtained.

The competitiveness of the different synthesis options is assessed based on the thermo-economic performance, expressed by the chemical and total energetic efficiency and the investment or production costs.

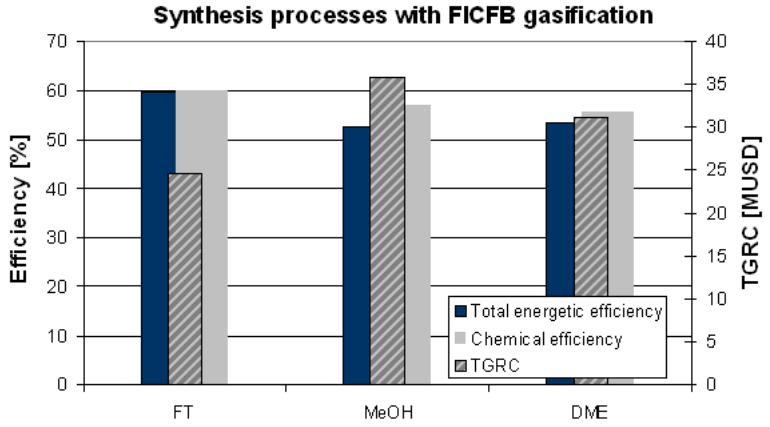

Figure 8.11: Thermo-economic performance comparison for the different synthesis processes with FICFB gasification

The thermo-economic performance of the three processes are quite high and of the same magnitude. Consequently, each process can be considered as potential alternative to produce biofuels in the future. The FT process has a higher thermo-economic performance because purification isn't included. Compared to the DME process, the methanol process has a somewhat lower thermo-economic performance.

A detailed analysis of the power balances (figure 8.13) and the energy supplied by the hot utility (figure 8.14), identifies the main reasons of this differences. The economic competitiveness of the different options is compared through the investment and production costs (figure 8.15). The revealed trends are confirmed by the aspect of the associated composite curves (figure 8.12).

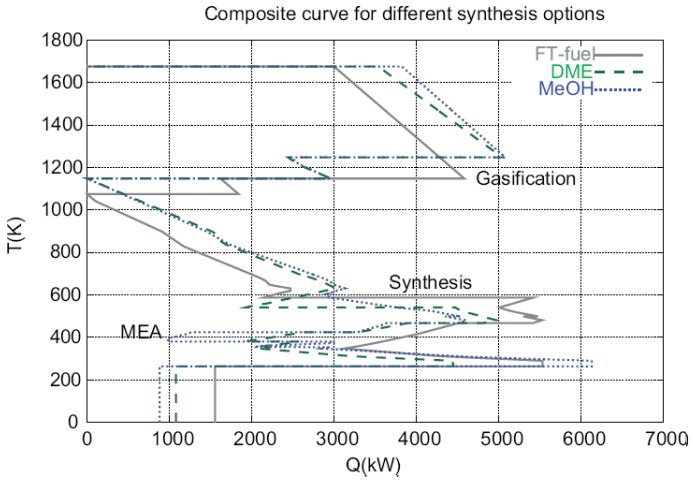

Figure 8.12: Composite curve comparison for the different synthesis processes with FICFB gasification including a steam network (omitted on the figure)

The comparison of the composite curves depicts one important difference between the FT process and the others. The CO_2 removal by MEA absorption is a large heat sink in the DME and MeOH process influencing the efficiency of the energy integration. The difference of the length of the plateau of the exothermic synthesis reactions is due to the different reaction heats. The slope of the lines corresponding to the gas cooling are identical because for each process the producer gas composition and hence its heat capacity are the same since the same pretreatment options are considered.

Power balance

The power consumption of the three processes is different because of the different synthesis pressures inducing different compression powers. The amount of power that is consumed increases with the operating pressure: FT (25 bar), DME (50 bar) and MeOH (85 bar). For the DME and MeOH process additional power is consumed by the CO_2 removal through MEA absorption. For the MeOH process, the amount of CO_2 removed to fix the stoichiometric ratio of the reactants to the optimal value is larger than the one removed in the DME process. Consequently, the methanol process consumes more power than the others. Even with the implementation of co-generation technology, not enough electricity is produced to cover the demands of the processes and additional electricity has to be imported. The steam turbine of the FT process can generate the most power (1526kW) because of the larger amount of excess heat being available. The difference is related to the MEA absorption interfering with the excess heat available for the Rankine cycle. The reduction of the steam demand for the CO_2 absorbent regeneration stripper would make a higher amount of high temperature excess heat available for the steam power cycle and hence increase the power generation.

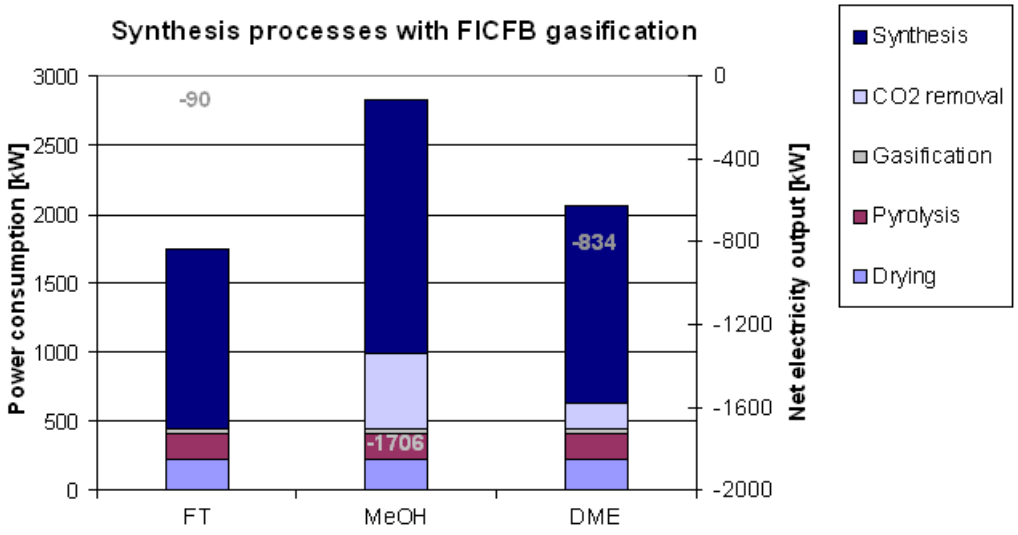

Figure 8.13: Power consumption split-up and net electricity output [kW] for the different synthesis options with FICFB gasification

Hot utility

The amount of energy that has to be supplied, above the pinch point, by combustion is highest for the MeOH process and lowest for the FT process. The relative contribution of the different types of combustibles is also different. Hot producer gas is combusted in the FT and DME process, whereas in the MeOH process the energy is supplied essentially from the waste steams. The proportion of char and torrified gas sent to combustion is similar in each process. In the DME process, the distillate is combusted primarily because the mass flow is high and the composition favorable for combustion. The flow rate of the offgas from the flash drums are very low; explaining the small contribution.

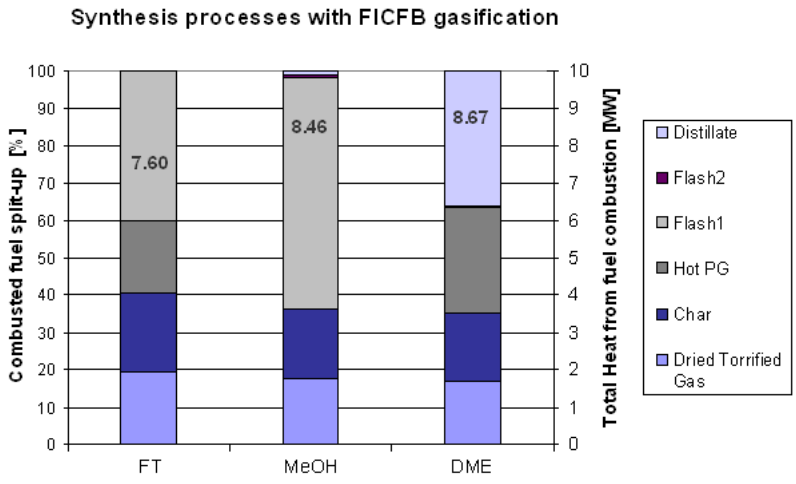

Figure 8.14: Energy supply from the fuel combustion for the different synthesis options with FICFB gasification

Economic Performance

The differences in the investment costs, come essentially from the additional costs for the MEA absorption unit in the MeOH and DME process. The synthesis unit costs, including the compressor costs, are of the same magnitude. For the FT process, the higher reactor costs (SAS) related to the complex construction are balanced with the lower compressor costs. The difference in the MeOH and DME synthesis costs is due to the higher compressor costs because the reactor costs themselves are in the same range.

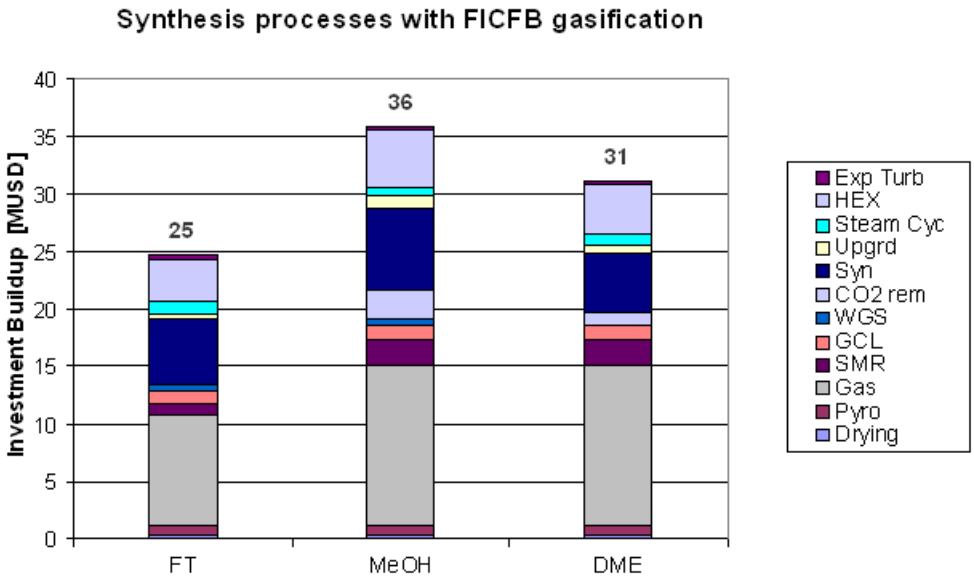

Figure 8.15: Investment buildup [MUSD] for the different synthesis options with FICFB gasification

The difference of the production costs, are essentially induced by the differences in the electricity costs and in a lesser extent by the different investment costs.

From an economic point of view the FT process is the most profitable and the MeOH process induces the highest costs. However, it is important to notice that additional costs would be associated with the FT upgrading and fractionating into diesel and gasoline.

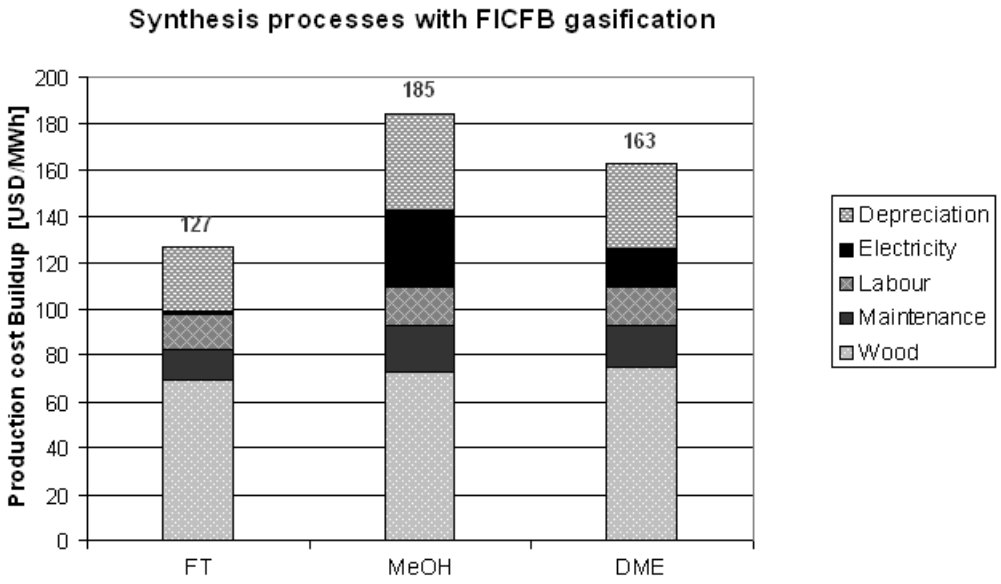

Figure 8.16: Production cost buildup [USD/MWh] for the different synthesis options with FICFB gasification

Further improvements

The comparison of the different synthesis processes leads to the conclusion, that CO_2 removal by MEA absorption, influences the thermo-economic performance of the DME and MeOH process. Even if the chemical performance is increased considerably by CO_2 removal, the energy and power consumption and consequently the additional costs are high. Alternative methods for CO_2 removal, consuming less power and energy, such as the Selexol or Rectisol process, could increase the thermo-economic performance of these processes. These alternatives could be designed in further studies to improve the model.

8.3 Thermo-economic and Environmental Performance

In the previous chapters the influence of some key process parameters and options on the thermo-economic performance were studied. In this chapter, the influence of process independent parameters are investigated, and the energy losses of the processes are identified. Finally, the environmental performance is evaluated by the CO_2 balance.

8.3.1 Economic Performance

The economic performance characterized by the installation and production costs, depends highly on the different process independent assumptions of the economic analysis (table C.1) and on the production scale. The general trends are exposed based on different sensitivity analysis performed for the MeOH process with FICFB gasification (final model, appendix E).

Raw material price

The raw materials constitute about half of the production costs (figure 8.16), consequently the wood purchase price is a relevant factor for the competitiveness of the production of fuels from biomass compared to the fuels from the fossil sources.

In the present work a wood price of 50 CHF/MWh (41.5 USD/MWh) was assumed. However, if biomass becomes available in large quantities at a lower price in future, the production costs would considerably drop and the biofuels become more competitive (figure 8.17). This depends hence largely on the evolvement of the international biomass market.

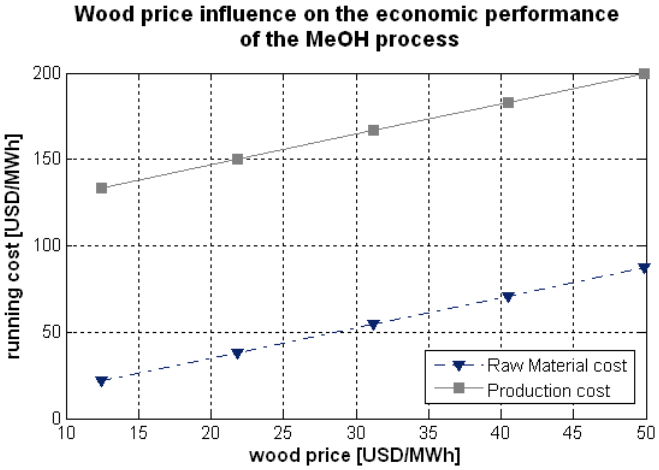

Figure 8.17: Influence of the wood price [USD/MWh] on the production costs including the raw material costs [USD/MWh] for the MeOH process

Electricity price

The electricity price is also a fundamental parameter. The electricity price evolution influence is related to the cogeneration technology. In the case where electricity is generated and can be exported from the process, high electricity export prices would reduce the production costs. This would be even more favorable as the produced electricity can be sold as green electricity since it is essentially generated from biomass. In this case, a difference between the electricity imported and exported price would change the economic evaluation further. On contrary, in the case where the process can't cover its own electricity demand, additional electricity has to be imported (as for the analyzed MeOH process) and hence the production costs increase with the electricity import price (figure 8.18). Consequently, the implementation of a good cogeneration system reducing the amount of electricity that has to be imported, is crucial.

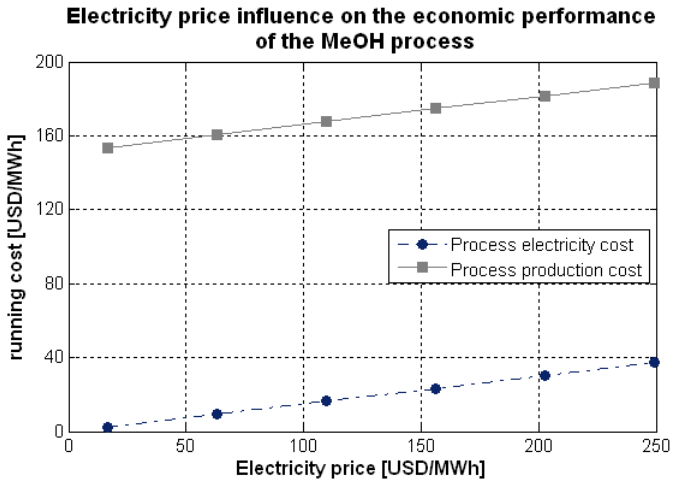

Figure 8.18: Influence of the electricity price [USD/MWh] on the production and electricity costs [USD/MWh] for the MeOH process

Interest Rate

The interest rate is another parameter that can influence the production costs because it is related to the depreciation costs (eq.: 6.14). Here, an interest rate of 6% was considered. An increase of the interest rate would go in pair with an increase of the production costs (figure 8.19).

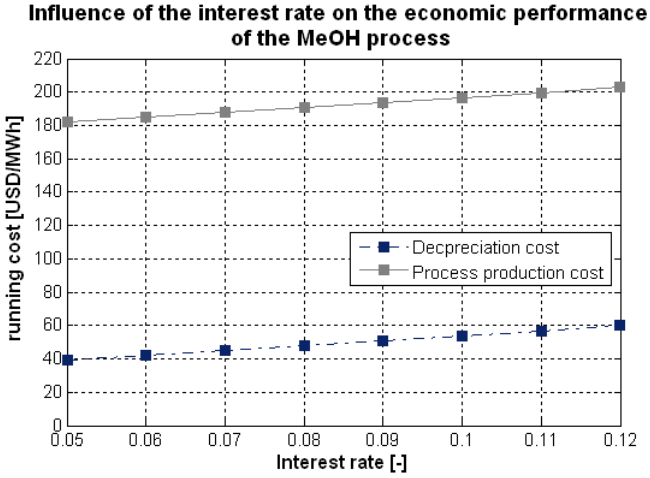

Figure 8.19: Influence of the interest rate [-] on the production costs including the depreciation costs [USD/MWh] for the MeOH process

Depreciation Period

The predicted lifespan of the installation affects the production costs through the depreciation costs (eq.: 6.14). The longer the discount period, the lower the estimated production costs (figure 8.20).

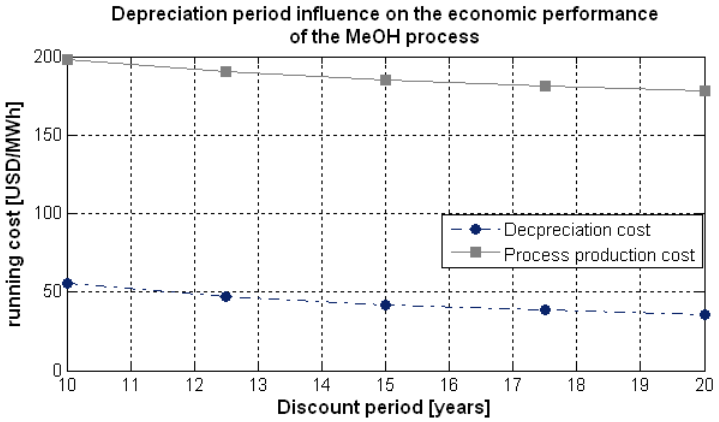

Figure 8.20: Influence of the discount period [years] on the production costs including the depreciation costs [USD/MWh] for the MeOH process

Scale-up

The economies of scale have a considerable influence on the production costs. The studies in the present work were all performed for a small scale production ($20MW_{th}$ nominal thermal capacity). Although scaling-up would increase the investment costs (figure 8.22), the production costs would decrease (figure 8.21) because of the non-linear relation between both. By increasing the plant capacity from low ($20MW_{th}$) to middle scale ($150MW_{th}$), the benefit is the biggest, further upscaling to $400MW_{th}$ reduces the production costs in a lesser extent.

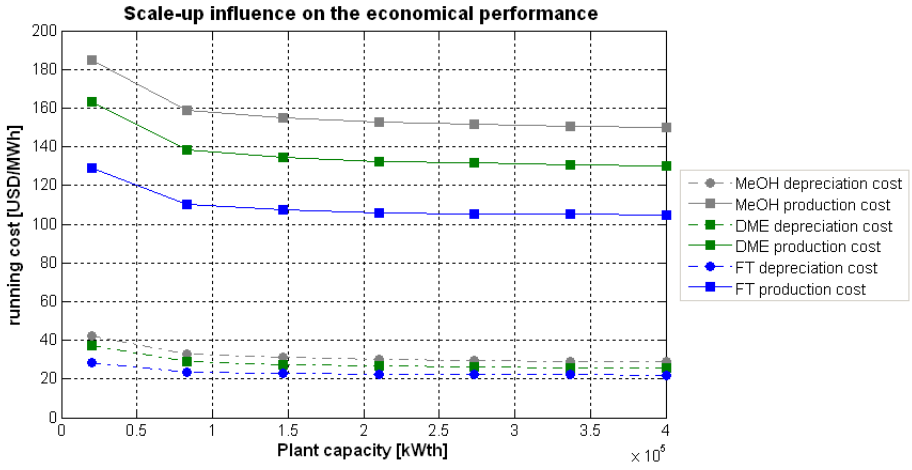

Figure 8.21: Influence of the nominal thermal capacity [kW] on the production and depreciation costs [USD/MWh] for the different synthesis processes

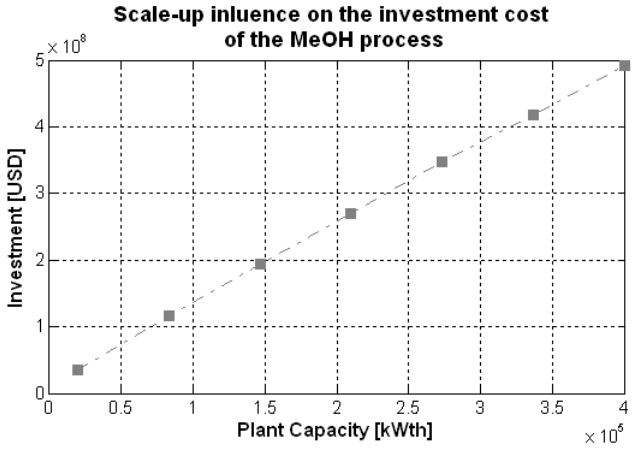

Figure 8.22: Influence of the nominal thermal capacity [kW] on the total investment costs [USD/MWh] for the MeOH process

8.3.2 Energy Losses

For all the different options that were analyzed, the best performances, expressed by the total energetic efficiency are in the range of 55-60%. From the input of $20MW_{th}$ (wood) around $12MW_{th}$ are recovered at the end in the fuel (FT-fuel, MeOH, DME). To improve the energy conversion further, it is important to identify where the rest is lost. The relative contribution of the different losses in the energy conversion are assessed on the basis of the MeOH synthesis process studied in the previous chapter 8.2.3.

Table 8.3 shows the different losses that are identified. The losses from the condensation come from the energy that is transferred from the condenser of the steam cycle to the cooling water. This corresponds to the amount of heat that cannot be converted into power, due to a limited energy efficiency of the combined cycle. The amount can be identified on the composite curve by the length of the corresponding plateau at 260K. For the different processes this amount is in the range of 3.5-5.5MW_{th}. For the MeOH process it accounts with 5.35MW for around 27% of the energy input.

The losses in the fumes are due to the non-utilization of the last part of the heat of combustion between the stack temperature and the basis for the LHV calculation (ambient temperature 289K). This loss accounts for about $0.3MW_{th}$.

Other contributions are thermal streams that are not considered in the energy integration, such as in steam drying where the energy loss in the dryer isn't taken into account, or in cold gas cleaning where the amount released by the artificial heat exchanger introduced to model the filter isn't considered. Another important factor is that the calculations are done by considering the LHV based on the dry biomass. Therefore, some losses are associated with the air drying, where the outlet air stream contains part of the removed water (vapor fraction 0.95%). Some losses come also from the material streams that are released but not valorized by recycling or combustion, such as in the DME process the methanol distillate of the third distillation column and in the MeOH process the bottom fraction of the second distillation containing a EtOH/H_2O mixture. All the losses are related to the assumptions of the modeling and the implementation of the energy integration. With the different contributions the balance is nearly closed.

Parameter		MeOH
Production [MW]	Fuel	11.41
Losses [MW]	Condensation	5.25
	Fumes	0.28
	Air drying	1.04
	Cleaning	0.54
	Wastewater (distillation)	0.08
	TOTAL	18.6
Consumption [MW]	Wood	20

Table 8.3: Energy balance of the MeOH process

8.3.3 Environmental Performance

Regarding the environmental problems, the alternative biofuel production processes presented here are of benefit for the future. As mentioned in the introduction, the production of fuels from biomass is more environmentally friendly because it can substitute the non-sustainable fossil fuels emitting a lot of CO_2.

For these biomass conversion processes the carbon cycle is closed and the net amount of greenhouse gas released to the atmosphere is zero, since the wood, used as feedstock, adsorbs exactly the same amount of carbon during its growth, as is emitted by the production and combustion of the gas. As the introduction of such processes in the energy system can substitute a certain amount of fossil natural gas, the overall CO_2 emissions can be decreased. Moreover, since pure CO_2 is removed in the MeOH and DME process, a negative CO_2 balance can be obtained by CO_2 sequestration.

To assess the environmental performance of the MeOH and DME process [2], the amount of yearly avoided CO_2 emissions by substitution with and without sequestration are evaluated according to the method described in appendix F.4. The numerical results of the environmental evaluation (appendix table F.2) prove that CO_2 emissions can be avoided by this production processes using essentially wood as feedstock. Upscaling of the production from 20 to $400 MW_{th}$ nominal thermal capacity, would be of benefit for the reduction of the greenhouse gas emissions (figure 8.23) since through substitution of fossil fuels more CO_2 emissions could be avoided.

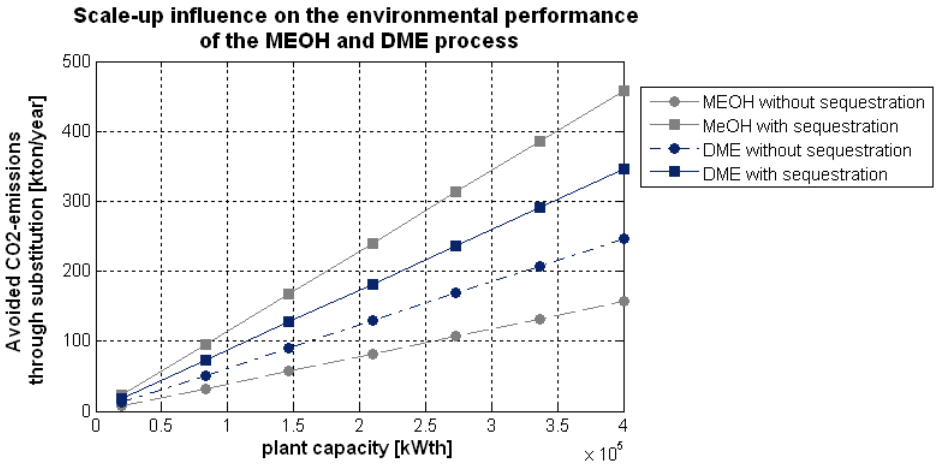

Figure 8.23: Influence of the nominal thermal capacity [kW] of the installation on the environmental performance expressed as yearly avoided CO_2 emissions by substitution

[2] The FT process is not considered because no CO_2 was removed and because the purification and fractionation into diesel and gasoline wasn't modeled

Chapter 9

Conclusion

A superstructure based thermo-economic model for alternative technologies to produce fuels from wood was presented with the purpose to evaluate the competitiveness with regard to the productivity, the energy integration efficiency and the economic performance.

The performance comparison reveals that all the different options are viable. The overall efficiency is in the range of 50 to 60%. The most critical choice is the choice of the gasification technology. Directly heated gasification has a lower performance and higher costs due to the costs and power consumption of the oxygen production for the oxidation. Entrained flow gasification yields a high efficiency, however more research has to be done on the technical realization of direct heating and on the industrial applications of indirect heating. The recommended technology for the analyzed processes is indirectly heated fluidized bed technology having proven industrial applications.

Key parameters for the productivity are the operating conditions and the producer gas quality characterized by the stoichiometric ratio of the reactants and influenced by the equilibrium of the water gas shift and the steam methane reforming reaction, the recycling and the CO_2 removal.

The process performance is highly influenced by the implementation of the energy integration. The optimization of the steam cycle or the combined cycle valorizing the waste heat in the power production, increases the total energetic efficiency.

Nowadays, the production costs for biofuels are still higher than for fossil fuels. However, in the long term, costs improvements are foreseen by the combined effects of larger production scales, cheaper biomass, technological learnings and developments in the gasification technology and the oxygen production, and increased fuel efficiencies through improved catalysts.

With regard to environmental concerns, these fuels produced from renewable resources (i.e. biomass) are carbon neutral and could reduce the CO_2 emissions through substitution of fossil fuels.

In the prospect of a more sustainable world, it is worth for R&D to investigate in these thermo-chemical processes producing fuels from biomass, since the problem of the energy supply and of the global warming could be solved partially by using biomass as energy resource.

Acknowledgments

I would like to thank Dr. François Maréchal for accepting this master project at the Industrial Energy Systems Laboratory and for his good advice.

I'm thankful to Martin Gassner for his kind assistance, his pertinent explanations, his help in solving any kind of problems and his support during the different stages of this project.

Special thanks go to my family and friends for their constant support during all my studies at the EPFL.

Bibliography

[1] European Commission. *Biomass-Green Energy for Europe.* Directorate-General for Research Sustainable Energy Systems, 2005.

[2] Europe in Figures-Eurostat yearbook 2008. *Energy.* Eurostat, 2008.

[3] European Environment Agency. *How much biomass can Europe use without harming the environment?* EEA Briefing 2005/02, 2005.

[4] Van der Drift A. and Boerrigter H. . Synthesis Gas from Biomass for Fuels and Chemicals. *ECN Biomass, Coal and Environmental Research* , ECN-C-06-001, 2006.

[5] Gassner M. Energy Integration and Thermo-economic Evaluation of a Process converting Wood to Methane. Diploma work, EPFL, Industrial Energy Systems Laboratory, Lausanne, 2005.

[6] Darbellay N. Thermodynamic Model and Energy Integration of Thermo-chemical Process producing Liquid Transportation Fuel from Biomass. Diploma work, EPFL, Industrial Energy Systems Laboratory, Lausanne, 2007.

[7] http://www.belsim.com.

[8] LENI: http://leniwww.epfl.ch.

[9] http://www.integrofuels.com/green.html.

[10] Energy research Centre of Netherlands: http://www.ecn.nl.

[11] International Energy Agency: Bioenergy Agreement Task 33 : Thermal Gasification of Biomass: http://www.gastechnology.org/iea.

[12] *Doğu* T. and Varisli D. Alcohols as alternates to petroleum for environmentally clean fuels and petrochemicals. *Turkish J. Chemistry*, 31:551–567, 2007.

[13] Table of fuel properties: http://www.walshcarlines.com/pdf/fueltable.pdf.

[14] Kaneko T. et al. *Coal Liquefaction.* Ullmann's Encyclopedia of Industrial Chemistry, 2001.

[15] Shadle L.J. and Berry D.A. and Syamlal M. *Coal Conversion Processes, Gasification.* Kirk-Othmer Encyclopedia of Chemical Technology, 2002.

[16] Hamelinck C.N. et al. Production of Fischer-Tropsch transportation fuels from biomass; technical options, process analysis and optimisation, and development potential. *Energy*, 29:1743–1771, 2004.

[17] Tijmensen M.J.A. et al. Exploration of the possibilities for production of Fischer-Tropsch liquids and power via biomass gasification. *Biomass and Bioenergy*, 23:129–152, 2002.

[18] http://www.wikipedia.org/.

[19] Lemercier R. Modélisation de la pyrolyse de biomasse. Semester work, EPFL, Industrial Energy Systems Laboratory, Lausanne, 2007.

[20] Lemercier R. Modélisation et intégration énergétique de la production de carburants biogènes par pyrolyse. Semester work, EPFL, Industrial Energy Systems Laboratory, Lausanne, 2008.

[21] Bergman P.C.A. and Kiel J.H.A. *Torrefaction for Biomass Upgrading.* Published at 14th European Biomass Conference & Exhibition, Energy Research Centre of Netherlands, ECN, 2005.

[22] http://www.techtp.com.

[23] http://www.wyssmont.com.

[24] Steynberg A.P. et al. *Fischer-Tropsch Technology*, volume vol.152. Studies in surface science and catalysis, Elsevier, Amsterdam, 2004.

[25] Olofsson I. and Nordin A. and Söderlind U. *Initial Review and Evaluation of Process Technologies and Systems Suitable for Cost-Efficient Medium-Scale Gasification for Biomass to Liquid Fuels.* ETPC (Energy Technology & Thermal Process Chemistry), University of *Umeà*, ISSN 1653-0551, ETPC Report 05-02, 2005.

[26] National Renewable Energy Laboratory: http://www.nrel.gov.

[27] http://www.ficfb.at.

[28] HoST: Engineers in Energy: http://www.host.nl.

[29] Hamelinck C.N. and Faaij A.P.C. Future prospects for production of methanol and hydrogen from biomass. *Utrecht University, Report NWS-E-2001-49*, 2001.

[30] VanEric E. Stein et al. *The impact of ITM Oxygen on Economics for Coal-based IGCC.* 27^{th} International Technical Conference on Coal Utilization & Fuel Systems, 2002.

[31] S. Diethelm. Integration of ceramic oxygen separation modules in high temperature industrial and energetic processes. Travail de diplôme postgrade, EPFL, Lausanne, 2001.

[32] Electric Power Research Institute: http://www.epri.com.

[33] Radgen P. et al. *Verfahren zur CO2-Abscheidung und -Speicherung.* Climate Change, Umweltbundesamt, 2006.

[34] Spath P.L. and Dayton D.C. *Preliminary Screening-Technical and Economic Assessment of Synthesis Gas to Fuels and Chemicals with Emphasis on the Potential for Biomass-Derived Syngas.* Technical Report, National Renewable Energy Laboratory (NREL/TP-510-34929), Colorado, 2003.

[35] Leibold H. et al. HTHP syngas cleaning concept of two stage biomass gasification for FT synthesis. *Powder Technology*, 180:265–270, 2008.

[36] Zwart R.W.R. Mozaffarin M. *Feasibility of Biomass/ Waste-Related SNG Production Technologies.* Petten, 2003.

[37] Fischer-Tropsch Archive: http://www.fischer-tropsch.org/.

[38] HB.H. Davis et al. *Fischer-Tropsch synthesis, catalysts and catalysis*, volume vol.163. Studies in surface science and catalysis, Elsevier, Amsterdam, 2007.

[39] Robert Bernard Anderson. *The Fischer-Tropsch Synthesis.* Orlando-Fla.a.o. Academic Press, 1984.

[40] Dry M.E. The Fischer-Tropsch Process: 1950-2000. *Catalysis Today*, 71:227–241, 2002.

[41] Chorkendorff I. and Niemantsverdriet J.W. *Concepts of Modern Catalysis and Kinetics.* WILEY-VCH Verlag, Weinheim, 2007.

[42] Jager B. and Espinoza R. Advances in low temperature Fischer-Tropsch synthesis. *Catalysis Today*, 23:17–28, 1995.

[43] Maretto C. and Krishna R. Modelling of a bubble column slurry reactor for Fischer-Tropsch synthesis. *Catalysis Today*, pages 279–289, 1999.

[44] Irion W.W. and Neuwirth O.S. *Oil Refining.* Ullmann's Encyclopedia of Industrial Chemistry, 2005.

[45] Yotaro Ohno. *A New DME Production Technology and Operation Results.* NKK Corporation, Japan, 2001.

[46] Müller M. and Hübsch U. *Dimethyl Ether.* Ullmann's Encyclopedia of Industrial Chemistry, 2000.

[47] Haldor Tospsoe Company: http://www.topsoe.com.

[48] JFE Holdings Inc.: http://www.jfe-holdings.co.jp/en/.

[49] Yotaro Ohno. *Development of DME Direct Synthesis Technology.* DME Project-JFE Holding, 2001.

[50] Yotaro Ohno. *Coal Conversion into Dimethyl Ether as an Innovative Clean Fuel.* DME Project-JFE Holding (12th ICCS), 2003.

[51] Fiedler E., Grossmann G., Kersebohm D.B., Weiss G., and Witte C. *Methanol.* Ullmann's Encyclopedia of Industrial Chemistry, 2000.

[52] Maréchal F., Heyen G., and Kalitventzeff B. Energy Savings in Methanol Synthesis: Use of Heat Integration Techniques and Simulation Tools. *Computers and Chemical Engineering*, 21, Issue suppl. 1:S511–S516, 1997.

[53] English A. and Rovner J. and Brown J. and Davies S. *Methanol.* Kirk-Othmer Encyclopedia of Chemical Technology, 2005.

[54] Gassner M. and Maréchal F. *Thermo-economic Model of a Process converting Wood to Methane.* submitted to biomass & bioenergy, 2006.

[55] Gazobois S.A.: http://www.gazobois.ch.

[56] Burdet I. *Fiche de spécifications, Procédé élémentaire: Torréfaction.* Laboratoire d'Energétique Industrielle, EPFL, 2006.

[57] Heyne S., Thunman H., and Harvey S. *Integration aspects for synthetic natural gas production from biomass based on a novel indirect gasification concept.* PRES 2008, 11th Conference on Process Integration, Modelling and Optimisation for Energy Saving and Pollution Reduction, Prague, 2008.

[58] Van Grambezen P. ir A.I.A. *Contribution l'étude cinétique de la synthése du méthanol par le procédé industriel sous basse pression.* Ecole militaire Bruxelles.

[59] Alleman X. and Charles R. Avant-projet d'usine Coproduction d'Ammoniac et de Méthanol. Avant-projet, Université de Liège, Liège, 1998.

[60] Maréchal F. and Kalitventzeff B. Process Integration: Selection of the optimal utility system. *Computers and Chemical Engineering*, 22 Suppl:S149–S156, 1998.

[61] Turton R. et al. *Analysis, Synthesis, and Design of Chemical Processes.* Prentice Hall, New Jersey, 1998.

[62] Ulrich G.D. and Vasudevan P.T. *Chemical Engineering Process Design and Economics A Practical Guide.* Process Publishing, Durham New Hampshire, 2 edition, 2004.

[63] Personal communication with Thomas Peyer, Erdgas Ostschweiz AG, June 2007.

[64] HB.H. Davis et al. Fischer-Tropsch synthesis: Overview of reactor development and future potentialities. *Topics in catalysis*, 32, 2005.

[65] Reed T. *The Fuel composition-conversion Diagram.* The Biomass Energy Foundation, Available from: www.woodgas.com.

[66] Prins M.J. et al. More efficient biomass gasification via torrefaction. *Energy*, 31:3458–3470, 2006.

[67] J. Gmehling and U. Onken. *Vapor-Liquid Equilibrium Data Collection, Alcohols: Methanol Supplement 5*, volume Vol I, Part 2g. DECHEMA Chemistry Data Series, Frankfurt am Main, 2005.

[68] J. Gmehling and U. Onken. *Vapor-Liquid Equilibrium Data Collection, Aqueous systems Supplement 2*, volume Vol I, Part 1b. DECHEMA Chemistry Data Series, Frankfurt am Main, 1988.

[69] H. Knapp and R. Dring and L.Oellrich and U. Plcker and J. M. Prausnitz. *Vapor-Liquid Equilibria for Mixtures of low Boiling Substances* , volume Vol VI. DECHEMA Chemistry Data Series, Frankfurt am Main, 1982.

[70] Sander R. *Compilation of Henry's law constants for inorganic and organic species of potential importance in environmental chemistry.* www.henrys-law.org, 1999.

[71] Personal communication with Prof. Georges Heyen.

[72] http://www.oanda.com/convert/fxaverage_result.

[73] Chen et al. Numerical Simulation of Entrained Flow Coal Gasifiers. *Chemical Engineering Science*, 55:3861–3883, 2000.

[74] Bockelie M.J. . *CFD Modeling for Entrianed Flow Gasifiers In Vision 21 Systems.* Presented at the Gasification Technologies Conference, 2000.

[75] Godat J. *Optimisation of the Proton Exchange Membrane Fuel Cell System using the Energetic Integration Analysis.* EPFL-STI-ISE-LENI, 2003.

[76] Maréchal F. and Palazzi F. and Godat J. Thermo-Economic Modelling and Optimisation of Fuel Cell Systems . *Fuel Cells*, 2005.

[77] Fox J.M. et al. and Bechtel Group Inc. *Slurry Reactor Design Studies: Slurry vs. Fixed-bed Reactors for Fischer-Tropsch and Methanol: Final Report.* US. Department of Energy, 1990.

[78] Dianhua Liu et al. Mathematical Simulation and Design of Three-Phase Bubble Column Reactor for Direct Synthesis of Dimethyl Ether from Syngas. *Journal of Natural Gas Chemistry*, 16:193–199, 2007.

[79] ecoinvent Centre: http://www.ecoinvent.ch.

Appendix A

Thermodynamic models

For the modeling of the flowsheets, different thermodynamic models predicting the chemical interaction properties are used to simulate the synthesis, the distillation (vapor-liquid equilibrium) and the heat exchange (enthalpy, specific heat, latent heat). The change of the thermodynamic model between the synthesis and upgrading section, allows to describe correctly the state of the matter under a given set of physical conditions and to predict the vapor-liquid equilibrium. The most common activity coefficient models are: NRTL, WILSON, SRK, UNIQUAC and UNIFAC. The choice of the model is determined by the ideality and non-ideality of the system and the pressure. The non-ideality results from the interaction between molecules through intermolecular forces caused by the following chemical groups: hydroxyl (-OH), ketone (-C=O), aldehyde (-CHO), halogens (-Cl, -Br) and carboxylic acid groups (-COOH).

The two models used to predict the behavior of the liquid and vapor phase are based primarily on the activity coefficient model UNIQUAC and on the equation of state model Peng-Robinson and Soave. The thermodynamic model used for each unit, as well as the corresponding binary interaction coefficients introduced in Belsim Vali are reported in this chapter. The values are taken from DECHEMA tables [67, 68, 69] and [58, 70].

In order to use the NRTL and UNIQUAC parameters reported in the DECHEMA tables in Belsim Vali, some conversions have to be done, that is to say; the values given in the DECHEMA tables have to be divided by the universal gas constant R=1.9872cal/mol/K (with the assumption that there is no temperature dependence).

DECHEMA (NRTL)	Thermodynamic signification	Belsim Vali
A12	g12-g22 [cal/mol]	ijC0·R (ijCT=0)
A21	g21-g11 [cal/mol]	jiC0·R (jiCT=0)
α12	α12	ijA0 (ijAT=0)

Table A.1: Relation between the NRTL parameters reported in the DECHEMA tables and the one introduced in Belsim Vali

DECHEMA (UNIQUAC)	Thermodynamic signification	Belsim Vali
A12	u12-u22 [cal/mol]	ijA·R (ijB=0)
A21	u21-u11 [cal/mol]	jiA·R (jiB=0)

Table A.2: Relation between the UNIQUAC parameters reported in the DECHEMA tables and the one introduced in Belsim Vali

For the syngas preparation units and the fuel synthesis section, the physical properties of the mixtures are estimated by using the Peng-Robinson equation of state. However, for the purification section UNIQUAC or NRTL model are used to predict the liquid phase activity

coefficients. The binary interaction parameters predict the vapor-liquid equilibrium in the mixtures (water, MeOH, EtOH and DME). The Lee-Kesler equation of state is used to predict the enthalpy departures.

	Vapor phase	Liquid phase
Fugacity	VIDEAL	LIDEAL
Enthalpy	VIDEAL	LIDEAL2
Volume	VIDEAL	Gunn-Yamada

Table A.3: Thermodynamic model definition for the producer gas stream

	Vapor phase	Liquid phase
Fugacity	Peng-Robinson	Peng-Robinson
Enthalpy	Peng-Robinson	Peng-Robinson
Volume	VIDEAL	Gunn-Yamada

Table A.4: Thermodynamic model definition for the MeOH synthesis unit

Peng-Robinson		
Compound 1	Compound 2	kij
N_2	MeOH	-0.2141
H_2O	MeOH	-0.0778
CO	MeOH	-0.2141
CO_2	MeOH	0.0583

Table A.5: Parameters for the Peng-Robinson model for the MeOH synthesis [58, 68]

	Vapor phase	Liquid phase
Fugacity	Soave	UNIQUAC
Enthalpy	Lee-Kesler	Lee-Kesler
Volume	VIDEAL	Gunn-Yamada

Table A.6: Thermodynamic model definition for the MeOH separation unit

UNIQUAC			
Compound 1	Compound 2	isGAM0	isGAMT
CH_4	H_2O	5.412	-0.255
CH_4	MeOH	6.2	0
N_2	H_2O	3.0	0
N_2	MeOH	3.0	0
H_2O	CO	6.963	0
H_2O	CO_2	8.696	-1543.5
H_2O	H_2	7.963	0
CO	MeOH	2.9	0
CO_2	MeOH	0.9928	-121.847
H_2	MeOH	4.7	0

Table A.7: Binary parameters for the UNIQUAC model [58] used for the MeOH separation

UNIQUAC			
Compound 1	Compound 2	Aij	Aji
H_2O	MeOH	239.67	-153.369
H_2O	EtOH	178.141	-31.028
MeOH	EtOH	-6.03875	-1.792
MeOH	DME	-145.458	433.938

Table A.8: Interaction coefficients for the UNIQUAC model [58] used for the MeOH synthesis

	Vapor phase	Liquid phase
Fugacity	Peng-Robinson	Peng-Robinson
Enthalpy	Peng-Robinson	Peng-Robinson
Volume	VIDEAL	Gunn-Yamada

Table A.9: Thermodynamic model definition for the DME synthesis unit

Peng-Robinson		
Compound 1	Compound 2	kij
N_2	MeOH	-0.2141
C_2H_6	MeOH	0.027
H_2O	MeOH	-0.0778
CO	MeOH	-0.2141
CO_2	MeOH	0.0583

Table A.10: Parameters for the Peng-Robinson model [58] used for the DME synthesis

	Vapor phase	Liquid phase
Fugacity	Soave	NRTL
Enthalpy	Lee-Kesler	Lee-Kesler
Volume	VIDEAL	Gunn-Yamada

Table A.11: Thermodynamic model definition for the DME separation unit

NRTL				
Compound 1	Compound 2	ijC0	jiC0	α
H_2O	DME	567.5851	-284.52093	0.3
H_2O	MeOH	-86.6043	386.7502	0.3
DME	MeOH	187.8019	-66.27415	0.3

Table A.12: Parameters for the NRTL model used for the DME separation [71]

	Vapor phase	Liquid phase
Fugacity	VIDEAL	LIDEAL
Enthalpy	VIDEAL	LIDEAL2
Volume	VIDEAL	Gunn-Yamada

Table A.13: Thermodynamic model definition for the FT-fuel

Appendix B

Process Modeling

In chapter 4 the general approach used to model the different process units is outlined. Supplementary specifications and the numerical values of the key modeling parameters of each unit are reported in the following paragraphs.

B.1 Drying

Air drying is governed by the transfer of water in the solid and the vapor pressure at its surface and the surrounding air. The overall mass transfer coefficient is fixed at $Up = 11.16 \cdot 10^{-3} bar^{-1}$, the pressure drop is set to 100mbar and the wood outlet temperature equals the air outlet temperature $T_{BMout} \cong 78^{o}C$.

Steam drying in contrast, is governed by heat transfer and the overall transfer coefficient is expected to be $Up = 1117 J/kgK$. The pressure drop in the dryer is fixed at 40mbar and the wood outlet temperature equals the water boiling temperature $T_{BMout} = 100^{o}C$. A heat loss of 18% (based on the transferred heat) is considered [54].

B.2 Pyrolysis

The conversion in the torrefaction reactor is modeled by specifying the outlet stream composition. The numerical values used for the weight fractions (WF) of each element, for the ratio between the outlet and inlet mass flow (MASSF_out_in) and for the composition of the gas phase in terms of H and O are given in table B.1.

$WFC\_OUT\_IN = 1.057$	$MASSF\_OUT\_IN = 0.87$
$WFH\_OUT\_IN = 0.916$	$R\_HC1\_HBMG = 0.501$
$WFO\_OUT\_IN = 0.942$	$R\_OCO\_OBMG = 0.175$

Table B.1: Modeling parameters for the pyrolysis [56]

The flowsheet of the torrefaction model is illustrated in figure B.1

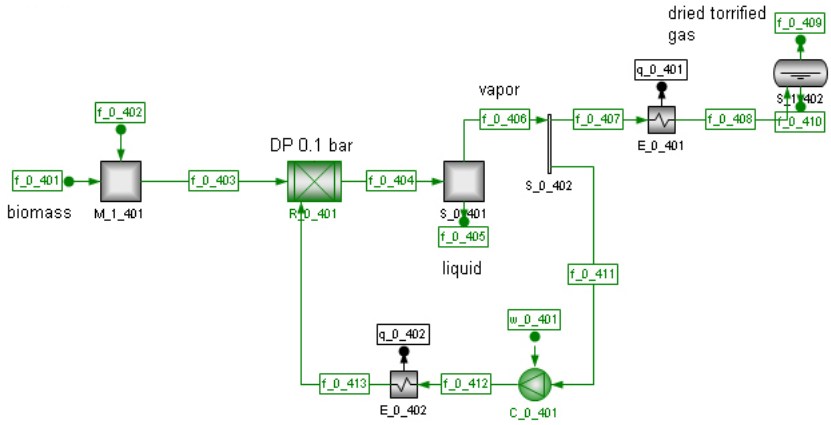

Figure B.1: Flowsheet of the torrefaction

B.3 Gasification

Table B.2 summarizes the key parameters specified in the models of the indirectly and directly heated entrained flow and fluidized bed gasification (base-cases). The additional options (gas5 and gas6) introduced for the steam methane reforming following the gasification, are modeled according to the corresponding base case FICFB or CFB gasifications performed at atmospheric pressure. The gasification temperature and pressure can be optimized for the different processes. For the reactors heat losses in the range of 1-10% are considered.

Gasifier type	EF	EF	FICFB	CFB
Gasifying agent	H_2O	O_2 $(+H_2O)$	H_2O	O_2 $(+H_2O)$
Heating mode	indirect	direct	indirect	direct
Label	gas1	gas2	gas3	gas4
Gasifying agent Temperature $[^oC]$	400	400	400	400
Pressure drop [mbar]	150	150	150	150
Pressure [bar]	30	25	1	30
$T_{reactor\_out}$ $[^oC]$	1350	1350	850	850
$T_{HTstage\_out}$ $[^oC]$	-	-	1350	1350
T_{quench} $[^oC]$	800	800	800	800
steam to biomass ratio	1	0.6	0.5	0.6
steam to oxygen ratio	-	0.1	-	-
ΔT_1	-	-	-280	-280
ΔT_2	-	-	-112	-112
k_p	-	-	4.9	2.9
ratio $\frac{C_2H_4}{CH_4}$	-	-	0.2045	0.476
ϵ_{cc}	-	-	90.3%	93.0%

Table B.2: Gasification model constants

B.4 Air Separation

Figure B.2 illustrates a simplified model of the oxygen transfer membranes containing a compressor (isentropic efficiency 0.85), an heat exchanger, a separator (representing the membrane) and an expansion turbine (isentropic efficiency 0.8).

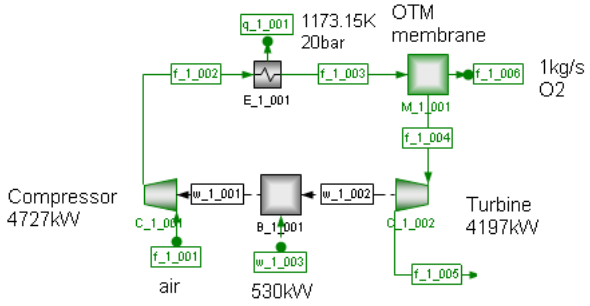

Figure B.2: Model of ion transfer membrane for O_2 production

As an alternative to the oxygen production through oxygen transfer membranes, air distillation could be considered. In a preliminary essay a simplified black box model was set up based on a complex model involving three successive distillations developed by Prof. Georges Heyen [71] for the production of 10kg/s of oxygen. The first air distillation (T=-174^oC and P=5.35bar) releases pure nitrogen at the top. The bottom fraction (T=-187^oC , 5.32 bar) is introduced in a second distillation column separating the remaining nitrogen with a small part of the other gases (top) from the bottom part containing mainly oxygen (96-98 wt%) and a small fraction of argon. A side draw from the second column and subsequent distillation in a third column, generates a stream containing mainly argon (74%). In this model the Murphey efficiency is set to 0.7. The size of each column expressed in term of plates is: 1st column 46 plates, 2nd column 66 plates and 3rd column 60 plates. The difficulty of this approach is to accurately model the energy integration taking into account the compression power and the cold utility. Since this process is performed at low temperature a refrigeration cycle has to be included. Due to the complexity related to the energy integration this option isn't investigated in more detail.

B.5 Cold Gas Cleaning

The concentration of contaminants in the producer gas is influenced by the nature of the biomass feedstock and their contaminant concentration (Cl, N, S), as well as the ash components. The typical impurities in wood gasification gases and the cleanness requirements for the different synthesis processes are displayed in table B.3 [25, 35, 36].

Component	PG from gasifier [36]	FT synthesis Sasol [35]	FT synthesis [25]	MeOH synthesis [25]
CO_2		$< 10\%$		
HCN	$280ppm$	$< 20ppb$	$< 10ppb$	$0.01ppmv$
NH_3	$2830ppm$	-	$< 10ppmv$	$10ppmv$
H_2S	$100ppm$	$< 10ppb$	$< 60ppb$	$< 0.1ppmv$
HCl	$25000ppb$	$< 10ppb$	$< 10ppb$	$< 0.001ppmv$
Halogens	-	-	$< 10ppbv$	$0.01ppmv$
Alkalis	$1630mg/Nm^3$	$< 10ppb$	$10ppbv$	$ppbv$ to $ppmv$
Tar	$10000\text{-}15000mg/Nm^3$	-	-	-

Table B.3: Gas cleaning requirements - Target levels of major contaminants [35, 25]

A simplified model of the cold gas cleaning section is illustrated in figure B.3 and the numerical values of the modeling parameters are reported in table B.4.

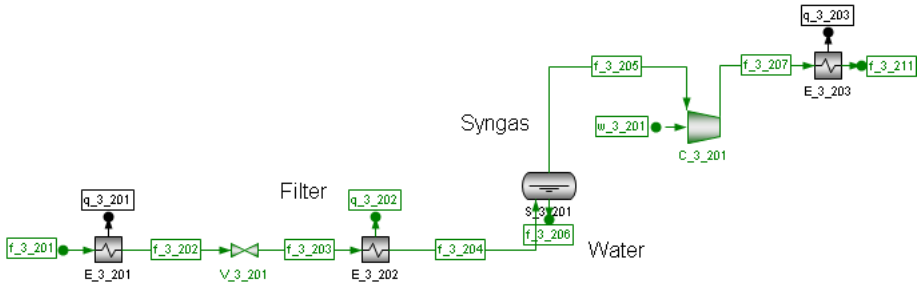

Figure B.3: Flowsheet of the cold gas cleaning section

Parameter	Value
Heat exchanger T_{out}	150^oC
Filter pressure drop	0.1bar
Filter T_{out}	25^oC
Flash temperature	25^oC
PG T_{GCcold_out}	400^oC
PG P_{GCcold_out}	25bar

Table B.4: Cold gas cleaning model constants

B.6 FT Reaction Modeling

The FT reaction taking place in a SAS fluidized bed reactor over a Co-catalyst is modeled based on data from [14]. The considered values of the olefinic fraction in the different hydrocarbon ranges and the value of the growth probability α are reported in table B.5.

Parameter	Value
$C_2 - C_4$	0.8
$C_5 - C_{12}$	0.7
$C_{13} - C_{18}$	0.6
Probability α	0.884

Table B.5: Parameters for FT- SAS synthesis: fraction of olefins in the different hydrocarbons ranges and polymerization probability [14, 42]

B.7 MeOH Reactor Modeling

As explained in [52, 59] the MeOH reactor being a multistage reactor of 4 beds is modeled as four reactors in series. The four beds are characterized by the relative flow rate and the inlet and outlet temperatures represented in table B.6.

Bed	Realtive flow	$T_{in}[^oC]$	$T_{out}[^oC]$
Bed 1	0.6	260	353
Bed 2	0.72	260	335.5
Bed 3	0.86	260	326.5
Bed 4	1	260	319

Table B.6: Parameters for the methanol reactor modeling

B.8 Distillation Modeling in Belsim

In Belsim Vali different methods can be used to model distillations. First, a distillation column can be designed by using a simulation unit; the simplest one being COL010 (used together with the controller CTL010 or CTL020). For a given inlet stream, the distillation column of type COL010 simulates the separation according to the fixed specifications for the distillate (i.e. purity of light and heavy compounds). The unit COL010 is however only appropriate for simple ideal systems for which ones the relative volatility is constant. Hence, for non-ideal systems, the generated results, especially the number of plates, are underestimated by using this approach.

In this case, as well as for azeotropes, a more elaborated model (COL07) has to be used. In order to run this unit, one has to define a distillation column (type: COL07B) coupled respectively to a condenser (type: COL07A) on the top and a reboiler (type: COL07A) on the bottom (illustrated in figure B.4). The degrees of freedom and hence the number of variables to be specified depend on the configuration. It is recommended to specify measurable quantities such as the flow rates rather than purities. In addition, a controller unit of the type COL070 has to be set up to manipulate the specified variables. Finally, it is import to give good estimations for the initialization values in order to obtain convergence and reliable results.

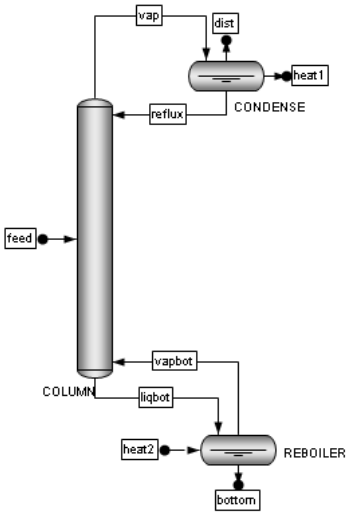

Figure B.4: Set-up of a distillation unit for simulation with Belsim SIMU (COL07)

B.8.1 Methodology for Distillation Modeling

In this work the distillation sections are modeled according to the following methodology. First, a simplified model is set-up in a simulation unit, containing a column of type COL010 with thermal streams representing the condenser and reboiler at the top and bottom respectively (figure B.5b). By knowing the inlet composition, the targeted purity of the light and heavy compound is estimated and specified. Table B.7 indicates the light and heavy keys of the different distillations and the related purity targets.

Distillation Column	MeOH 1st	MeOH 2nd	DME 1st	DME 2nd	DME 3rd
Light key	CO_2	MeOH	CO_2	CO_2	MeOH
Purity [%]	99.0	99.0	99.9	99.9	99.9
Heavy key	MeOH	H_2O	DME	MeOH	H_2O
Purity [%]	0.1	0.15	5	0.75	0.5

Table B.7: Purity of key light and heavy compounds of the different distillations modeled with COL010

The simulations generate then the number of stages and the reflux ratio. If these values are not realistic, for example, if the reflux ratio is extremely high (e.g. 5), the purity is adapted until a good compromise is found. These values (i.e. number of stages, distillate and reflux rate) are then introduced in the more detailed simulation model containing a column of the type COL07 (condenser represented explicitly) (figure B.5a)). The results of the different essays show, that in fact the simplified model (COL10) generates in some cases, essentially for non-ideal systems, too optimistic values. In order to reach the targeted purity, the number of stages and/or the reflux ratio has then to be increased. For economic reasons, it is in general better to work with moderate reflux ratios because high reflux ratios increase the energy consumption and the costs.

For simple ideal-systems the results computed with the column of type COL010 are however quite accurate and consequently the simulation with a column of type COL07 can be omitted and the results (from COL010) can be used directly.

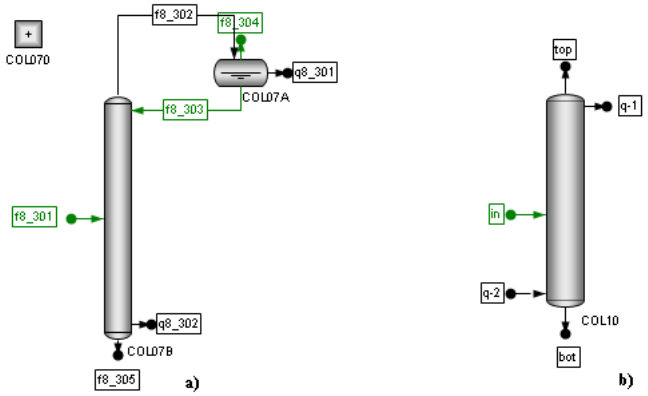

Figure B.5: Set-up of two different distillation simulation units (COL07, COL010) in Belsim SIMU

Finally, these results are transferred in a VALI PFD, where a model is set-up with a distillation column of the type COLVAL with thermal streams representing the condenser and reboiler heat load. In this model, the values of the composition and mass flow rate at the bottom and of

the heat load are fixed. Moreover, the streams are initialized with the values from the simulation units.

Table B.8 shows the influence of the number of plates and the reflux ratio on the methanol purity in the distillate of the second column in the methanol purification. Since the goal is the produce MeOH having a purity of at least 99.9%, a reflux rate of 1.3 and a column with 45 plates seems to be a good compromise in this case.

Column	Reflux ratio	N plates	feed plate	MeOH wt% in distillate
COL010	1	40	20	99.41
COL07	1	40	22	99.34
COL07	1	50	20	99.86
COL07	1.3	40	20	99.87
COL07	1.3	45	20	99.928
COL07	1.3	50	23	99.944
COL07	1.5	45	22	99.931

Table B.8: 2nd distillation in MeOH process: analysis of the separation as a function of the reflux ratio, the number of stages and the type of simulation unit used

Inconvenience of the Distillation Modeling

The methodology used for the distillation modeling induces some inconveniences; essentially regarding the convergence after the change of one parameter. In fact, the specifications fixed in the COLVAL column in VALI PFD are only valid for one set of operating conditions because they are adapted from the results of the SIMU unit obtained for a fixed composition, temperature and pressure. Consequently, the model does not converge, if one parameter is changed. For each change, the distillation has therefore to be resimulated in a SIMU unit and these results has again to be transferred to the VALI PFD. Since this operation is quite time consuming, only some key parameters are varied in this work to study the influence. For each case, the specifications for the number of plates and the reflux rate are set to the same value, in order to allow to make a relative comparison of the performance. However, to be completely accurate, the characteristics of the distillation could be optimized for each case.

B.8.2 Distillation Modeling Parameters

DME

The characteristics of the DME purification model are presented in the table B.9:

Parameter	1st distillation	2nd distillation	3rd distillation
$\epsilon_{Murphey}$	85%	85%	85%
N^o plates	8	11	16
Feed plate	1	5	5
Reflux	0.7	0.7	2.6
Inlet T [^oC]	27	142	87.5
Inlet P [bar]	32	32	2

Table B.9: Parameters for the DME purification

MeOH

The characteristics of the methanol purification model, are given in table B.10 and the corresponding flowsheet is illustrated in figure B.6:

Parameter	1st distillation	2nd distillation
$\epsilon_{Murphey}$	85%	85%
N^o plates	22	45
Feed plate	11	20
Reflux	1.3	1.3
Inlet T $[^oC]$	115	85
Inlet P [bar]	8	2

Table B.10: Parameters for the methanol purification

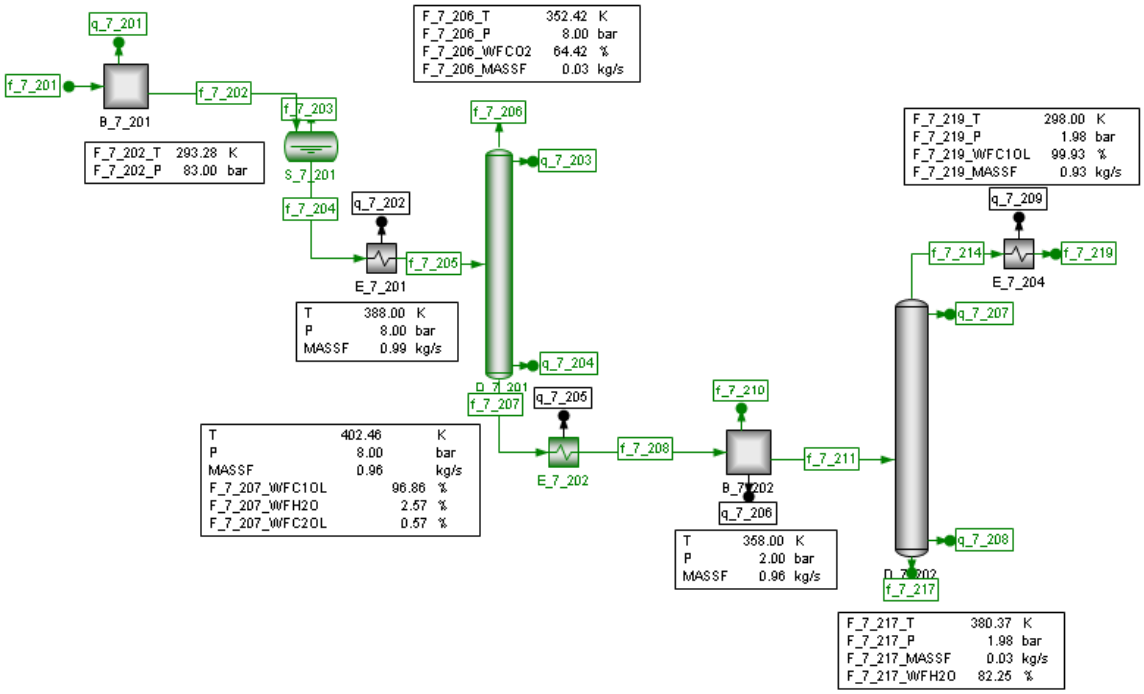

Figure B.6: Flowsheet of the methanol upgrading

B.9 Modeling of a Flash Drum

The temperature and pressure of the flash drums are chosen in such a manner to minimize the losses of product in the vapor fraction and to maximize the separation of the light gases. The tool that is used to study this, is the Thermo3 application of Belsim Vali computing the liquid and vapor phase compositions of a stream for different operating conditions (i.e. pressure and temperature). Different plots can be generated, for example the mass flows or weight fractions of different compounds in the liquid or vapor phase as a function of the temperature or pressure. From the plot the best compromise to meet the opposite objectives can be determined. Figure B.7 illustrates the vapor mass flow of the different components with the temperature for a fixed pressure in the second flash drum in the DME separation section after indirect fluidized bed gasification.

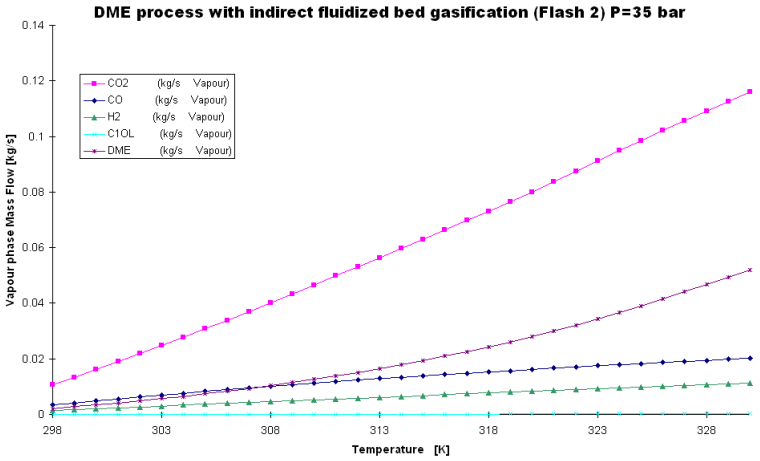

Figure B.7: Determination of the flash drum temperature for the DME process (P=35bar)

By increasing the temperature for a fixed pressure, the vapor fraction increases logically and consequently more products are under vapor form. The plot shows, that an acceptable compromise is T=$308 - 310^oC$, because the loss of DME in the vapor phase is low and nearly all CO and H_2 is contained in the vapor phase and a large amount of CO_2 is removed from the DME product.

B.10 Summary of the Synthesis Conditions

Table B.11 compares the process conditions for the three different synthesis options.

Type	FT	DME	Methanol
PG Pressure [bar]	25	25	25
Reactor Pressure inlet [bar]	25	50	85
Pressure Drop [bar]	0	0	2
PG Temperature [^oC]	340	340	340
Reactor Temperature inlet [^oC]	340	277	260
Reactor Temperature outlet [^oC]	340	277	319

Table B.11: Summary of the synthesis conditions

B.11 Power Recovery

Power recovery is modeled in the Vali PFD Utility according to the flowsheets illustrated in figure B.8.

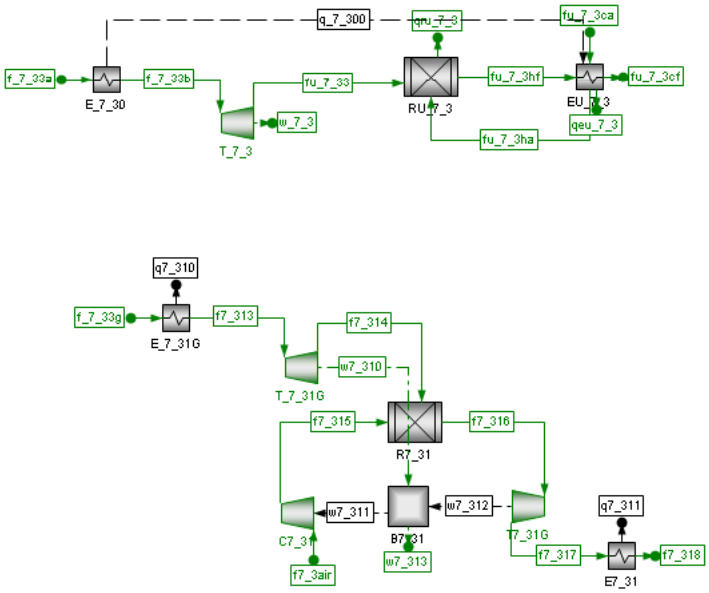

Figure B.8: Utility modeling: Expansion turbine model (top), Gas turbine model (bottom)

The model on the top illustrates the expansion to normal conditions (isentropic efficiency 0.8), followed by the combustion (RU_7_3) in the presence of air (fu_7_3ha). The key parameter is the temperature of the combusted stream (fu_7_3hf) fixed at 1427^oC.

The model on the bottom illustrates the combine gas turbine-Rankine cycle model containing an air compressor (C7_31)(isentropic efficiency 0.85), an expansion turbine (T_7_31G) (isentropic efficiency 0.8), a combustion chamber (R7_31) and finally a turbine (T7_31G) (isentropic efficiency 0.8) and a heat exchanger to reach normal conditions. At high pressure, the offgas is mixed with pressurized air and combusted at around (1100-1300^oC). The power is generated by the expansion of the resulting hot flue gas and part of the power is used for the air compression. Key parameters are the combustion pressure and the temperature after the combustion (around 1127^oC). These values can be optimized to increase the power generation.

Appendix C

Process Economics

C.1 Economic Evaluation Assumptions

The different assumptions for the economic analysis are listed in table C.1. All the costs have been updated to year 2007 by using the Marshall Swift index accounting for the cost inflation. The currency exchange rates have been averaged from 2004 to 2008 (01.10.2008) [72].

Parameter	Value
Marshall and Swift index (2007)	1399
Dollar exchange rate (USD_CHF)	1.203 CHF/US$
Dollar exchange rate (USD_EUR)	0.762 €/US$
Expected lifetime	15 years
Interest rate	6%
Average plant operation	90%
Annual working days	356 days/year
Number of operators	4/shift
Operator's salary	91070 CHF/year
Wood costs	50 CHF/MWh
Electricity price (export)	270 CHF/MWh
Electricity price (import)	270 CHF/MWh

Table C.1: Assumptions for the economic analysis

The electricity costs are based on green electricity and the costs for imported or exported electricity are considered to be the same [63].

C.2 Capital Cost Estimation Methodology

The capital costs are estimated based on the general methodology outlined in [61, 62]. For each equipment the purchase costs C_P are given, assuming atmospheric pressure and carbon steel construction, by a correlation of the type:

$$log_{10}C_P = K_1 + K_2 log_{10}A + K_3(log_{10}A)^2 \tag{C.1}$$

where K_i are constants and A is the characteristic size parameter (power for compressor, length/diameter for the reactors and heat transfer area for the heat exchangers).

The bare module costs (C_{BM}) representing the purchase costs adjusted by material (F_M) and pressure (F_P) factors taking into account the specific process pressures and materials, is given by:

$$C^o_{BM} = (B_1 + B_2 F_M F_P) IC_p \tag{C.2}$$

where I is the actualization factor expressed by the ratio of the Marshall and Swift Equipment Cost Index at actual time to the cost data's reference time.

The total grass roots costs defining the total investment costs for a new production site are then calculated from the bare module cost by using further multiplication factors to take into account indirect expenses like labor, transportation, fees, contingencies and auxiliary facilities.

$$C_{GR} = (1 + \alpha_1) \sum_{i=1}^{n} C_{BM,i} + \alpha_2 \sum_{i=1}^{n} C_{BM,n,i} \tag{C.3}$$

where $C_{BM,n,i}$ represents the bare module costs of the i^{th} equipment for the base case conditions (i.e. atmospheric pressure and carbon steel material) and $C_{BM,i}$ the costs at the operating conditions. The two factors represent additional costs related to the construction of the plant being dependent (α_1) or independent (α_2) of the process conditions. The numeric values that are used are: α_1=0.18 (contingencies 0.15 and fees 0.03) and α_2=0.35 (auxiliary facilities, site development and buildings).[61]

C.3 Process Equipments

The following tables summarize the major process equipments for the different options of feed preparation, pyrolysis, gasification, gas cleaning, synthesis and upgrading. For each installation the construction material and operating pressure are reported.

Section	Equipment	Material	Operating pressure
Air Drying	Direct Rotary Dryers	Carbon Steel	1 bar
	Centrifugal Fans	Carbon Steel	1 bar
Steam Drying	Fluid Bed Dryer	Carbon Steel	1 bar
	Centrifugal Fans	Carbon Steel	1 bar

Table C.2: Major equipments for feed preparation

Section	Equipment	Material	Operating pressure
Torrefaction	Turbo-Dryer	Carbon Steel	1 bar

Table C.3: Major equipments for pyrolysis

Section	Equipment	Material	Operating pressure
Indirectly heated entrained flow	Water Feed Pump	Cast Steel	1 bar(suction)
Steam blown gasifier	Bucket Conveyor	Carbon Steel	1 bar
	Reactor	Nickel Alloy	1-30 bar
Directly heated entrained flow	Centrifugal O_2 Compressor	Carbon Steel	1 bar(inlet)
Oxygen-steam blown gasifier	Water Feed Pump	Cast Steel	1 bar(suction)
	Bucket Conveyor	Carbon Steel	1 bar
	Gasification Reactor	Nickel Alloy	1-30 bar
Indirectly heated fluid bed	Water Feed Pump	Cast Steel	1 bar(suction)
Steam blown gasifier	Bucket Conveyor	Carbon Steel	1 bar
	Gasification Chamber	Nickel Alloy	1-10 bar
	Combustion Chamber	Nickel Alloy	1-10 bar
Directly heated fluid bed	Centrifugal O_2 Compressor	Carbon Steel	1 bar(inlet)
Oxygen-steam blown gasifier	Bucket Conveyor	Carbon Steel	1 bar
	Gasification Reactor	Nickel Alloy	1-30 bar

Table C.4: Major equipments for gasification

Section	Equipment	Material	Operating pressure
ITM	Oxygen transfer membranes	Ceramic membranes	
	Centrifugal Compressor	Carbon Steel	1 bar (inlet)
	Radial Gas turbine	Carbon Steel	1-30 bar

Table C.5: Major equipments for air separation by ion transfer membranes

Section	Equipment	Material	Operating pressure
Reforming	Reactor	Carbon Steel	1 bar
CO_2 removal	MEA absorption unit	Carbon Steel	1 bar

Table C.6: Major equipments for reforming and CO_2 removal

Section	Equipment	Material	Operating pressure
Hot Gas cleaning	Reactor	Nickel Alloy	1-30 bar
Cold Gas cleaning	Cyclone	Nickel Alloy	1-30 bar
	Bag Filter	Carbon Steel	1-30 bar
	Scrubber	Carbon Steel	1-30 bar
	Guard Beds	Carbon Steel	1-30 bar
Water-gas shift	Shift Reactor	Nickel Alloy	25 bar
	Centrifugal Water Feed Pump	Cast Steel	1 bar (inlet)

Table C.7: Major equipments for gas cleaning

Section	Equipment	Material	Operating pressure
FT synthesis	Compressor	Carbon Steel	1-30 bar (inlet)
	SAS-reactor	Nickel Alloy	25 bar
	SB-reactor	Nickel Alloy	25 bar
	FB-reactor	Nickel Alloy	25 bar
	CFB-reactor	Nickel Alloy	25 bar
MeOH synthesis	Compressor	Carbon Steel	1 bar (inlet)
	Compressor	Carbon Steel	25 bar (inlet)
	Reactor	Nickel Alloy	85 bar
	Compressor	Carbon Steel	1-25 bar (inlet)
	Flash drum	Carbon Steel	82 bar
DME synthesis	Compressor	Carbon Steel	1 bar (inlet)
	Compressor	Carbon Steel	25 bar (inlet)
	Reactor	Nickel Alloy	50 bar

Table C.8: Major equipments for synthesis

Section	Equipment	Material	Operating pressure
MeOH Dist	Flash drum	Carbon Steel	83 bar
	1st Distillation Column (N=22)	Carbon Steel	8 bar
	2nd Distillation Column (N=45)	Carbon Steel	2 bar
DME Dist	1st Flash drum	Carbon Steel	50 bar
	2nd Flash drum	Carbon Steel	40 bar
	1st Distillation Column (N=8)	Carbon Steel	32 bar
	2nd Distillation Column (N=11)	Carbon Steel	32 bar
	3rd Distillation Column (N=16)	Carbon Steel	2 bar

Table C.9: Major equipments for upgrading

Section	Equipment	Material	Operating pressure
Power recovery equipments	Expansion Turbine	Carbon Steel	5-40 bar
	Gas Turbine	Carbon Steel	5-40 bar
	Steam Turbine	Carbon Steel	50-180 bar (inlet)

Table C.10: Major equipments for power and energy recovery

Section	Equipment	Material	Operating pressure
Steam network	Heat exchanger network	Carbon steel	1-50 bar

Table C.11: Major equipments for the steam network

C.4 Sizing and Capital Cost Estimation

For each process unit, the sizing (based on the general approach outlined in section 6.1.2) and capital cost estimation is described in the following paragraphs and the sizing parameters are summarized in table C.12.

C.4.1 Drying

Flue gas dryer costs are calculated based on direct rotary dryers' costs with the following design parameters: solid velocity $u_w = 0.03m/s$, percentage of cross section occupied by solids $p_w = 12\%$.

The diameter is calculated by eq.6.2 and the length is determined by the overall heat transfer coefficient $[W/m^3K]$ given by the following equation, [62].

$$U = \frac{240 * G^{0.67}}{d} \tag{C.4}$$

$$l = \frac{\Delta\dot{m}\Delta h_{vap}}{UA\Delta T_{lm}} \tag{C.5}$$

where G is the average superficial velocity $[\frac{kg}{sm^2}]$

Steam dryer costs are calculated based on fluid bed dryers' costs with the following parameters: steam velocity $u_{mean} = 1.40m/s$ and ratio between the height of the dryer and the height of the bed given by: $h = 1.27 * h_{bed}$ where the height of the bed is estimated from eq.C.4.

C.4.2 Pyrolysis

The torrefaction reactor is considered as a Turbo-dryer® from Wyssmont and a residence time of 15 minutes is assumed. The costs are evaluated by the scaling method with data from [22]. The purchase costs for a dryer of d=15ft(4.57m) and h=29ft(8.84m) are 670'000US$ and the ones for a dryer of d=15ft(4.57m) and h=23ft(7.01m) are 565'000US$. A scaling factor of 0.735 is calculated. The density of dry wood is expected to be $80kg/m^3$. It is assumed that only 20% of the reactor's volume is occupied by the reactive compounds and that the h/d ratio is 3.

C.4.3 Gasification

Each gasification option's equipments are sized based on the different design characteristics. For all the options the costs of a bucket conveyor needed to carry the dried biomass to the gasifier are included in the gasification expenses. The height of the conveyor is assumed to be proportional to the gasifier height. A ratio of $\frac{h_{conv}}{h_g} = 3$ is chosen based on data from the Guessing plant.

The costs of a centrifugal pump defined by the power and pressure are included for the steam-blown and oxygen-steam blown gasifiers. For the directly heated gasifications the costs of a centrifugal oxygen feed compressor having an efficiency of 0.8 are added.

The expenses of the directly heated fluidized bed reactor are estimated with the correlation for fluid beds, while the cost of the indirectly heated fluidized bed reactor are estimed by the FICFB reactor costs. The sizing parameters are reported in table C.12.

The FICFB reactor operated at Guessing plant consists of a gasification zone fluidized with steam and a combustion chamber fluidized with air. The costs of both chambers are calculated with correlations for fluid beds by using the parameters of the Guessing plant. The mean velocity is derived from the gas composition.[27]

The entrained flow reactors are modeled like horizontal vessels with a length to diameter ratio of 10 and a residence time of 2 sec [73, 74].

In order to take into account internals, special constructions and new technology, a multiplication factor of 4 is introduced for the gasification reactors costs.

The different sizing parameters for the gasification are summarized in table C.12.

C.4.4 Air Separation

In the case of directly heated gasification by internal oxidation the costs for air separation are included.

The costs of the ion transfer membranes for O_2 production include the costs of the transfer membranes themselves and the costs of a centrifugal compressor and a radial gas turbine. The costs of the transfer membranes are scaled from data from Air Products publication [30]. The reported installed costs are 13'000 US$/TPD O_2 (1'123'200 US$/kg/s O_2). The compressor costs are calculated based on an efficiency of 0.8 and the compression power with the corresponding correlation. The turbine costs are also determined by the corresponding correlation.

C.4.5 Steam Methane Reforming

The costs for the steam methane reformer are estimated by summing the catalyst and the reactor costs determined from scaling from known costs. The evaluation procedure, as well as the characteristics for the sizing and the cost estimation are detailed in section C.5 [75, 76]. The costs are essentially defined by the methane conversion and the methane flow rate in the reactor. The catalyst chosen for the steam methane reforming is Ni/Al_2O_3.

C.4.6 Gas Cleaning

Cold gas cleaning

For estimating the costs related to cold gas cleaning, the costs of the various equipments needed to remove the impurities are summated. The key parameter for the cost estimation of the cyclones, the bag filter and the Venturi scrubber is the volumetric flow rate. The costs for the ZnO guard beds are estimated by scaling the volume per Nm^3/s of treated gas from literature data [17]. By knowing the volume, the height and the diameter are calculated by assuming a ratio h/d=3. With these parameters the costs are determined based on the costs of a vertical vessel and tower packings.

Hot Gas cleaning

The costs for hot gas cleaning are evaluated by the scaling method. The costs reported in [17] are in the order of 14.3MUS$ for a plant capacity of $400MW_{HHV}$. It is assumed that there is no effect of scaling and the overall installation factor is 1.

Shift reactor

The costs of the shift reactor are evaluated, in analogy with the costs of the SMR reactor (section C.5), by summing the catalyst and reactor costs. According, to the process temperature an appropriate catalyst is: 1%Pd/Al_2O_3. By knowing the catalyst characteristics, the total molar flow rate, the CO and H_2O flow rate and the CO-conversion, the size and the costs are estimated. The values used for the WGS-reactor cost estimations are given in appendix in table C.13.

CO_2 removal

The costs for CO_2 removal are estimated for chemical absorption with MEA by using the scaling method. The following values are found in literature [29]: $22MUS\$_{1994}$ (installed costs) for 42 tonnes CO_2 per hour with a scaling exponent of 0.8.

C.4.7 Synthesis

The synthesis costs are composed of the reactor cost themselves and the costs of a compressor increasing the pressure to the synthesis pressure. In the case of cold gas cleaning, the compression from atmospheric pressure to 25 bar takes place before the shift reactor, while in the case of hot gas cleaning the compression only occurs before the synthesis. The costs for this compression are in each case included in the synthesis costs.

Fischer-Tropsch

The costs of the different options for the Fischer-Tropsch synthesis reactor are estimated based on sizing data available from commercial plants [77, 43, 24]. The key parameters (u_{mean}, h relation) are given in table C.12.

The fixed bed reactor and the slurry phase reactor costs are determined based on the correlation for vertical vessels.

The Sasol advanced Synthol reactor and the circulating fluidized bed reactor costs are estimated from the fluid bed reactor correlation.

DME

The costs for the DME reactor are determined for a slurry reactor with $u_{mean} = 0.2m/s$ [49]. The parameters for the height correlation are fitted from [49, 50, 78] and given in table C.12. Moreover, the costs of a compressor and a flash drum are added.

MeOH

The costs of the methanol synthesis section are composed of the expenses for the reactor, a compressor and a flash drum. The costs of the reactor are simply estimated by the values of u_{mean} and the ratio h/d for the two types of reactors: fixed bed reactor and slurry phase reactor [77] (table C.12). Moreover, a factor is introduced to take into account the total area and not only the area occupied (FB: 92%, SB: 49%)[77]. The costs are then estimated with the correlation for a vertical vessel.

C.4.8 Upgrading

DME

The costs of the DME purification include the costs of flash drums and distillation columns. The price of the columns related to the number of stages (8, 11 and 16) is estimated based on the correlation for vertical vessels and towerpackings.

MeOH

The costs for methanol purification are estimated by the costs of a flash drum and two distillation columns (22 and 45 plates).

C.4.9 Power Recovery Equipment

The expansion turbine costs are calculated by introducing the value of the overall power generated through the expansion of the different fuels in the correlation for radial gas turbines including the cost of an electric drive.

The costs of the gas turbine including a compressor, a combustion chamber and a turbine, is also estimated by using the overall power produced and the correlation for gas turbines.

In general, radial gas turbines are, compared to axial gas turbines, more efficient but limited in size (axial: 4000kW and radial gas turbines: 1500 kW).

In the case where a Rankine cycle is implemented, the costs for the steam turbine are evaluated based on the shaft power computed from the energy integration by using the correlation from [61] and including the costs of an electric drive. These costs are defined as steam cycle costs hereafter.

C.4.10 Heat Pump

A heat pump, is a vapor-compression refrigeration cycle containing a condenser, an expansion valve, an evaporator and a compressor. The costs of this cycle are dominated by the costs of the compressor because the costs of a valve are negligible and the costs of the condenser and evaporator are taken into account in the heat exchanger network costs. Therefore, the costs for the heat pump are estimated based on the compression power defining the compressor costs. The value of the compression power is computed from the energy integration.

C.4.11 Summary of Parameters for Sizing

Table C.12 summarizes the model constants used for the reactor sizing.

Reactor	$u_{mean}[m/s]$	h_0	n	h/d
Air drying	0.03	-	-	-
Steam drying	1.40	-	-	-
FICFB-Gasification	0.645	4.07	0.188	-
FICFB-Combustion	5.250	8.47	0.188	-
FT- SB [77]	0.136	2.004	1.158	-
FT - FB [77]	0.433	5.472	0.848	-
FT- SAS [77, 24]	0.2	9.728	0.477	-
FT - CFB [24]	1.5	57.83	-0.172	-
DME -Slurry reactor [49]	0.2	21.77	0.073	-
MeOH -FB [77]	0.317	-	-	1.62
MeOH -SB [77]	0.135	-	-	3.15

Table C.12: Assumptions for sizing of reactors

C.5 Reforming and WGS Reactor

The steam methane reforming and the water-gas shift reaction are performed in a shell and tube reactor with the catalyst in the tube and the heat exchange in the shell. As the heat exchange cost is computed from the composite curve, it is not considered in the reactor sizing and costing procedure described hereafter.

The cost evaluation comprises the catalyst volume and cost estimation and the reactor volume and cost assessment. This cost estimation method is developed in detail in [75, 76].

The volume of the catalyst in the reactor k, $V^k_{catalyst}$, corresponds to the volume required to achieve the target conversion of reactant (X) and is computed from the reaction kinetics ($-r^k_r$).

$$V^k_{catalyst} = \frac{\dot{n^k_{r,in}}}{\rho^k_B} \int_0^X \frac{dX}{-r^k_r} \tag{C.6}$$

where $n^k_{r,in}$ is the molar flow rate of reactant coming out of reactor k [mol/s] and ρ^k_B the bulk density of catalyst used in reactor k [kg/m^3].

The catalyst costs are then evaluated from the volume by knowing the volume cost $\pi^k_{catalyst}$:

$$C^k_{catalyst} = V^k_{catalyst} \cdot \pi^k_{catalyst} \tag{C.7}$$

The volume of the reactor V^k_{Rct} is estimated from the catalyst volume by introducing a proportionality constant F^k_V.

$$V^k_{Rct} = F^k_V \cdot V^k_{catalyst} \tag{C.8}$$

Finally, the costs of the reactor volume C^k_{volume}, is computed by scaling from a reference case with known costs C^k_{ref} and volume V^k_{ref}.

$$C^k_{volume} = C^k_{ref} \cdot F^k \cdot \left(\frac{V^k_{Rct}}{V^k_{ref}}\right)^{\gamma} \tag{C.9}$$

where γ is the scale exponent and F^k the proportionality constant taking into account the scaling due to pressure and material factors.

The values for the sizing and costing of the steam methane reformer and the water-gas shift reactor are summarized in table C.13. The appropriate catalyst is chosen in accordance with the process temperature; for the SMR reforming the selected catalyst is Ni/Al_2O_3 and for the WGS reaction 1%Pd/Al_2O_3.

Parameter Catalyst	SMR Ni/Al_2O_3	WGS 1%Pd/Al_2O_3
α	0	0.14
β		0.38
k [kmol/kgs]	227.8	1.93
Bulk density ρ_B [kg/m^3]	1200	1200
Activation NRJ [J/mol]	129790	79967.8
$\pi^k_{catalyst}$ [USD/m^3]	100000	16800
C^k_{ref} [USD]	21936	5774.6
V^k_{ref} [m^3]	0.0167	0.104
F^k_V	1.17	1.17
Exponent for volume calculation γ	0.6	0.6

Table C.13: Assumptions for sizing of the SMR and WGS reactor [75, 76]

Appendix D

Scenarios

Scenario	A	B	C	D	E	F	G	H
Synthesis	DME	DME	MeOH	MeOH	FT	FT	FT	MeOH
Drying	air	air	air	air	air	air	air	air
Gasification type	EF/FICFB	FICFB	FICFB	FICFB	FICFB	FICFB/CFB	FICFB	FICFB
Heating mode	d/ind	ind	ind	ind	ind	ind/d	ind	ind
Reforming T [K]	-/1123.15	1623.15	1623.15	1223.15	1050	var/var	var	var
Reforming steps	1	1	1	1	1	1	3	1
Gas Cleaning	cold	cold	cold	cold	cold	cold	cold	cold
CO_2 removal [%]	95	95/var	fixed	fixed	0	0	0	fixed
Gas Recyling [%]	80	var/80	var	90	var	0	0	90
H_2/CO	var	1.3	-	-	2	2	2	-
$\frac{H_2-CO_2}{CO+CO_2}$	-	-	2	2	-	-	-	2
CO-conversion	-	-	-	-	85	80	85	
Steam cycle	S0	S3	S2	S2	S1	S1	S1	S2
Char combustion	y	y	y	y	y	y/n	y	y
PG combustion	hot	hot	hot	hot	hot	hot	hot	hot
Offgas combustion	y	y	y	y	y	y	y	y
Gas Turbine	n	n	n	n	n	n	n	n

Table D.1: Parameters choices for the different scenarios studied (Heating mode: d=direct and ind=indirect; Steam cycle characteristics: S0, S1, S2 and S3 refering to section E.2; Combustion: y=yes, n=no)

Scenario	I	J	K	L	M	N	O
Synthesis	DME	FT	MeOH	FT	DME	FT	FT
Drying	air	air	steam	air	air	air	air
Gasification type	CFB	FICFB	FICFB	FICFB	FICFB	EF	FICFB
Heating mode	d	ind	ind	ind	ind	ind	ind
Reforming T [K]	1123.15	1623.15	1223.15	1050.15	1223.15	-	var
Reforming steps	1	3	1	1	1	-	1
Gas Cleaning	cold	cold	cold	cold	cold	cold	cold
CO_2 removal [%]	95	0	fixed	0	95	0	0
Gas Recyling [%]H_2/CO	1.3	2	-	2	1.3	2	2
$\frac{H_2-CO_2}{CO+CO_2}$	-	-	2	-	-	-	-
CO-conversion	-	85	-	var	85	85	85
Steam cycle	var	S1	S2 modi.	S1	S3	S1	S1
Char combustion	n/y	y	y	y	y	y	y
PG combustion	hot	hot/cold	hot	hot	hot	hot	hot
Offgas combustion	y	y	y	y	y	y	y
Gas Turbine	n/y	n	n	n	n	n	n

Table D.2: Parameters choices for the different scenarios studied (Heating mode: d=direct and ind=indirect; Steam cycle characteristics: S0, S1, S2 and S3 refering to section E.2; Combustion: y=yes, n=no)(continuation)

Base-case	1		2									
Options			gas1	gas2	gas3d	gas3i3	gas3i1	gas4d	gas5ii	gas5dd	gas6i	gas6d
Synthesis	FT	FT	FT	FT	FT	FT	FT	FT	FT	FT	FT	FT
Drying	air/steam	air/steam	air	air	air	air	air	air	air	air	air	air
Gasification type	CFB	CFB	EF	EF	FICFB	FICFB	FICFB	CFB	FICFB	CFB	FICFB	CFB
Heating mode	d	ind	ind	d	ind	ind	ind	d	ind	d	ind	d
Reforming T [K]	1000.15	1050.15	-	-	1623.15	1623.15	1623.15	1623.15	1050.15	1000.15	1050.15	1000.15
Reforming steps	1	1	-	-	1	3	1	1	1	1	1	1
Gas Cleaning	cold	cold	cold	cold	cold	cold	cold	cold	cold	cold	cold	cold
CO_2 removal [%]	0	0	0	0	0	0	0	0	0	0	0	0
Gas Recyling [%]	0	0	0	0	0	0	0	0	0	0	0	0
H_2/CO	2	2	2	2	2	2	2	2	2	2	2	2
CO-conversion	85	85	85	85	85	85	85	85	85	85	85	85
Steam cycle	S1	S1	S1	S1	S1	S1	S1	S1	S1	S1	S1	S1
Char combustion	n	y	y	n	y	y	y	n	y	n	y	n
PG combustion	hot	hot	hot	hot	hot	hot	hot	hot	hot	hot	hot	hot
Offgas combustion	y	y	y	y	y	y	y	y	y	y	y	y
Gas Turbine	n	n										

Table D.3: Parameters choices for the different options of the two base-case FT processes (Heating mode: d=direct and ind=indirect; Steam cycle characteristics: S0, S1, S2 and S3 refering to section E.2; Combustion: y=yes, n=no)

Appendix E

Final models

In this section the key parameters of the final models of the different synthesis processes are summarized. For each process the considered options are: air drying, indirectly heated fluidized bed gasification, steam methane reforming at optimal temperature and cold gas cleaning and an optimized steam network is included in the energy integration. The performance of the processes characterized by these parameters are compared in chapter 8.2.3.

E.1 Synthesis

The characteristics of the final models for the synthesis of FT, DME and methanol are summarized in table E.1

Parameter	FT	DME	MeOH
$T_{synthesis}in$ [^oC]	340	277	260
$T_{synthesis}out$ [^oC]	340	277	319
$P_{synthesis}$ [bar]	25	50	85
$\frac{H_2}{CO}$ [-]	2	1.3	-
$\frac{H_2-CO_2}{CO+CO_2}$ [-]	-	-	2
CO_2 removal [%]	-	95	fix $\frac{H_2-CO_2}{CO+CO_2}$=2
CO-conversion [%]	85	-	-
Recycling loop [%]	-	80	90

Table E.1: Summary of parameters for the final synthesis models

E.1.1 List of streams

The characteristics of the main process streams for the three different processes are summarized in the tables E.2- E.7. The composition and mass flow at the outlet of the gasification, gas treatment, synthesis and upgrading section are reported, as well as the main hot and cold streams corresponding to the integrated process (figure 8.12).

Main process streams composition

Section	Gasification	WGS	Synthesis	Upgrading
Composition [%mol]				
CH_4	0.61	0.6	1.72	1.25
H_2	48.83	55.64	13.28	2.16
CO	36.54	27.82	7.66	2.75
CO_2	6.32	14.07	25.83	65.84
N_2	0.08	0.08	0.15	0.05
H_2O	7.61	1.78	46.67	0.07
$oC_2 - C_4$	0	0	1.16	5.15
$pC_2 - C_4$	0	0	0.29	1.40
$oC_5 - C_{12}$	0	0	1.73	11.35
$pC_5 - C_{12}$	0	0	0.3	2.00
$oC_{13} - C_{18}$	0	0	0.38	2.50
$pC_{13} - C_{18}$	0	0	0.25	1.67
$pC_{20} - C_{24}$	0	0	0.58	3.81
LHV [MJ/kg]	14.48	14.02	11.10	25.47
$\dot{m}$ [kg/s]	1.35	1.29	1.29	0.47
Load [MW]	19.5	18.1	14.3	12.01

Table E.2: Gas composition [%mol], calorific value, mass flow and heat load at process section outlet for the FT process

Section	Gasification	WGS	Synthesis	Upgrading
Composition [%mol]				
CH_4	0.01	0.01	0	0
H_2	48.27	57.25	0.54	0
CO	38.47	28.63	1.09	0
CO_2	4.48	13.89	0.23	0
N_2	0.08	0.08	0.01	0
H_2O	8.69	0.13	0.53	0
MeOH	0	0	96.92	99.97
EtOH	0	0	0.39	0.03
DME	0	0	0.29	0.58
LHV [MJ/kg]	14.57	14.32	19.73	19.83
$\dot{m}$ [kg/s]	1.35	1.37	0.59	0.57
Load [MW]	19.67	19.62	11.65	11.41

Table E.3: Gas composition [%mol], calorific value, mass flow and heat load at process section outlet for the MeOH process

Section	Gasification	WGS	Synthesis	Upgrading
Composition [%mol]				
CH_4	0.01	0.01	0	0
H_2	48.27	51.81	26.33	0.29
CO	38.47	39.85	2.18	0
CO_2	4.48	5.53	29.80	0.04
N_2	0.08	0.09	0.21	0
H_2O	8.69	2.71	7.22	0
MeOH	0	0	3.64	0.10
DME	0	0	30.62	99.57
LHV [MJ/kg]	14.57	15.72	16.14	28.8
$\dot{m}$ [kg/s]	1.35	1.13	0.96	0.38
Load [MW]	19.67	17.76	15.49	11.13

Table E.4: Gas composition [%mol], calorific value, mass flow and heat load at process section outlet for the DME process

Main hot and cold process streams

Unit	Stream	Type	Tin [K]	Tout [K]	q [kW]
Airdry	0_107-0_108	Cold	303.30	473.15	3657.7
Airdry	0_105-0_109	Hot	355.65	298.15	2741.7
Torrefaction	1_403-1_404	Cold	533.15	623.0	1509.9
Torrefaction	1_406-1_407	Hot	533.15	298.15	1201.5
Gas5	2_506-2_507	Cold	298.23	465.28	324.70
Gas5	2_507-2_508	Cold	465.28	465.28	902.59
Gas5	2_508-2_509	Cold	465.28	673.15	212.73
Gas5	2_521-2_521	Cold	1123.20	1123.20	2960.5
Gas5	2_522-2_531	Cold	1050.10	1050.10	1838.6
CGCL	3_201-3_202	Hot	1050.10	423.15	1654.3
CGCL	3_207-3_211	Hot	836.41	674.48	406.66
WGS	4_103-4_104	Cold	298.31	497.07	81.617
WGS	4_104-4_105	Cold	497.07	497.07	176.53
WGS	4_105-4_106	Cold	497.07	674.48	41.476
WGS	4_107-4_111	Hot	673.15	644.65	328.95
WGS	4_111-4_112	Hot	644.65	613.00	86.158
Synthesis	6_101-6_111	Hot	613.00	613.00	3274.2
Upgrading	7_101-7_102	Hot	612.93	298.15	1705.9

Table E.5: Main hot and cold streams of the FT process with FICFB gasification and reforming at 1050K corresponding to figure 8.12

Unit	Stream	Type	Tin [K]	Tout [K]	q [kW]
Airdry	0_107-0_108	Cold	303.30	473.15	3657.7
Airdry	0_105-0_109	Hot	355.65	298.15	2741.7
Torrefaction	1_403-1_404	Cold	533.15	623.0	1509.9
Torrefaction	1_406-1_407	Hot	533.15	298.15	1201.5
Gas5	2_506-2_507	Cold	298.23	465.28	324.70
Gas5	2_507-2_508	Cold	465.28	465.28	902.59
Gas5	2_508-2_509	Cold	465.28	673.15	212.73
Gas5	2_521-2_521	Cold	1123.20	1123.20	2960.5
Gas5	2_522-2_531	Cold	1223.10	1223.10	2601.4
CGCL	3_201-3_202	Hot	1223.10	423.15	2294.6
CGCL	3_207-3_211	Hot	845.95	674.49	456.76
WGS	4_103-4_104	Cold	298.31	497.07	86.330
WGS	4_104-4_105	Cold	497.07	497.07	186.73
WGS	4_105-4_106	Cold	497.07	674.48	43.871
WGS	4_107-4_111	Hot	673.15	477.60	880.96
WGS	4_111-4_112	Hot	477.60	613.00	383.52
Syn	6_200-6_201	Hot	613.00	613.00	1.367
Syn	6_201-6_201a	Hot	613.00	298.00	885.82
Syn	6_202-6_203	Hot	446.45	341.00	303.48
Syn	6_204-6_205	Cold	338.18	341.00	19.138
Syn	6_206-6_206a	Cold	341.00	533.00	1561.1
Syn	6_211-6_212	Hot	628.46	533.00	462.05
Syn	6_214-6_214a	Hot	611.05	533.00	477.01
Syn	6_216-6_216a	Hot	602.12	533.00	468.88
Syn	6_218-6_219	Hot	594.76	298.00	2932.2
Syn	6_223-6_224	Cold	300.58	341.00	262.47
MEA	MEAHT	Cold	423.00	423.00	2016.2
MEA	MEALT	Hot	383.00	383.00	2016.2
Upgrd	7_201-7_202	Hot	298.00	291.64	10.051
Upgrd	7_204-7_205	Cold	298.46	388.00	210.49
Upgrd	7_205-7_206	Hot	388.00	337.24	9.5736
Upgrd	7_205b-7_207	Cold	388.00	401.76	38.853
Upgrd	7_207-7_208	Hot	401.76	358.00	541.59
Upgrd	7_211-7_217	Cold	358.00	371.71	895.46
Upgrd	7_211b-7_214	Hot	358.00	355.75	904.15
Upgrd	7_214-7_219	Hot	355.75	298.00	773.36

Table E.6: Main hot and cold streams of the MeOH process with FICFB gasification and reforming at 1223K corresponding to figure 8.12

Unit	Stream	Type	Tin [K]	Tout [K]	q [kW]
Airdry	0_107-0_108	Cold	303.30	473.15	3657.7
Airdry	0_105-0_109	Hot	355.65	298.15	2741.7
Torrefaction	1_403-1_404	Cold	533.15	623.0	1509.9
Torrefaction	1_406-1_407	Hot	533.15	298.15	1201.5
Gas5	2_506-2_507	Cold	298.23	465.28	324.70
Gas5	2_507-2_508	Cold	465.28	465.28	902.59
Gas5	2_508-2_509	Cold	465.28	673.15	212.73
Gas5	2_521-2_521	Cold	1123.20	1123.20	2960.5
Gas5	2_522-2_531	Cold	1223.10	1223.10	2601.4
CGCL	3_201-3_202	Hot	1223.10	423.15	2045.5
CGCL	3_207-3_211	Hot	845.95	673.15	409.58
WGS	4_103-4_104	Cold	298.31	497.07	0.96E-3
WGS	4_104-4_105	Cold	497.07	497.07	0.21E-2
WGS	4_105-4_106	Cold	497.07	674.48	0.485E-3
WGS	4_107-4_111	Cold	673.15	864.95	433.56
WGS	4_111-4_112	Hot	864.95	613.00	596.89
Syn	6_301-6_302	Hot	610.77	298.00	662.33
Syn	6_302a-6_303	Cold	379.98	550.00	363.32
Syn	6_304-6_305	Hot	550.00	550.00	2545.5
Syn	6_306-7_302	Cold	550.00	550.00	11.283
Syn	7_302-7_32	Hot	550.00	332.00	372.35
Syn	7_34-7_35	Hot	330.55	308.00	31.593
Syn	7_37-7_37a	Cold	307.09	308.00	2.2567
MEA	MEAHT	Cold	423.00	423.00	667.89
MEA	MEALT	Hot	383.00	383.00	667.89
Upgrd	7_38-7_303	Hot	308.00	277.96	34.672
Upgrd	7_38b-7_304	Cold	308.00	404.92	106.88
Upgrd	7_304-7_304a	Cold	404.92	415.00	52.714
Upgrd	7_304a-7_305	Hot	415.00	376.37	68.671
Upgrd	7_305-7_312	Hot	376.37	298.15	16.944
Upgrd	7_304b-7_306	Cold	415.00	470.55	84.095
Upgrd	7_306-7_307	Hot	470.55	360.65	39.479
Upgrd	7_307-7_308	Hot	360.65	355.29	128.41
Upgrd	7_307b-7_309	Cold	360.65	393.37	173.94
Upgrd	7_308-7_310	Hot	355.29	298.15	48.422
Upgrd	7_309-7_311	Hot	393.37	298.15	20.025

Table E.7: Main hot and cold streams of the DME process with FICFB gasification and reforming at 1223K corresponding to figure 8.12

E.2 Steam Network

The steam network introduced before optimization of the characteristic parameters was defined by the arbitrary values reported in table E.8.

Parameter	Value
Steam production pressure	80 bar
Steam superheat temperature	823K
Bleeding temperature (1)	423K
Bleeding temperature (2)	473K
Bleeding temperature (3)	293K
Condensation	292K

Table E.8: Initial parameters for the Steam Cycle (S0)

The steam network introduced to improve the overall performance of the different processes has the following characteristics (table E.9).

Parameter	FT process (S1)	MeOH (S2)	DME (S3)
Steam production pressure 1	80 bar	50 bar	50 bar
Steam production pressure 2	120 bar	120 bar	120 bar
Bleeding temperature (1)	433K	433K	433K
Bleeding temperature (2)	473K	473K	473K
Bleeding temperature (3)	293K	293K	293K
Condensation	292K	292K	292K

Table E.9: Parameters for the steam network included in the final models

Appendix F

Additional Data

The results computed from the thermo-economic models are analyzed and discussed in chapters 7 and 8. Here, additional figures and tables illustrating some conclusions drawn in these chapters are reported.

F.1 Unit Performance

F.1.1 FT process: CO-Conversion

CO-conversion influence on the chemical efficiency of the different hydrocarbons fractions and non-hydrocarbon fraction (non HC: CO,H_2O, CO_2, H_2) of the crude FT-fuels.

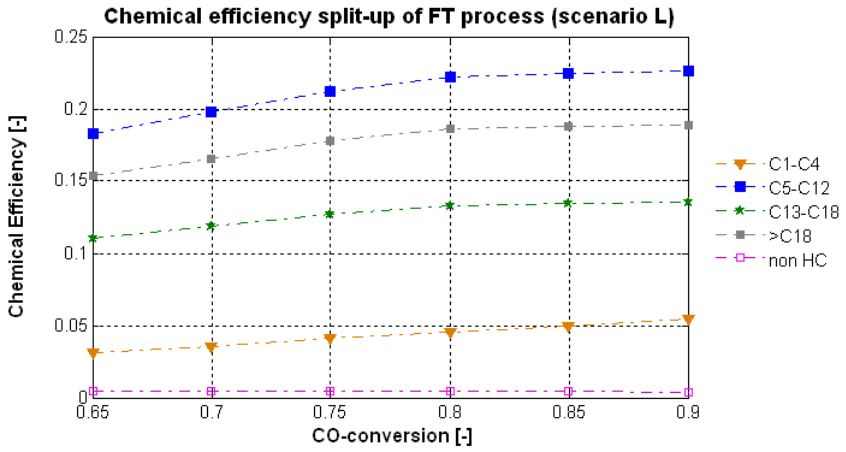

Figure F.1: Fuel efficiency variation with CO-conversion in the different hydrocarbons ranges for FT process (scenario L)

F.1.2 Gasification and Reforming Pressure

The gasification pressure influences the thermo-economic performance, by influencing the composition of the producer gas and hence the synthesis productivity and by influencing the compression power and hence the energy integration and the production costs (figure F.2).

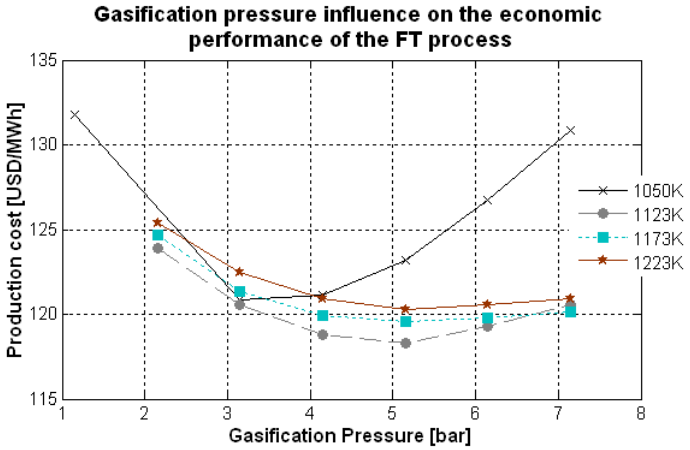

Figure F.2: Gasification pressure influence on the production cost of the FT process with indirectly heated fluidized bed gasification for different methane reforming temperatures (scenario O)

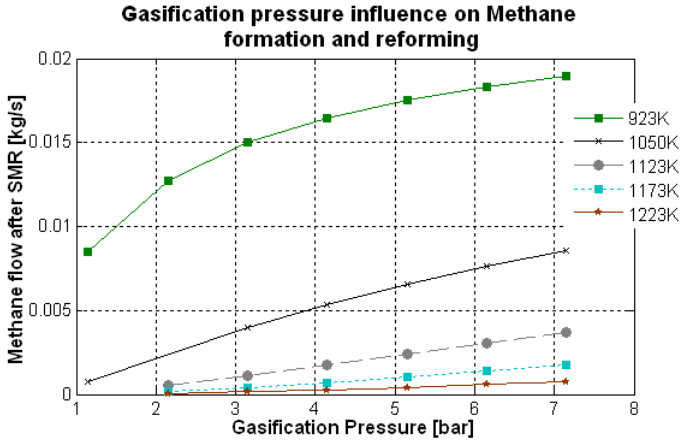

Figure F.3: FT-process: Gasification pressure influence on the methane content in the producer gas after indirectly heated fluidized bed gasification and SMR for different reforming temperatures (scenario O)

F.1.3 Steam Reforming Temperature

The stepwise reforming at different temperatures (973, 1333 and 1623K) increases the efficiency only slightly compared to the single reforming at 1623K. Figure F.4 illustrates the variation of the efficiency with the reforming configuration (set-up 0 and set-up 3) for the different synthesis options.

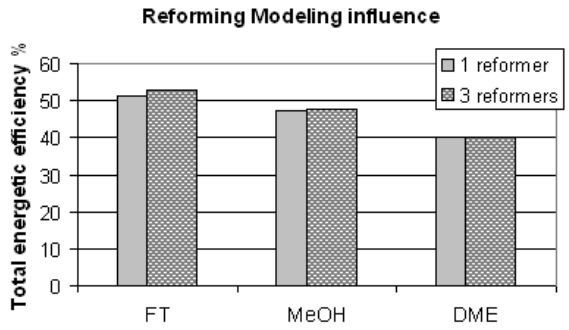

Figure F.4: Reforming modeling influence on the performance of the different synthesis processes (similar to scenario G)

F.1.4 Hot Utility

Figure F.5 illustrates the difference in the energy integration for different types of fuels combusted to cover the heat demand above the pinch.

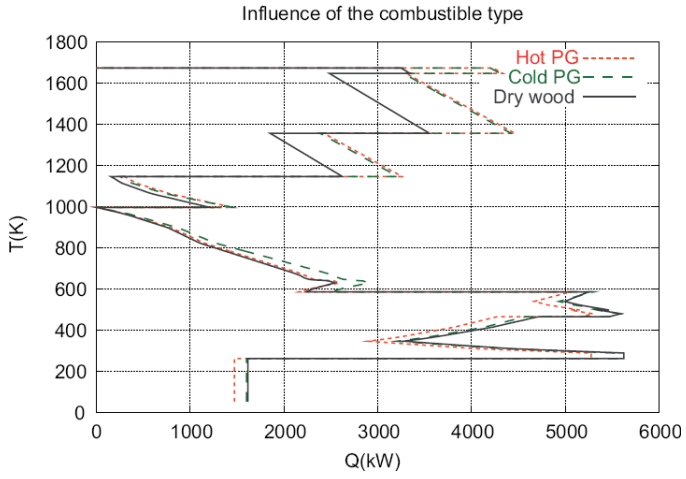

Figure F.5: Composite curves (steam network not shown) for the FT process for different types of combustibles (scenario J)

F.2 Literature Comparison

To prove the accurateness of the developed models, a comparison is made with literature data in chapter 8.1.

The composite curves including a steam network, corresponding to the MeOH and FT processes used for the comparison with the ECN processes [16, 29] are illustrated in figures F.6 and F.7.

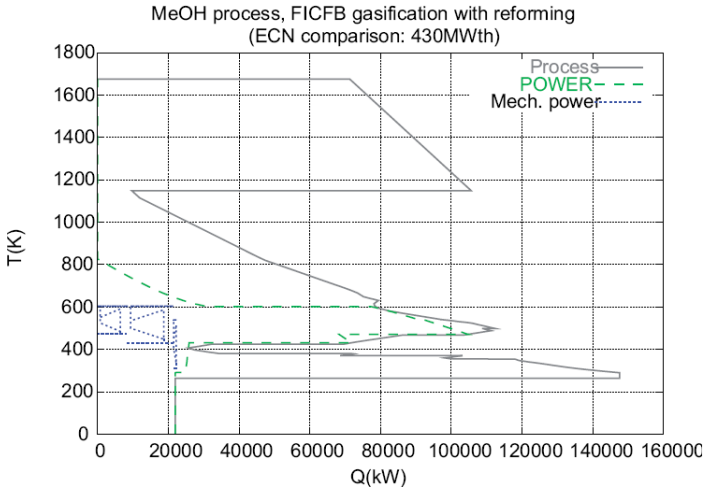

Figure F.6: Composite curve of the MeOH process with FICFB gasification and reforming for a nominal thermal capacity of $430 MWth_{HHV}$

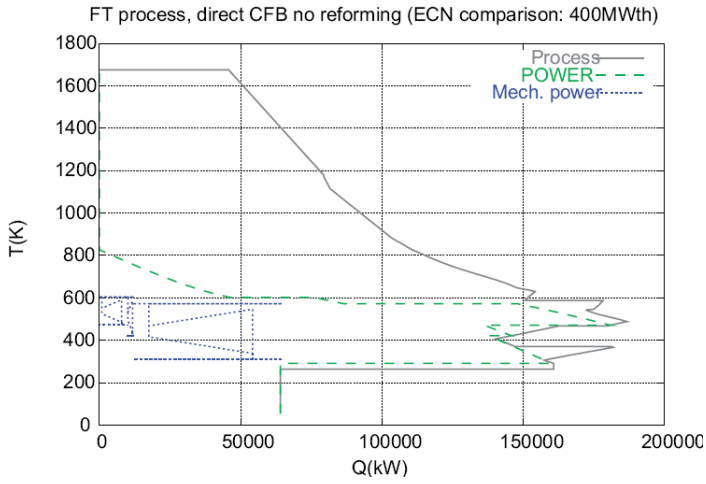

Figure F.7: Composite curve of the FT process with CFB gasification and without reforming for a nominal thermal capacity of $400 MWth_{HHV}$

F.3 Process Options Comparison

F.3.1 Gas Cleaning

The cleaning technology and the degree of impurities influence the process performance. Figure F.8 illustrates the composite curves for hot and cold gas cleaning for the FT process with FICFB gasification.

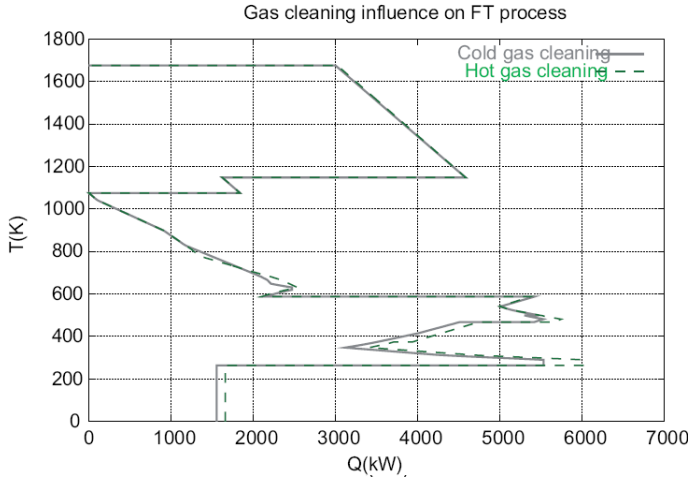

Figure F.8: Composite curves for the different cleaning options for the FT process including a steam network (not shown)(base-case 1: air drying, indirectly heated CFB)

F.3.2 Steam Methane Reforming

The integrated composite curves (figure F.9) illustrate the influence of the introduction of a steam methane reforming step for the FT process with directly heated CFB gasification.

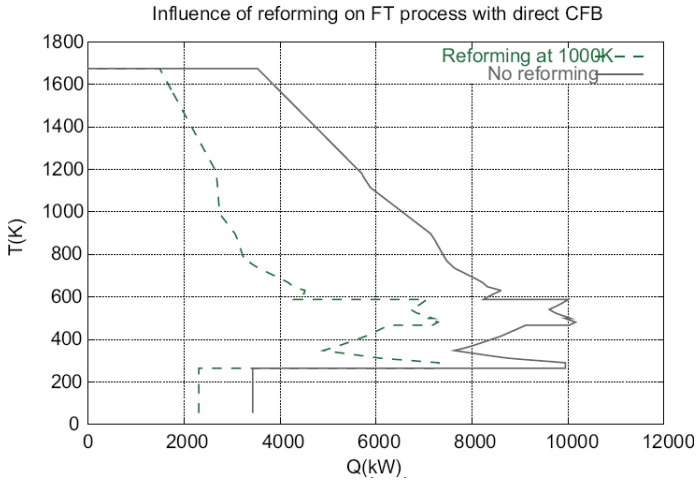

Figure F.9: Composite curves for the FT process with directly heated CFB gasification with and without reforming (steam network not shown)

F.4 Evaluation of avoided CO_2 emissions

The notion of avoided CO_2 emissions is related to the idea that the production of syngas from a renewable source with zero net emissions of CO_2 can replace part of the natural gas demand from fossil sources and consequently lower the total net greenhouse gas emissions.

To assess the amount of avoided CO_2, the CO_2 emissions from the complete oxidation of MeOH and DME are calculated based on the lower heating value (table F.1). The emissions from the production and transport of MeOH and DME from a fossil feedstock are taken from [79] and reported in table F.1.

CO_2 emissions [kg/MWh]	Combustion	Production
MeOH	234.37	116.59
DME	238.52	163.75

Table F.1: CO_2 emissions from combustion and production (from fossil feedstock)

From the thermodynamic model, the amount of pure CO_2 removed before the synthesis and the amount at the combustion outlet are computed for both processes. By considering the emissions related to the wood harvesting and transport (6.25kg/MWh), and to the electricity production (110 kg/MWh)[1], the emissions of use are calculated. The avoided emissions are then evaluated from the emissions from the fuel production from a fossil source by subtracting the emissions of use from the biomass conversion process. If sequestration is considered, the amount of captured CO_2 at the process outlet is subtracted from the emissions of use respectively added to the avoided CO_2 emissions. The results for the CO_2 emissions assessment are summarized in table F.2.

CO_2 emissions [kg/MWh fuel]	MeOH no capture	MeOH capture	DME no capture	DME capture
Outlet pure CO_2	171.99		58.39	
Combustion outlet	144.62		268.58	
Emissions of use	27.41	-144.58	19.47	-38.92
Avoided by substitution	89.18	261.17	144.28	202.67
Yearly avoided [kton/year]	7.8	22.9	12.34	17.34

Table F.2: Environmental evaluation of the MeOH and DME process

[1]The current Swiss electricity mix including imported electricity is allocated with specific CO_2 emissions of $110 g/kWh_{el}$ [79]

List of Figures

List of Tables